Structural Engineering Report No. ST-00-3

NONLINEAR ANALYSIS OF CONTINUITY PLATE AND DOUBLER PLATE DETAILS IN STEEL MOMENT FRAME CONNECTIONS

Yanqun Ye, Jerome F. Hajjar, Robert J. Dexter, Sara D. Prochnow, and Sean C. Cotton

September 2000

Department of Civil Engineering
Institute of Technology
University of Minnesota
Minneapolis, Minnesota 55455

Abstract

This research studies the nonlinear behavior of steel girder-to-column connections with particular focus on the effects of column stiffener details. The objective of the research is to gain further knowledge of the connection behavior, and to assess and clarify the need for and the design provisions for column stiffeners, i.e., continuity plates and doubler plates. Both the non-seismic and seismic AISC design provisions particular to those stiffeners are considered. In this work, connection stiffener behavior is studied through three-dimensional finite element analyses using the ABAQUS. This research compliments experimental research that includes nine monotonically-loaded pull plate specimens and five cyclically-loaded cruciform specimens. The failure modes of local flange bending (LFB) and local web yielding (LWY) are studied in detail. All of the test specimens were modeled to corroborate with the experimental work and additional configurations were analyzed to further characterize the connection stiffener behavior. In addition, several new details were investigated that eliminate the need to weld doubler plates along the column k-line. These details include attaching the doubler plate to the column flanges with fillet welds such that the doubler plate remains flush or nearly flush with the column web, and a box detail in which two doubler plates are welded to the column flanges located 1/3 to 2/3 of the distance between the web and the girder flange tip from the column web using complete joint penetration welds. The box detail doubler plates also serve as continuity plates.

The finite element analyses revealed that current design provisions regarding local flange bending and local web yielding, which were based on test results of small sections, are reasonably conservative and are also generally applicable to larger sections (W14). Continuity plates may not be needed in connections with thicker column flanges, and fillet welded continuity plates equal to half of the girder flange thickness performed satisfactorily. The size of the continuity plate clip near the column fillet was also found to have little effect on the connection or stiffener behavior. The study of the box detail showed that the box detail is effective both as a continuity plate and as a doubler plate, and a parametric study was completed to determine the optimal location of the box detail doubler plates. The computational studies, combined with the experimental research, aim to provide a better understanding of the welded steel moment connection behavior and advance safe and economical stiffener design.

Acknowledgments

The authors would like to thank Dr. Theodore V. Galambos, Paul M. Bergson, Lawrence A. Kloiber, and Angela M. Kingsley for their assistance with this research. This research was sponsored by the American Institute of Steel Construction and the Department of Civil Engineering at the University of Minnesota. Supercomputing resources were provided by the Minnesota Supercomputing Institute. This support is gratefully acknowledged.

Any opinions, findings, and conclusions or recommendations expressed in this material are those of the author and do not necessarily reflect the views of the sponsors.

Table of Contents

Appendix

List of Tables

List of Figures

Chapter 1

Introduction

After the 1994 Northridge earthquake, a large number of steel buildings with welded steel moment resisting frames (WSMF) were found to have fractures in the girder–to–column connection region. Although there were no collapses due to this kind of failure, the widespread nature of the connection failures caused concern among engineers. Welded steel moment resisting frames are commonly used and are considered one of the most effective structural systems for lateral resistance. The girder-to-column connections are expected to sustain a high percentage of their design strength while undergoing plastic deformation.

After the Northridge earthquake, a wide range of research investigations were undertaken to study the cause of the damage and to provide design guidelines for new and existing buildings. The fractures were caused primarily by weld filler metal with very low Charpy V-Notch (CVN) toughness combined with poor detailing, including leaving a backing bar in place, creating a notch and defects at the weld root (FEMA, 1995a). However, even though there is no evidence that column stiffening details had any effect on these fractures, there has been a tendency to overdesign the connection stiffening details, such as requiring thicker column transverse stiffeners (continuity plates), doubler plates, and stiffener welds than are necessary. The overdesign does not necessarily insure better connection behavior and in fact may contribute to cracking during fabrication in some cases due to restraint and associated high residual stress. Fabrication cost also increases with overspecified details (Carter, 1999).

Current design provisions regarding connection stiffeners have undergone several revisions since the earthquake. However, the present provisions are largely based on experiments conducted in the 1960's and the 1970's (Graham et al., 1960; Krawinkler et al., 1971; Bertero et al., 1973). Since the Northridge earthquake, additional research has been conducted to assess these design provisions and recommend new guidelines (FEMA, 1995; FEMA, 1997; AISC, 1997; AISC, 1999; FEMA, 2000a). Recent studies have shown that, for example, the continuity plate thickness may be less than the full thickness of the girder flange and the panel zone deformation should be controlled to achieve better overall connection behavior (El-Tawil et al., 1998; Ricles et al., 2000; FEMA, 2000a). Furthermore, it was observed that the welds connecting stiffeners to the connections have a strong influence on weld residual stress, which can contribute to cracking during fabrication (e.g., Yee et al., 1998). To complement these ongoing research efforts, further research is needed to evaluate existing AISC non-seismic and seismic design recommendations for continuity plate and doubler plate detailing.

1.1 Objective and Scope of Research

The objective of the current research is focused on the behavior of steel moment frame connections with various stiffener detailing for the column transverse stiffeners and web doubler plates. The results from this research will provide further understanding of steel moment frame connection behavior as well as advance safe and economical stiffener detailing.

The scope of the complete project included the following components:

- Literature review:

  A literature review was conducted on previous research on the development of AISC connection stiffener design criteria. This included documentation of all available test data and analytical studies of the connection stiffeners.

- Experimental research:

  1. Nine pull plate tests were conducted to investigate the behavior of column transverse stiffeners. The focus was on the study of the non-seismic design provisions regarding the local flange bending (LFB) and local web yielding

(LWY), including both common and new alternatives for the connection stiffener details.

2. Five full-scale cruciform girder-to-column tests were conducted to investigate the column panel zone behavior, including both the continuity plate and the doubler plate design provisions. The full-scale tests investigated both non-seismic and seismic specifications and new alternatives for the connection stiffener details.

- Computational research:
  1. Finite element modeling of all test specimens
  2. Parametric finite element analyses

This thesis is focused on the computational research. Nonlinear three-dimensional continuum finite element analyses were conducted to study the connection behavior of all the test specimens. The results were used to assist specimen selection, determine instrumentation plans, and establish failure criteria. Additional parametric studies were conducted to evaluate the connection behavior with different connection details and to extrapolate the test results to a wider range of member sizes and details. The main variables included the column and girder sizes, material properties, and alternative stiffener details.

The experimental research is reported in more detail in other companion reports (Prochnow et al., 2000; Cotton et al., 2001). The scope of this research is limited to hot-rolled wide flange shapes used for both the girders and the columns. All materials are A992 or A572/50 steel. Girder and column sizes common to WSMFs are investigated. Both the computational and experimental work will provide valuable information on the girder-to-column connection behavior. This will help to clarify connection stiffener design criteria and recommend new design guidelines where appropriate.

1.2 Organization of Thesis

This thesis includes seven chapters. Chapter 1 is a general introduction to the research objectives and outlines the organization of the thesis. Chapter 2 includes background information related to the research, containing both current design criteria and previous analytical work on moment frame connection behavior. Chapter 3 focuses on the finite element modeling of the test specimens. The geometric models, material models, loading and boundary conditions, element type, as well as mesh refinement issues are presented in this chapter. Chapter 4 and Chapter 5 present computational results of the pull plate specimens and cruciform specimens, respectively. Comparisons to the available test results are also included. Parametric studies of connection stiffener behavior are discussed in Chapter 6. Chapter 7 contains a summary and conclusions.

Chapter 2

Background

2.1 Current Design Provisions for Column Transverse Stiffeners and Doubler Plates

The AISC LRFD Specification (1993) includes non-seismic design provisions pertaining to the design of column continuity plates and doubler plates. In addition, the AISC Seismic Provisions for Structural Steel Buildings (1997) provides seismic provisions for moment frame connection design. The SAC joint venture has also recently provided guidelines that incorporate results of more recent research (FEMA, 2000a). All of these design requirements include the assessment of the following limit states in the connection region:

- Local flange bending (LFB)
- Local web yielding (LWY)
- Local web crippling (LWC)
- Panel zone (PZ) shear yielding

Column stiffeners are required when the connection fails to provide adequate strength according to these limit states. These limit state design provisions are summarized briefly below. Background on these equations is summarized in Dexter et al. (1999).

2.1.1 Local Flange Bending

Local flange bending occurs when the column flanges are subjected to the out-of-plane tensile force transferred by the girder flange. Due to the relatively small out-of-plane bending stiffness in the column flange, the column flange will be subjected to two-way bending both along the width of the column flange and along the length of the column. The extensive localized bending in the column flanges will cause the distortion of the connection region and may contribute to the rupture of the girder flange-to-column flange weld due to excessive plastic strain.

For non-seismic design, AISC (1993) states that a pair of transverse stiffeners extending at least one-half the depth of the web shall be provided adjacent to a concentrated tensile force centrally applied across the flange when the required strength of the flange (R_u) exceeds the nominal resistance of the column flange (ϕR_n), which is governed by the following equation:

$$\phi R_n = \phi 6.25 t_f^{\,2} F_{yf} \qquad \text{(Equation K1-1, 1993) (2.1)}$$

where

ϕ = resistance factor = 0.9

t_f = thickness of the column flange

F_{yf} = minimum specified yield stress of the column flange

In the AISC (1997) seismic provisions, the design equations for continuity plates have been removed due to lack of concesus on appropriate provisions in the wake of the Northridge earthquake. Instead, it is stated that the continuity plates shall be provided to match the tested connection. FEMA (2000a) provides further recommendations regarding continuity plates based on recent research. Two equations are included to determine the need for continuity plates. Transverse continuity plates are required when the column flange thickness is less than the value given by Equations (2.2) and (2.3):

$$t_{cf} < 0.4\sqrt{1.8 b_f t_f F_{yb} / F_{yc}} \qquad (2.2)$$

$$t_{cf} < b_f / 6 \qquad (2.3)$$

where:

t_{cf} = minimum required thickness of column flange when no continuity plates are provided

b_f = beam flange width

t_f = beam flange thickness

F_{yb} = minimum specified yield stress of the girder flange

F_{yc} = minimum specified yield stress of the column flange

When continuity plates are required, FEMA (2000a) states that the thickness should be at least one half of the thickness of the beam flange for one-sided connections and should be equal to the thicker of the girder flanges for two-sided connections.

2.1.2 Local Web Yielding

Local web yielding occurs when the column web is unable to resist the tensile or compressive concentrated force applied by the girder flange. The concentrated applied force from the girder flange is assumed to spread to a certain distance along the column web. AISC (1993) states that the strength provided by the web is governed by the following provision:

$$R_u \leq \phi R_n = \phi(5k + N)F_{yw}t_w \quad \text{For interior conditions} \qquad \text{(Equation K1-2, 1993) (2.4)}$$

$$R_u \leq \phi R_n = \phi(2.5k + N)F_{yw}t_w \quad \text{For end conditions} \qquad \text{(Equation K1-3, 1993) (2.5)}$$

where:

ϕ = resistance factor = 1.0

k = distance from outer face of the column flange to the end of the fillet on the column web

N = length of bearing surface

F_{yw} = minimum specified yield stress of the column web

t_w = column web thickness

Either a doubler plate or a pair of transverse stiffeners, extending at least one-half the depth of the web shall be provided when the required force is greater than the strength of the web at the toe of the fillet. In the AISC (1997) seismic design provisions, there is again no specific provision given regarding local web yielding in conjunction with continuity plate use being based on tests. FEMA (2000a) makes no specific reference to local web yielding.

2.1.3 Local Web Crippling

When the column web is subjected to a compressive force applied by the compressive girder flange, AISC (1993) indicates that the web crippling provision shall be checked. Either transverse stiffeners or a doubler plate is necessary when the required force exceeds the nominal strength. Recent studies on the full range of girder/column combinations showed that local web crippling never controls the connection stiffer requirement (Dexter et al.,1999). Thus, this research did not specifically consider local web crippling design criteria.

2.1.4 Panel Zone Provisions

For panel zone shear yielding, either a doubler plate or diagonal stiffeners shall be used when the required strength exceeds the resistance strength of the panel zone. In the AISC (1993) provisions, the nominal strength is determined from the following equations for low column axial load:

(a). When the effect of panel zone deformation on frame stability is not considered

$$R_v = 0.60 F_y d_c t_w \qquad \text{(Equation K1-9, 1993) (2.6)}$$

(b). When frame stability and plastic panel zone deformation are considered

$$\phi R_v = \phi 0.6 F_{yc} d_c t_p \left(1 + \frac{3 b_{cf} t_{cf}^2}{d_g d_c t_p} \right) \qquad \text{(Equation K1-11, 1993) (2.7)}$$

where:

ϕ = resistance factor = 0.9

R_v= nominal panel zone shear strength

b_{cf} = column flange width

d_c = column depth

d_g = girder depth

t_p = panel zone thickness

A reduction in strength is taken in the presence of high column axial load.

In the AISC (1997) seismic provisions, the same equation as Equation (2.7) is used to check the panel zone strength. However, the ϕ factor is changed to 1.0. In addition, a check on the panel zone slenderness is required:

$$t \geq \left(d_z + w_z\right)/90 \qquad \text{(Equation 9-2, 1997) (2.8)}$$

where:

t = column web or doubler plate thickness, or total thickness if doubler plates are plug welded

d_z = panel zone depth

w_z = panel zone width

The intent of Equation (2.8) is to avoid a thin panel zone from buckling at larger inelastic deformations, which may cause loss of shear capacity as the buckling occurs.

FEMA (2000a) specifies that the panel zone strength shall be based on a balance of shear yielding of the panel zone and flexural yielding of the girder. That is, better connection behavior is achieved when the flexural strength of the girder and the shear strength of the panel zone are reached approximately at the same time (Roeder, 2000). The required panel zone thickness is determined from this balanced yielding criteria:

$$t = \frac{M_{yg} \dfrac{h - d_g}{h}}{(0.9)0.55 F_{yc} d_c (d_b - t_{gb})} \qquad (2.9)$$

$$M_{yg} = F_{yg} S_g \qquad (2.10)$$

where:

F_{yg} = minimum specified yield stress of the girder

S_g = elastic section modulus of the girder

h =story height defined as the distance between girder centerlines of adjacent stories.

When the thickness of the column web is less than the required thickness calculated form Equation (2.9), doubler plates are required. Alternatively, the panel zone strength shall be designed to match the tested connection.

2.1.5 Required Design Strength

The connection stiffeners are designed based on the difference between the required strength and the nominal strength. The required strength for the connection is based on the material properties of the girder flange. For the non-seismic provisions, the strength is generally based on nominal yield strength of the girder flange (AISC, 1993). The required strength demand for checking continuity plate requirements, R_u, is then calculated as:

$$R_u = F_{yg} A_{gf} \tag{2.11}$$

where:

A_{gf} = girder flange area

For FEMA (2000a), the required strength demand is calculated as:

$$R_u = 1.8 F_{yg} A_{gf} \tag{2.12a}$$

The 1.8 factor included in the seismic equations accounts for the strain hardening properties of the steel (FEMA, 2000a). For seismic design, it is expected that a certain amount of plastic deformation is needed to dissipate energy, thus avoiding brittle failure. Plastic hinging is expected to occur outside the critical connection region. By using these factors, the seismic design provisions put a higher strength requirement on the column than for non-seismic provisions. However, girder flanges seldom actually reach the strength as specified in Equation (2.12a). To provide a more realistic assessment of the probable required strength while still considering both the effects of overstrength and strain hardening of the steel, an equation for the required strength that stems from the criterion for checking strong column-weak beam compliance (AISC, 1997) is often used in this study for corroborating the experimental research and conducting parametric studies:

$$R_u = 1.1 R_y F_{yg} A_{gf} \tag{2.12b}$$

where:

R_y = 1.1 for rolled shapes made from A572/50, A992, A572/65 or A913 steel

In the AISC (1997) design provisions, the required strength, R_u, for checking the panel zone is calculated from the load combination or alternatively determined from the moment capacity of the girder using equilibrium in the panel zone. One possibility for this calculation would be based on using a girder strength similar to that used in the strong column-weak beam check of AISC (1997):

$$R_u = 1.0\sum \frac{1.1 R_y M_p}{d_g} - V_c \tag{2.13}$$

where:

M_p= plastic moment of the girder

V_c = column shear

In the FEMA (2000a) design guidelines, the required strength of the panel zone is based on the concept of the balanced yielding of the panel zone and the girder. The required strength is determined from the moment capacity of the girder (Equation 2.9).

2.1.6 Strong Column Weak Beam (SCWB) Requirement

Steel frames are designed to undergo controlled plastic deformation in certain areas under seismic loading. Plastic hinges are expected to form outside the connection region in the girder rather than in the column. The SCWB design requirements specified in the current AISC (1997) Seismic Provisions for Special Moment Frame (SMF) and Intermediate Moment Frame (IMF) structures are intended to help ensure good ductile behavior. According to these provisions, the moment ratio between the column and the girder shall satisfy the following equations:

$$\frac{\sum_{column} M_{pc}^{*}}{\sum_{girder} M_{pg}^{*}} > 1.0 \tag{2.14}$$

$$\sum_{column} M_{pc}^{*} = \sum_{column} Z_c \left(F_{yc} - \frac{P_{uc}}{A_g} \right) \tag{2.15}$$

$$\sum_{girder} M_{pg}^{*} = \sum_{girder} (1.1 R_y M_p + M_v) \tag{2.16}$$

where:

M_{pc}^{*} = column moment above or below joint

M_{pg}^{*} = expected girder flexural strength at the intersection of the girder and column centerlines

Z_c = plastic section modulus of the column

P_{uc}/A_g = required axial stress of column

M_p = nominal plastic moment of the girder

M_v = additional moment due to shear amplification

In addition to this check, FEMA (2000b) recommended another similar equation for the welded flange-welded web connection to limit column yielding caused by an increased girder bending moment due to strain hardening:

$$\frac{\sum Z_c (F_{yc} - \frac{P_{uc}}{A_g})}{\sum Z_g \frac{F_{yg} + F_{tg}}{2}} > 1.1 \qquad (2.17)$$

where:

Z_g = plastic section modulus of the girder

F_{tg} = tensile strength of girder

2.2 Related Computational Research on WSMF Connection Behavior

Past studies of the performance of girder-to-column connections include both experimental and analytical work. An overview of recent research shows that analytical work has played an important role in the research findings. Following is a brief summary of some recent analytical studies on connection stiffeners, particularly focused on past finite element analysis research. Dexter et al. (1999) contains a more detailed literature review on both the experimental and analytical research on connection stiffener design.

- **Lee, Goel, and Stojadinovic (1997)**

This study conducted at the University of Michigan showed that the restraint near the column-to-girder interface in welded steel moment connections may lead to low cycle fatigue failures of these connections. The finite element studies focused on the stress flow in the girder web and flanges in the vicinity of the connection region. Models using shell elements (4–node linear shell elements) as well as models using solid elements (8–node linear solid elements) were analyzed using the ABAQUS program. The two models showed similar stress and strain distribution patterns. However it was noted that for thicker flanges, a single layer of shell elements cannot adequately represent the stress and strain pattern through the flange thickness. The analyses using solid elements showed higher stress concentrations near the girder flange welds.

Extensive finite element analyses showed that, due to the restraint of the Poisson effect and restraint of warping due to shear deformation in the girder-to-column connection region, the stress in the girder flange is much higher near the connection region than the result obtained from beam theory. A "truss analogy" was proposed as a simple and realistic method to represent the load path in the moment connection region. As an alternative connection detail, a free flange design method was proposed. The free flange configurations relieve the constraints at the girder-to-column interface. Tests and parametric studies indicated that the free flange connection detail met the rotational capacity requirement and exhibited good ductile performance. However, excessive panel zone deformation still should be controlled to ensure satisfactory behavior of this free flange connection.

- **Leon, Hajjar, and Gustafson (1998) and Hajjar, Leon, Gustafson, and Shield (1998)**

Experimental research and corroborating three-dimensional nonlinear finite element analyses using the ABAQUS program were undertaken to investigate the failure of steel moment frame connections during the Northridge earthquake with a focus on the effect of the composite floor slabs. For the analyses, one half of the specimen was modeled by applying boundary conditions at the plane of symmetry. The girder shear tabs, doubler plates, continuity plates, welds, concrete, and a part of the column section were modeled with 8-node solid elements with incompatible models (ABAQUS element C3D8I). The column section starting at 22.5 inches away from the girder flange was modeled with two-node cubic beam elements (ABAQUS element B33). Multipoint constraints (MPC) were applied to enforce the compatibility between two types of elements. REBAR elements were used to model slab reinforcement. Contact elements (slide line) were used to model the interface between the concrete slab and steel girder. The doubler plate was fused to column web, and continuity plates were fused to the doubler plate and column flanges. The shear tab was assumed to be fully attached to the girder web.

The results from the study show that the presence of composite floor slabs increases the strain in the bottom flange region, which may increase the potential for fracture. A recommendation was made to consider the asymmetric behavior in the connection due to the composite floor slab in design.

- **El-Tawil, Mikesell, Vidareson, and Kunnath (1998)**

Detailed three-dimensional nonlinear finite element analyses of connection subassemblages were performed using ABAQUS to study the inelastic behavior of pre-Northridge fully restrained welded-bolted connections. The computational model was based on Berkeley specimen PN3, which is considered to represent the typical connection practices used before the Northridge earthquake. First-order solid elements and shell elements both with reduced integration were used in the analyses. The intersection between the beam bottom flange and the column was composed of brick elements (ABAQUS element C3D8R). The remaining part of the subassemblage was modeled by 4-node shell elements (ABAQUS element S4R5) to reduce the computational expense. Multipoint constraints were used to enforce compatibility between different types of elements. Both geometric nonlinearity and material nonlinearity were accounted for. The parametric studies included geometric details such as the access hole geometry, presence/absence of the continuity plate, thickness of the continuity plate and column flange, girder depth, and panel zone thickness. The material parameters included the yield-to-ultimate stress ratio. A series of parametric studies yielded the following results: Steel with a high yield-to-ultimate stress ratio (0.95) can result in a large reduction in the plastic hinge length of the beam, which leads to earlier local buckling; the potential for ductile fracture at the root of the access hole is higher with a larger size of access hole; the 0.8 factor used in the panel zone strength equation (AISC 1997) need to be modified for one-sided connections and requiring continuity plates in all connections was justified by finite element analyses. However, analyses showed that continuity plates with 60% of the required thickness performed satisfactorily for one-sided connection.

- **Yee, Paterson, and Egan (1998)**

Finite element simulation using ABAQUS was performed to evaluate continuity plate details. Both continuity plate details (clipped corners and coped corners) and weld types (CJP and fillet welds) were modeled. One quarter of the connection section using eight-node solid elements was modeled with symmetrical boundary constraints applied at all symmetrical planes. Only the continuity plate-to-web weld was modeled. Heat transfer due to welding was modeled and was nonlinear and time dependent. Free convection boundary conditions were assumed for all exposed surfaces. The material properties of all components were temperature-dependent based on A572/50 steel.

The evaluation of the local restraint effect (due to welding and geometry detail) in the continuity plate-to-column web interface showed that the weld type and continuity plate detail design greatly affected the restraint stress. The highest stress (a principal stress of approximately 93 ksi) occurred when larger CJP weld and clip details were used. They concluded that potential cracking during fabrication may be caused by low toughness and high strength in the column k-area and excessive weld restraint stress from a large weld volume.

- **Deierlein and Chi (1999)**

This research investigated the fracture behavior of welded girder-to-column connections and various design and detailing parameters' influence on fracture resistance. Both pull plate tests and connection subassembly tests were modeled using the ABAQUS program. Two-dimensional analyses used 8-node quadrilateral and 6-node triangular elements, while the three-dimensional model consisted of 20-node brick elements with 8-point integration. Two-dimensional elements assumed in-plane stress except at the crack tip, where plain strain elements were used to simulate high constraints. The mesh convergence study around the crack tip was based on the accuracy of the evaluation of the J-integral. Residual stresses were simulated by thermo-mechanical and eigenstrain modeling techniques. The material models used in the analyses were based on the nominal stress-strain properties of A572/50 documented by Frank (1999) and the weld metals were based on test results reported in Johnson et al. (FEMA, 2000c).

The study showed that the continuity plates effectively reduced the crack tip opening displacement (CTOD) demands for a postulated weld root crack on the bottom flange and have a greater effect on connections with a relatively weak panel zone. Column flange thickness directly affects CTOD demands at a weld root crack. The fracture toughness demand in the welds is larger for column with thinner flanges. CTOD demands are smallest where inelastic panel zone deformations are minimized. The CTOD fracture toughness demands are also influenced by flaw size and location. Panel zone deformation has the largest influence on the toughness demand for the required moment and inelastic rotation demand. Welding induced residual stress also seems to be most significant for elastic behavior at low stress levels. Comparison of analyses of girder-to-column connections and pull plate specimens confirmed that pull plate tests provide an effective check on the through thickness strength of column flanges and the fracture resistance of groove welds.

- **Dexter and Melendrez (1999)**

More than forty pull plate tests were performed to determine strength, deformation and fracture behavior of the wide-flange column section, especially in the through-thickness direction. Three-dimensional finite element analyses were performed to simulate the test results. By using symmetry, only one-eighth of the T-joint specimen was used. Twenty-node quadratic solid brick elements with reduced integration (ABAQUS element C3020R) were used to achieve accuracy. The model consisted of a pull plate, pull plate-to-column weld, column section, and continuity plate. Stress and strain properties were input as a piecewise-linear curve. Residual stresses were not modeled. A displacement controlled loading history was applied at the pull-plate. The limit load, stress distribution, and behavior of the column flange under triaxial constraint were well predicted in the analyses.

The results from both the laboratory tests and finite element analyses suggest that the through-thickness strength of columns is greater than the longitudinal strength when constrained. The through-thickness failure of column sections is unlikely in moment frames with similar T-joint welds and need not be explicitly checked in design.

- **Roeder (1997, 2000; FEMA, 2000b)**

Analyses were performed on two buildings that experienced column cracking during the Northridge earthquake. Plane frame analyses were performed to study the relative stiffness of various components. Three-dimensional models were used to examine the full static and dynamic response. Local finite element analyses of the connection area were also conducted to study the panel zone yielding and cracking potential. Shell elements were used in the local analyses to model the beam, column, continuity plates, and panel zone region. The local analyses showed that high tensile stress in the girder flange center was caused by the larger stiffness of the column web in the welded connection. The girder flange-to-column flange interface was susceptible to hydrostatic tensile stress and cracking. Panel zone yielding caused sharp curvature of the girder and column flanges, which also contributed to the stress and strain concentration.

Observations from the failures in the actual buildings were compared to the past experiments and finite element case study. The change in structural system design and welding processes helped to explain the causes of the fracture. Larger girder depths and high panel zone inelastic deformations tend to decrease connection ductility. In addition, modern automatic feed processes with a larger volume of weld metal placed per unit time may lead to connections that are more sensitive to cracking due to internal flaws.

From comparisons of recent SAC tests and analytical studies on panel zone behavior, the author pointed out that the primary yield mechanism in welded flange connections consists of flexural yielding of the girder and panel zone shear yielding. A balanced design in which girder flexural yielding and panel zone shear yielding are reached at approximately the same time was recommended for connections to achieve greatest ductility. Similar studies on continuity plate behavior showed that in some cases, the connection can perform satisfactorily without continuity plates. It was noted that the requirement of sizing the continuity plate thickness equal to the girder flange thickness may be relaxed, but more research is needed to provide further evaluation of the design guidelines.

- **Ricles, Mao, Lu, and Fisher (2000)**

Extensive experimental and analytical studies have been carried out at Lehigh University on the behavior of welded unreinforced flange moment connections since Northridge earthquake. Recent research includes cyclic tests of nine full-scale connection specimens and fifteen pull-plate tests. Analytical work includes three-dimensional nonlinear finite element analyses of all the specimens as well as a parametric study to gain further understanding of the connection behavior.

The finite element analyses were conducted using the ABAQUS program. Eight-node brick elements with standard integration were used in the connection region and three-dimensional beam elements were used outside the connection region where the members remained elastic. Sub-modeling techniques were used in regions where a finer mesh and close examination of the local behavior was needed. Models with applied monotonic increasing static loads and models with cyclic variable amplitude loads were both analyzed.

The parametric study included the following key variables: (1) weld access hole size and geometry; (2) panel zone capacity; (3) girder web-to-column flange attachment detail and; (4) continuity plate thickness. The results from the analyses showed that the access hole size and geometry affect the plastic strain in the access hole region. An access hole configuration was recommended for all the test specimens based on the analysis results that will minimize the plastic strain. The authors suggested that the panel zone strength be designed based only on the column web strength and neglect the post-yield strength, thus limiting the panel zone deformation to less than 50% of the total plastic rotation. The analyses on continuity plates indicated that the ratio of the girder flange width to the column flange thickness ($b_{f,bm}/t_{c,f}$) could be used in sizing continuity plates. Furthermore, it was suggested to use full penetration groove welds at the girder web-column interface with supplemental fillet welds around the shear tab edges. This attachment detail was shown to inhibit web local buckling and reduce the strain demand at the girder tensile flange access hole region.

Chapter 3

Finite Element Model Development

As a part of this research program, finite element analyses were conducted to study the connection behavior. The analyses included models of all the specimens tested in this research, as well as appropriate parametric studies. For these analyses, the model geometry, material properties, boundary conditions, and loading history reflected the actual experimental configurations. Some simplifications were made in the finite element model so as to achieve computational efficiency. The results from the finite element analyses were compared with those from the experiments. In addition, a parametric study was undertaken to predict connection behavior beyond the range of what was covered in the tests. The analysis program used was ABAQUS, version 5.8-1 (HKS, 1994).

3.1 Pull Plate Experiments

3.1.1 Geometry Model

The pull-plate specimens consisted of a column stub, two pull-plates, and column stiffeners (Prochnow et al., 2000). The pull plate was used to simulate the bottom girder flange subjected to tension. The parameters which varied between the specimens included the size of the column stubs, the existence and size of stiffeners, and the stiffener weld details (Table 3.1). One–quarter of each specimen was used in the finite element model. There are two planes of symmetry: a horizontal plane passing through the mid-height of the column web and a vertical plane passing through the mid-plane of the column web

(Figure 3.1). A small restrictor plate was attached to the pull plate in the specimens, simulating an access hole. This was not modeled in the finite element analysis.

The fillet region in the W sections helps to reduce the stress raiser near the intersection of the column flange and web. However, the exact geometry dimensions of the fillet regions vary from different rolling processes. In the analyses, the fillet region was modeled implicitly by adding triangular elements in the column flange and web intersection region, thus avoiding the sharp corner effect.

The weld models used in the analyses were based on the geometry of the actual specimens. The complete joint penetration (CJP) weld connecting the pull plate to the column flange, the fillet weld and CJP welds connecting the continuity plates to the column web and column flanges, and the fillet and CJP welds connecting the doubler plates to the column flanges were modeled explicitly according to the test specimens. A typical unstiffened pull plate model consisted of 4725 nodes and 3273 elements. A finite element model with a doubler plate consisted of 6898 nodes and 4721 elements. Figure 3.2 to Figure 3.4 show the typical pull plate models.

3.1.2 Element Type and Finite Element Meshing

The element type chosen throughout all the models was an 8-node solid element (ABAQUS element C3D8). The displacement field includes three components for each node.

Gap elements were used when modeling the components connected by a fillet weld (e.g., the fillet welds connecting the continuity plate to the column web) as seen in Figure 3.5. The two base metals were fused only through the fillet weld region. The two surfaces of the base metal were not fused, thus allowing the two members to deform separately. The gap element allows separation of two nodes but prevents the two nodes to which it is attached from penetrating each other. Friction was not modeled in these regions.

3.1.3 Loading and Boundary Conditions

To ensure that the symmetrical conditions were satisfied in the one-quarter model, out-of-plane displacement restraints were applied at all nodes that lay in the plane of symmetry. The other two degrees-of-freedom were free. Uniform vertical displacements were applied at all nodes on the top surface of the pull plate to model the displacements applied by the testing machine in the experiments. Monotonic loading histories were modeled through the use of load steps and increments (Table 3.2). To obtain enough points corresponding to stress and strain history data, the applied displacements were divided into several steps and each step was further divided into several increments and iterations based on the convergence rate of the numerical solution. The end displacement values were monitored during each step to insure the desired displacements were achieved. The corresponding load levels were later back calculated from the stress results at the end of the pull plates.

For the pull plate model, there were no physical constraints in the X direction (direction "1" in Figure 3.2) along the column stub in the experiments. However, for the pull plate models, additional restraints in the X direction were applied at three nodes through column web thickness in the center of the column stub to stabilize the mesh. Both models with and without the additional X restraints were run for comparison. The results were identical for the two cases.

Typically four layers of elements were used through the thickness of the pull plate, the column web, and the continuity plate; three layers of elements were used through the column flange thickness; seventeen elements were used along the half width of the column flange; and eleven elements were used along the half depth of the column web.

As local flange bending and local web yielding are localized phenomena, high stress and strain are expected to occur near the center of the pull plate, column flange, and column web. Smaller elements were used near the area of the pull plate/column flange intersection region. To reduce the computational expense, larger elements were used towards the end of the pull plate and the column stub where the stress and strain gradients were small.

A mesh refinement study was conducted on an unstiffened specimen with a two-foot column stub length, refining the mesh everywhere where high stress and strain gradients were observed. The original unstiffened pull plate model consisted of 3272 elements and 4725 nodes. The refined mesh consisted of 5758 elements and 8789 nodes. The displacement, stress, and strain results were compared at several locations of interest, indicating the coarser mesh to be sufficient for these studies. The results of the mesh refinement are presented in Appendix A.

3.1.4 Material Models

The mechanical properties of the base metal and weld metal are discussed in this section. Both results from coupon tests and from other studies were considered. Simplified piecewise linear stress-strain curves were used as input data for the finite element analyses.

3.1.4.1 Stress–Strain Properties of A992 Steel for Structural Shapes

Frank (1999) documented the stress-strain behavior of structural steels. The variability of standard strength parameters such as the yield and tensile strength were reported. The base metal properties used in the finite element analyses were based on the results from Frank (1999), as well as on coupon test results of the pull plate specimens.

Figure 3.6 shows the schematic stress-strain properties measured during the tensile tests in Frank (1999). The full stress-strain curves were measured as much as possible. The static yield strength (F_{sy}) was obtained by stopping the loading of the test specimen during the tests and measuring the load after holding the deformation for at least three minutes. The dynamic yield strength (F_y) was the value measured on the yield plateau. In the figure, E is Young's modulus; F_{uy} is the upper yield point; E_{sh} is the strain-hardening modulus; ε_{sh} is the strain at strain-hardening initiation; F_u is the ultimate tensile strength; and ε_u is the strain at the ultimate tensile strength.

For hot-rolled sections, the webs normally have 4% to 7% higher yield strengths than the flanges. Both coupons from the web and flange in the rolled sections were taken by Frank (1999). For A992 steel, the web yield strength was about 5% greater than the flange yield strength. For A993 QST steel, the web properties were not signifcantly different than the flange properties. Figure 3.7 shows the stress-strain curves for the A992 steel used in the parametric study based on Frank's research. The curve was defined by the nominal yield strength F_{yn} (e.g., 50 ksi for A992 steel) and by the nominal yield strain $\varepsilon_{yn}=F_{yn}/E$, where E is Young's modulus, which was taken as 29,000 ksi for all analyses. The plateau strength was shown by Frank (1999) to be 9% higher than the nominal yield strength F_{yn}. The ultimate strength F_u was shown to be 45% higher than F_{yn}. These values were used in the parametric studies. In contrast, for the analyses corroborating the pull plate specimens, the actual mill report data was used for F_y and F_u, as reported in Table 3.3 for points 1, 2, and 3 in Figure 3.7.

3.1.4.2 Stress–Strain Data Used in Finite Element Model

The material properties used as ABAQUS input were defined as piecewise linear curves based upon the shape shown in Figure 3.7. Isotropic hardening and the Von Mises yield criteria were used. This uniaxial test engineering stress-strain data (σ_{nom}, ε_{nom}) from Figure 3.7 and Table 3.3 was converted to true stress-log plastic strain (σ_{true}, ε_{ln}^{pl}), as required for ABAQUS, using the following equation:

$$\sigma_{true} = \sigma_{nom} * (1 + \varepsilon_{nom}) \tag{3.1}$$

$$\varepsilon_{\ln}^{pl} = \ln(1 + \varepsilon_{nom}) - \frac{\sigma_{true}}{E} \tag{3.2}$$

Due to the greater hot working in the column web of the rolled section, the yield strength in the web is usually somewhat higher than the flanges. In addition, the material properties of the k-line region are different from other locations because of the roller straightening procedure during fabrication. The k-line region usually has a higher hardness, higher yield and tensile strength, and lower toughness (Frank, 1999). No obvious yield plateau is observed as in other locations. The standard pull plate models included a different material model for the column web compared to that of the flange. The yield strength and the ultimate strength were increased 5 ksi in the column web (other than elements near the k-line). For the elements in the k-line region, in addition to the 5 ksi increase of the ultimate strength, the yield strength was increased to 95% of the ultimate strength and no yield plateau was used. In Chapter 4, the analysis results using separate web and k-line properties are used throughout. Analyses using the same mill report properties throughout the cross section are also included in specific cases for comparison.

3.1.4.3 Stress-Strain Properties of Weld Metal

Past research on weld metals has shown that there is a much higher variability of the weld metal properties than that of base metals. The properties are mainly affected by the chemical composition of the weld metal and the cooling rate after welding (FEMA, 2000c). For E70 weld metals, a typical yield strength ranges from 70-75 ksi; the ultimate strength varies from 80-90 ksi. Table 3.3 shows the weld metal model used in the finite element analysis.

For the finite element analyses input data, the yield strength of the weld metal was taken as F_y=75 ksi. The ultimate tensile strength was taken as 80 ksi corresponding to 4% strain. The elastic modulus E was taken as 29000 ksi. Possion's ratio ν was taken as 0.3. The stress-strain curve was similar to that used for the base metal, except that a shorter yield plateau and more gradual strain-hardening progression were used for the weld metal. It is noted that the weld properties are highly dependent on the welding procedure used.

3.1.5 Analysis Type

Static nonlinear analyses were carried out to study the pull plate specimen behavior. The analysis accounted for both material and geometry nonlinearity. Large deflections and small strains were assumed. The analyses in this research did not model residual stresses, thermal effects, or fracture.

3.2 Cruciform Experiments

3.2.1 Geometry Model

The cruciform experiments each consisted of a column with two girders attached at the mid-height of the column (Cotton et al., 2001). The column was supported by a pin at its top and bottom. Two actuators were located at each girder tip, 140 inches away from the column centerline. A cyclic displacement loading history was applied at the girder tip. Five cruciform specimens were tested with different column sizes and connection details. Table 3.4 outlines the details of the specimens. The P_z, P_g and P_c values are the girder end load required to reach the nominal strength of the panel zone, girder, and column respectively (see Appendix D). To minimize the number of variables included, only one girder size was chosen (W24x94). Figure 3.8 shows the typical test set up.

To reduce the computational cost, only one-half of each test specimen was modeled by using symmetry. The symmetrical plane lay in the mid-plane of the column and girder webs. The shear tab was modeled as two-sided with half of its thickness on each side of girder web, while in the actual test the shear tab was one-sided. For specimen CR2, only a one-sided doubler plate was used to allow the instrumentation of the column web, but in the finite element model, it was treated as two-sided with half of its thickness on each side to simplify the finite element model.

The connection details of the finite element models reflected the test set-up. The girder flange-to-column flange CJP weld, the continuity plate-to-doubler plate welds, the continuity plate-to-column flange welds, the doubler plate-to-column flange welds, and the girder web-to-column web welds were modeled explicitly. The welds connecting the doubler plates to the column flanges were modeled by fusing the doubler plates through the welds along the edges of the doubler plates. The shear tab was fused to the girder web. The access hole was modeled according to the dimensions used in the specimen. The column fillet regions were modeled implicitly by adding a triangular element between the flange and web.

In the experiments, the doubler plates were attached to the column web and flanges by welds only at the four edges (or two edges for the box detail, specimen CR4). To account for the fact that the two surfaces at the interface of the doubler plate and column web may separate during deformation, the doubler plate and column web were fused only along the welds in the finite element model. The remaining parts were allowed to deform separately. Ideally, gap or contact elements should be used between two surfaces so as to allow pressure and friction forces to develop when the two surfaces come in contact. However, the analyses showed that the overlap of nodes at the interface did occur at high inelastic deformation, but the magnitude was very small (less than 0.005 inch). Thus, contact elements were not used in the current models. It is recognized that this modeling might reduce the out-of-plane stiffness of the web and doubler plate at high inelastic deformation because fewer kinematic restraints were applied to doubler plates.

3.2.2 Element Type and Finite Element Meshing

The cruciform models consisted of eight-node solid linear elements (ABAQUS elements C3D8 and C3D8R) and two-node linear beam elements (ABAQUS element B21). Three-dimensional solid elements were used in the connection region and 60 inches (approximately 2.5 times the girder depth) from the column face in the girder and 28 inches (approximately 2 times the column depth) above and below the girder face in the column. For the solid continuum element, the displacement field includes three translational components for each node. The stress and strain includes three normal and three shear components for each Gauss point. The two-node beam elements were used in the remaining region where the members remained elastic to reduce the computational expense. The beam element section properties were defined as rectangular cross sections with equivalent cross section properties to that of the W shapes. Half of the experimental member cross sectional area and moment of inertia were given to the beam element because of the half symmetry used in the finite element model. Five gauss points were used along the height of the section. For the beam elements, the displacement field includes translational and rotational components; the stress and strain has axial and transverse shear components at each Gauss point, with stress-resultants computed through integration. The beam elements are based on Timoshenko beam theory and include the transverse shear deformation. The shear transformation is treated as linear elastic, independent of axial and bending response. Multipoint constraints (MPC) were applied at the interface of the solid and beam elements to obtain compatibility. Figure 3.9 shows a typical cruciform model.

Eight-node solid elements with full integration (C3D8) were used for the column web and the doubler plates and reduced integration elements (C3D8R) were used for the remaining solid elements. It was noted that when reduced integration elements were used in the doubler plates, singular modes occurred in the highly inelastic range. (e.g., strain along a horizontal line in the doubler plate oscillated when higher strain occurred.) This is related to the modeling methods used for the doubler plate as discussed earlier. For the regions in the panel zone, where the primary stress is shear stress, the full integration elements used in those regions performed well without over stiffening the elements.

The finite element meshing for the cruciform specimens was similar to that of the pull plate specimens. Four layers of solid elements were used through the thickness of the girder flange, the girder web, and the column web. Three layers of solid elements were used through the thickness of the column flanges. Smaller elements were used near the connection region where higher stress and strain gradients were expected and larger elements were used towards the end of the column and the girder where stress and strain gradients were not sensitive to finite element mesh. A typical finite element model for the cruciform specimen consisted of 24310 elements and 88342 nodes. Shown in Figure 3.9 to Figure 3.11 are details of the finite element meshes for the cruciform models.

To examine the finite element meshing, mesh refinement studies were done on the cruciform specimen model. Based on the mesh studies for the pull plate models, only localized mesh refinement was done for the cruciform models. The location chosen was based on the stress and strain distribution pattern in the connection region. Mesh refinement was focused on the area near the girder flange to column flange welds and near the girder web access hole region, where higher stress and strain gradients were expected to occur. The final mesh was determined when the analyses in those regions were converged. The results of the mesh refinement study are presented in Appendix B.

3.2.3 Loading and Boundary Conditions

The boundary conditions represented the constraints used in the test set-up. The column was pinned at the bottom and roller supported at the top with vertical translation permitted. The end constraints at the column allowed the column to have in-plane rotation at both ends and vertical deflection at the top end. Out-of-plane degrees-of-freedom were restrained for the nodes lying in the symmetrical plane. The multipoint constraints applied at the interface of the beam/solid elements ensured that initially plane sections at the interface remained plane after deformation.

A displacement-controlled loading history was applied at the tip of each girder in opposite directions for the two girders. Due to the consideration of computational expense, the quasi-static cyclic loading history used in the tests was not modeled. Instead, a monotonically increasing loading history was used as shown in Table 3.5. The maximum displacement at each step was the same as the peak values used in the tests. Displacement was proportionally increased to the maximum values within each step. The applied displacements were divided into several steps and each step was further divided into several increments and iterations based on the convergence rate of the numerical solution. The applied displacement at the girder tip was monitored during the analyses to ensure that the desired displacement was obtained. Column axial load was not considered in the tests and was not modeled in the analysis. The results obtained from this monotonic loading are believed to represent fairly well the envelope of the cyclic response (Leon et al., 1998).

3.2.4 Material Models

Material properties for the cruciform specimens were based on mill reports for the girder, column, and welds. The yield stress and ultimate stress were obtained from the mill report. The shape of stress-strain curves were based of the study of Frank (1999) as discussed in Section 3.2. Table 3.6 shows the detailed material properties used in the analyses.

3.2.5 Analyses Type

Static nonlinear analyses were carried out to study the subassembly connection behavior. The analysis accounted for both material and geometry nonlinearity. Residual stress, thermal effects and fracture were not considered in the analyses.

Table 3.1: Pull Plate Specimens

Specimen	Column	Continuity Plate	Doubler Plate	Non-Seismic $\phi R_n/R_u$	
				LWY	LFB
l-LFB	W14x132	NA	2@0.5’’	0.79	0.80
2-LFB	W14x145	NA	2@0.5’’	0.86	0.89
1-LWY	W14x132	NA	NA	0.79	0.80
2-LWY	W14x145	NA	NA	0.86	0.89
3-UNST	W14x159	NA	NA	1.0	1.06
1-HCP	W14x132	0.5 t_{bf}	NA	0.79	0.80
1-FCP	W14x132	1.0 t_{bf}	NA	0.79	0.80
1-DP	W14x132	NA	2@0.75	0.79	0.80
1B-HCP	W14x132	0.5 t_{bf}	NA	0.79	0.80

Table 3.2: Loading Histories for Pull Plate Specimens

Load Step	Pull Plate End Displacement (in.)	Percent of Total Elongation (%)
1	0.0192	0.1
2	0.0385	0.2
3	0.0962	0.5
4	0.1539	0.8
5	0.1924	1.0
6	0.2886	1.5
7	0.3848	2.0
8	0.481	2.5
9	0.5772	3.0
10	0.962	5.0
11	1.5392	8.0

Table 3.3: Material Model Variables for Pull Plate Specimens

Material Variables	*E* (ksi)	ν	Stress - Strain Curve Data	
			Stress (ksi)	**Plastic Strain**
W14x145 column (A992)	29000	0.3	53	0
			53	0.0133
			70.5	0.1496
W14x132 column (A992)	29000	0.3	57	0
			57	0.0133
			73.5	0.1496
W14x159 column (A992)	29000	0.3	53.5	0
			53.5	0.0133
			72	0.1496
Pull plate, doubler plate (box detail) continuity plate (~t_f) (A572/50)	29000	0.3	52	0
			53	0.0133
			70.5	0.1496
Continuity plate (~0.5 t_f) (A572/50)	29000	0.3	64	0
			64	0.0133
			84	0.1496
Doubler plate (web) (A572/50)	29000	0.3	56	0
			56	0.0133
			73	0.1496
Weld (E70)	29000	0.3	75	0
			75	0.01
			80	0.04

Table 3.4: Cruciform Specimens

Parameter	Specimen				
	CR1	**CR2**	**CR3**	**CR4**	**CR5**
Beam	W24x94	W24x94	W24x94	W24x94	W24x94
Column	W14x283	W14x193	W14x176	W14x176	W14x145
Doubler plate	None	Fillet	Fillet	Box	Fillet
DP thickness	NA	0.625 in.	2@0.5 in.	2@0.75 in.	2@0.625 in.
Continuity	NA	NA	~0.5 t_f	NA	NA
P_z/P_g	1.02(1.1)*	0.93(1.01)	1.05(1.20)	1.31(1.49)	1.04(1.20)
P_c/P_g	2.34	1.54	1.39	1.39	1.13

* number in parenthesis is the value using girder and column mill report data rather than nominal yield stress

Table 3.5: Loading Histories for Cruciform Specimens

Load Step	Experimental Girder End Displacement			FEM Girder End Displacement (in.)
	θ	Number of Cycles	Girder End Displacement Δ_{tip}=140" x θ (in.)	
1	0.00375	6	0.53	0.53
2	0.005	6	0.7	0.7
3	0.0075	6	1.05	1.05
4	0.01	4	1.4	1.4
5	0.015	2	2.1	2.1
6	0.02	2	2.8	2.8
7	0.03	2	4.2	4.2
8	0.04	2	5.6	5.6
9	0.05	2	7.0	7.0

Table 3.6: Material Model Variables for Cruciform Specimens

Material Variables	*E* (ksi)	*ν*	Stress-Strain Curve Data	
			Stress (ksi)	Plastic Strain
W14x145 column (A992)	29000	0.3	57	0
			57	0.0133
			76	0.1469
W14x176 column (A992)	29000	0.3	57	0
			57	0.0133
			75	0.1469
W14x159 column (A992)	29000	0.3	54	0
			54	0.0133
			74	0.1469
W14x283 column (A992)	29000	0.3	54	0
			54	0.0133
			74	0.1469
W24x94 girder (A992)	29000	0.3	50	0
			50	0.0133
			68	0.1469
Doubler plate, continuity plate (A572/50)	29000	0.3	54	0
			54	0.0133
			72	0.1496
Weld (E70)	29000	0.3	75	0
			75	0.01
			80	0.04

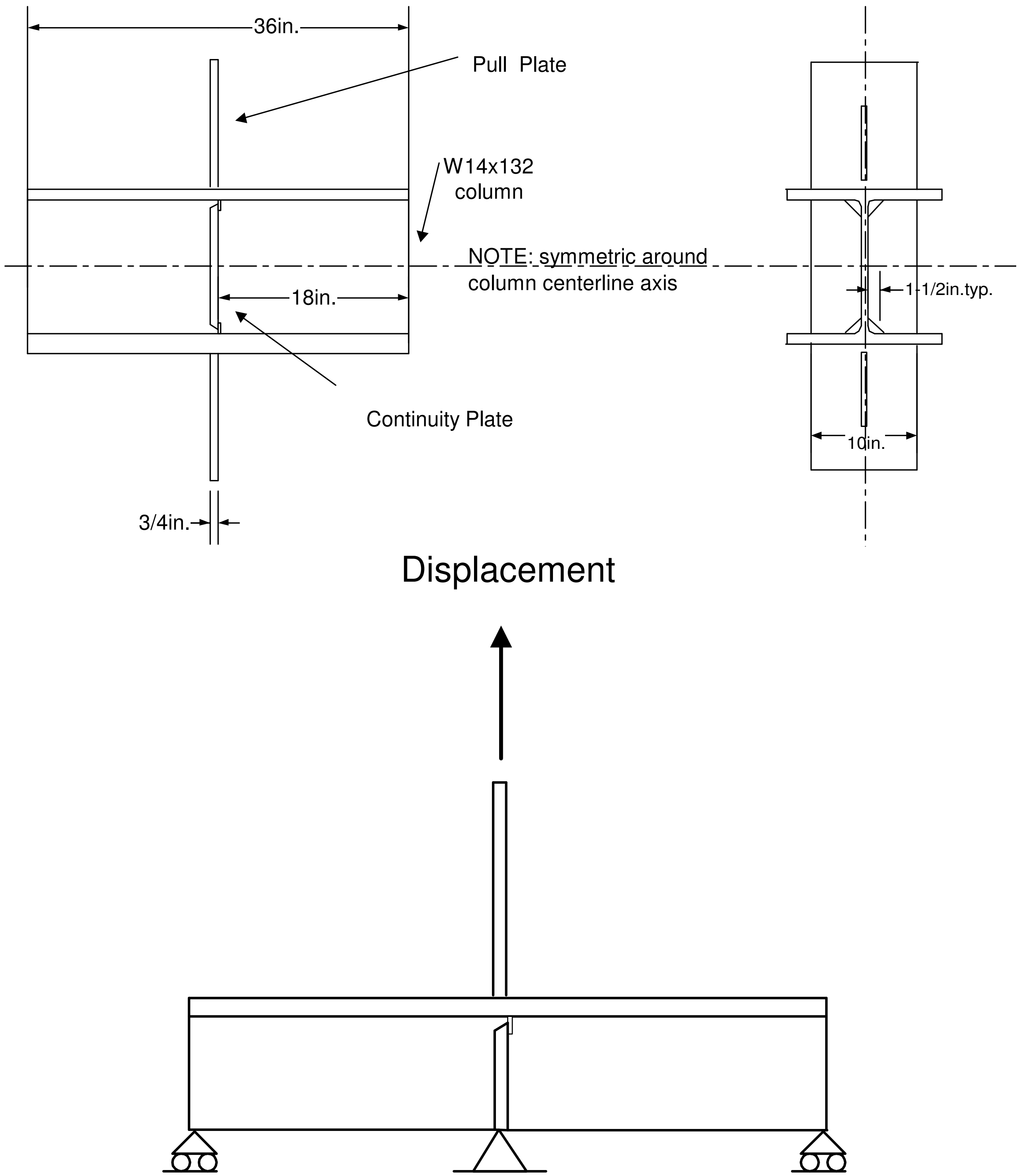

Figure 3.1: One-Quarter Symmetric Model of Pull Plate Specimen

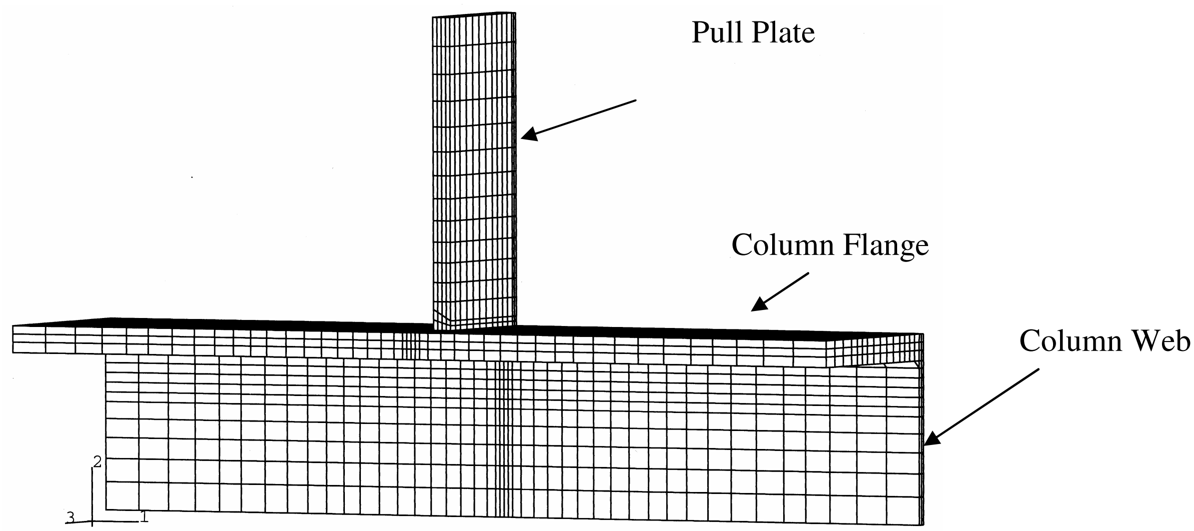

Figure 3.2: Typical Unstiffened Models

(1-LWY, 2-LWY and 3-UNST)

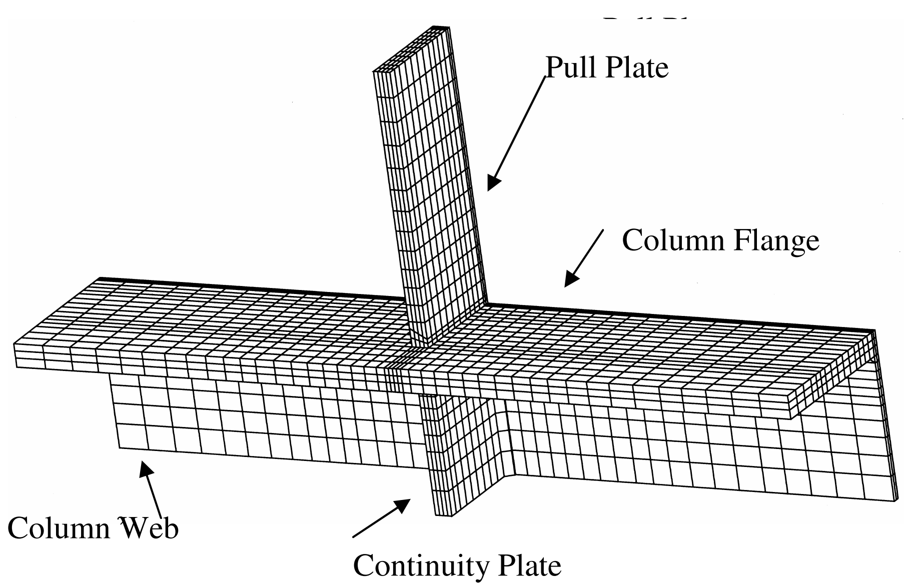

Figure 3.3: Typical Model With Continuity Plate

(1-HCP and 1-FCP)

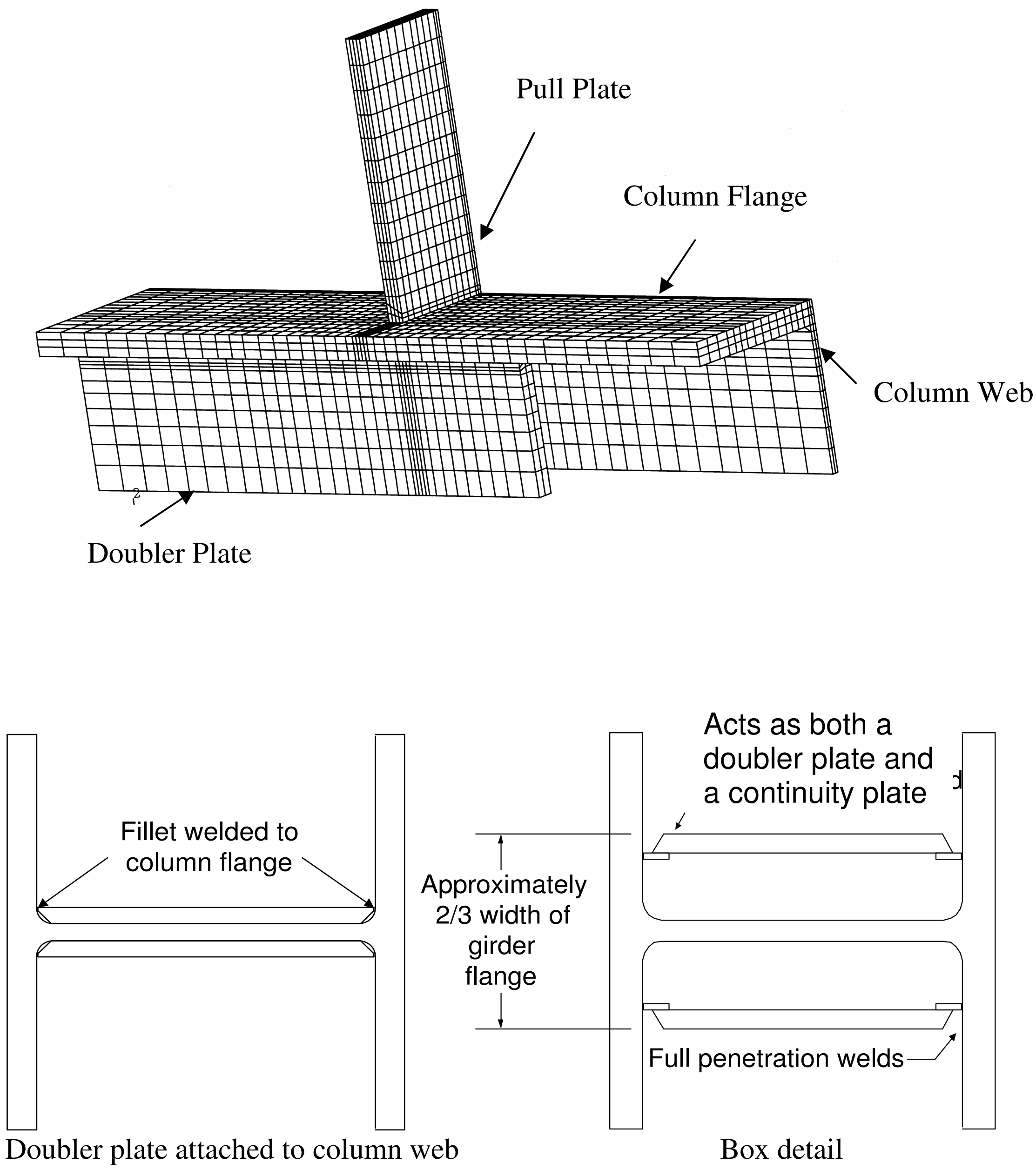

Figure 3.4: Typical Model with Doubler Plate (1-LFB, 2-LFB, and 1-DP)

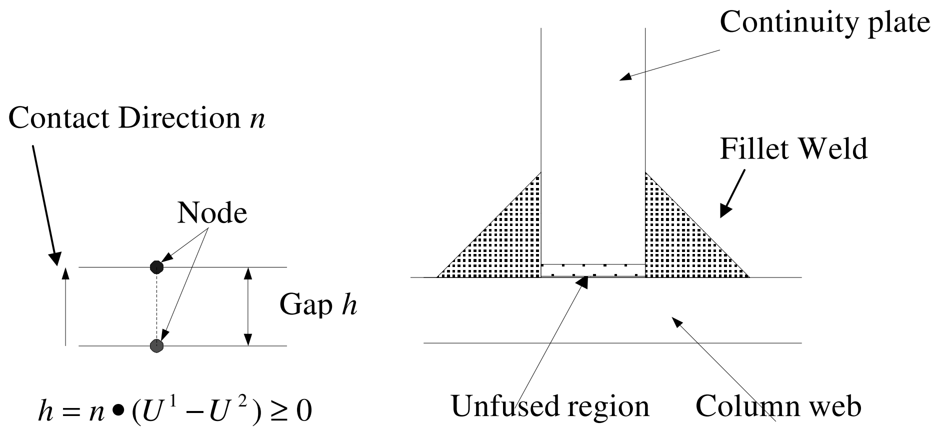

Figure 3.5: Gap Element Used in Finite Element Models

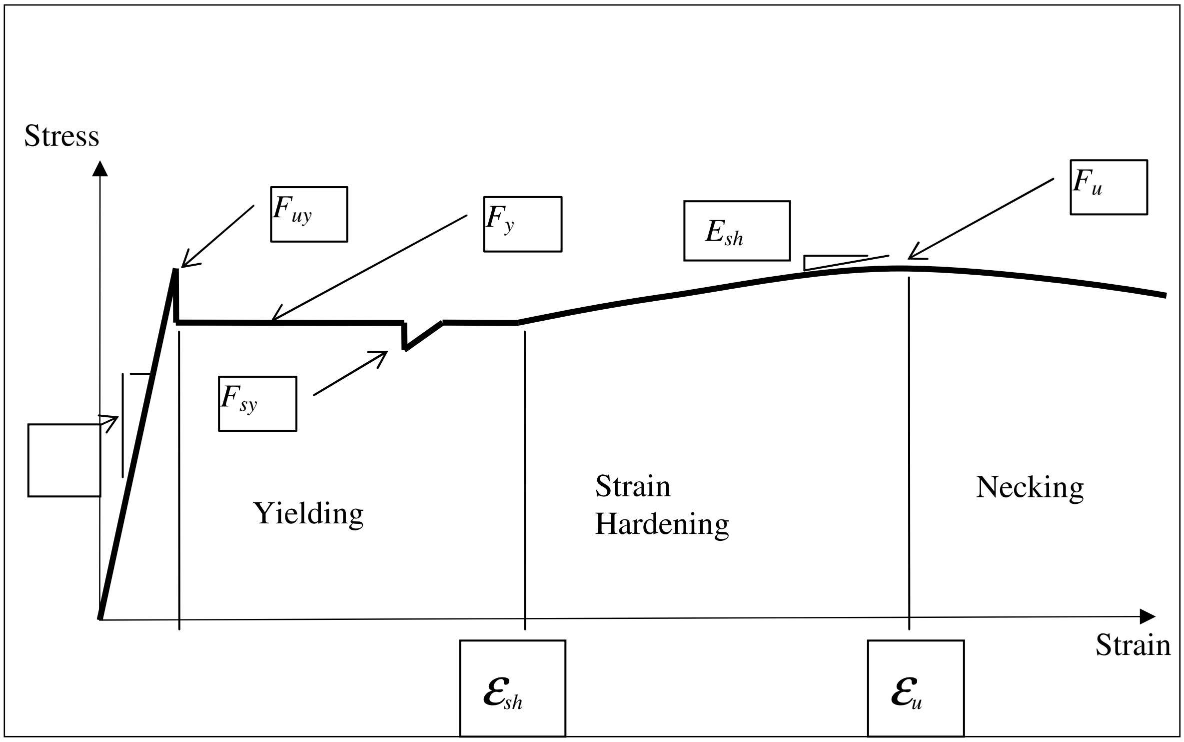

Figure 3.6: Schematic Stress-Strain Properties from Tensile Coupon Test

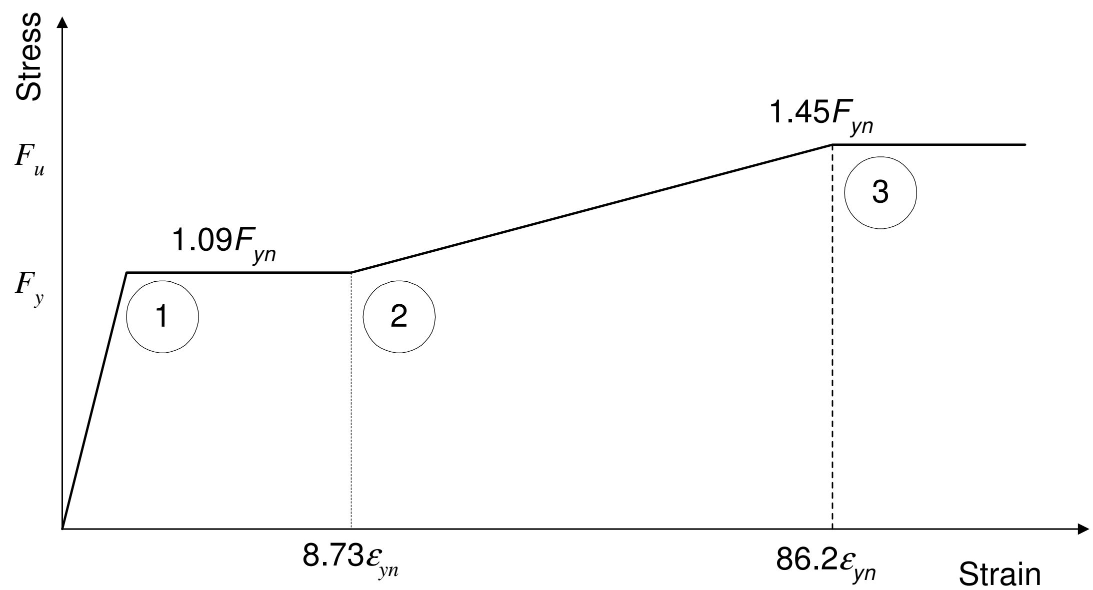

Figure 3.7: Stress-Strain Curve for A992/50 Steel

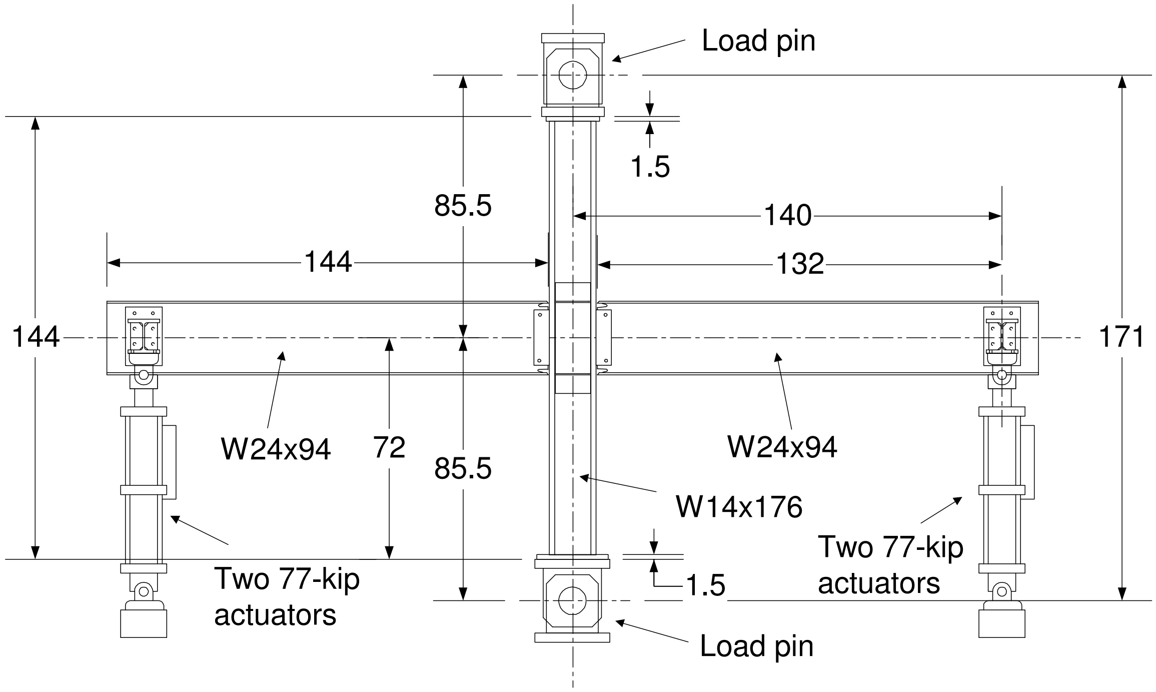

Figure 3.8: Cruciform Experimental Test Set-Up

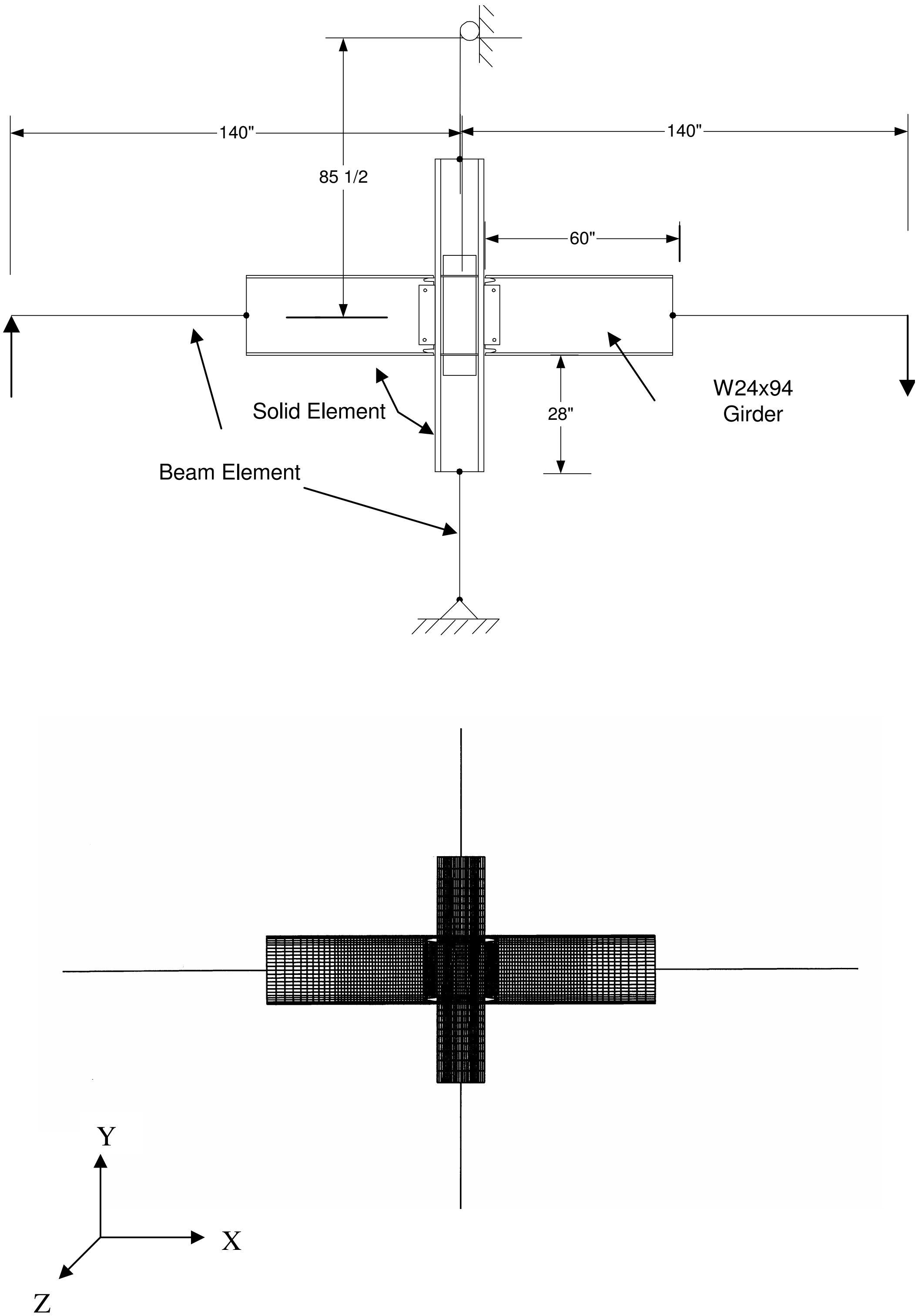

Figure 3.9: Finite Element Model of Cruciform

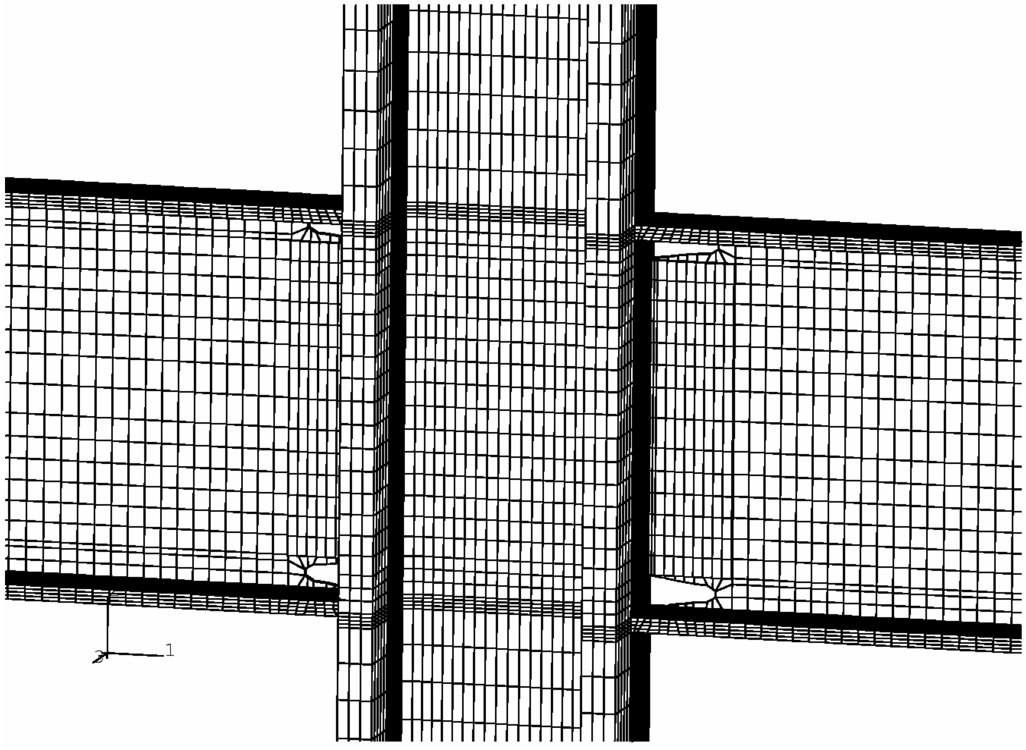

Figure 3.10: Unstiffened Cruciform Model (Specimen CR1)

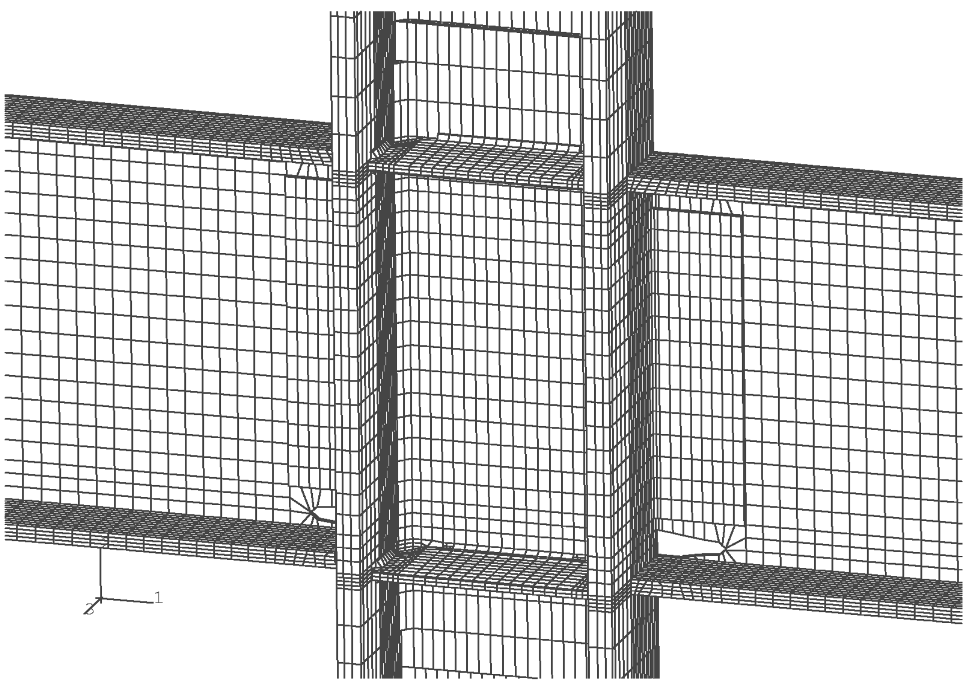

Figure 3.11: Cruciform Model with Continuity Plate and Doubler Plate (Specimen CR3)

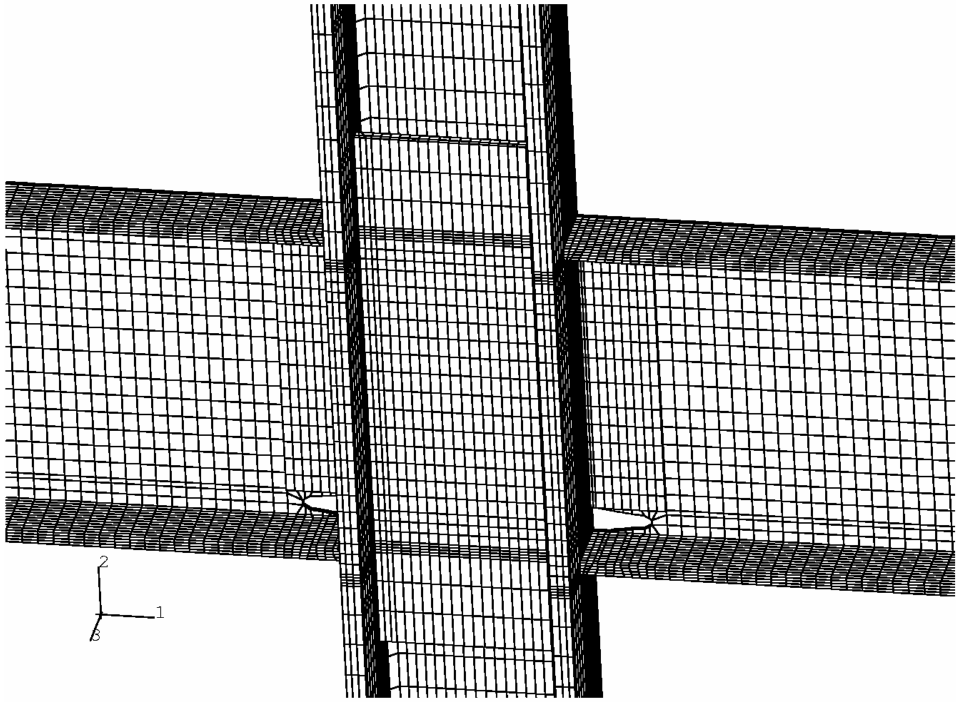

Figure 3.12: Cruciform Model with Doubler Plate (Specimens CR2, CR4, and CR5)

Chapter 4

Analysis of Pull Plate Specimens

As part of this research, nine pull plate tests were performed to study the local web yielding and local flange bending limit states of the connection assemblages under static load. Table 3.1 provides the detailed geometric configurations. As specimens 1-HCP and 1B-HCP had similar experimental results, only 1B-HCP is shown here. As shown in Figure 3.1, the pull plates were loaded axially at each end to represent the tensile girder flanges in steel moment-resisting connections. Details of the experiments, including loading history, gage locations, and data reduction, may be found in Prochnow et al. (2000).

The finite element analysis results of pull plate tests are presented in this chapter. The results are compared with the experimental data to verify the finite element models as well as to provide further understanding of the connection behavior. After a discussion of the load-deformation behavior, the specimens will be investigated in groups, looking at different column failure modes and stiffening details.

4.1 Load-Deformation Behavior

Shown in Figure 4.1 is the load versus specimen elongation behavior for the specimens and analyses. The applied loads were calculated by integrating the stress component in the pulling direction across the cross sectional area of the pull plate near the loaded end. The specimen elongation is defined as the total elongation of the specimen divided by the nominal length of the specimen. The finite element analysis results agreed well with the experimental results. All the specimens broke in the pull plate at an ultimate load of approximately 520 kips (547 kips for specimen 1B-HCP). All specimens showed similar load deformation behavior: an initial elastic stage, followed by a yield plateau and strain hardening stage to the ultimate load. Significant yielding occurred at a load level of approximately 380 kips and a nominal elongation of 0.5%-0.8% for specimens 1-LFB, 2-LFB, 1-LWY, 2-LWY, and 3-UNST. For specimens 1B-HCP, 1-FCP, and 1-DP, where the specimens were stiffer due to the existence of continuity plates or box detail doubler plates, significant yielding occurred at a load level of 390 kips and 0.2% of specimen nominal elongation. Both the computational and experimental results indicated that the specimen load capacity was governed by the pull plate strength. The load-deformation behavior of the specimens corresponded well to the pull plate stress-strain properties. The difference between the analysis and experiments could be attributed to the actual inhomogeneous material properties in the specimens, as will be discussed later.

Shown in Figure 4.2 is a contour plot of the equivalent plastic strain ($PEEQ = \sqrt{\frac{2}{3} * \varepsilon_{ij}^{\;pl} \varepsilon_{ij}^{\;pl}}$) for specimen 1-LWY at 0.8% specimen elongation, corresponding to the nominal pull plate yield strength of 385 kips. A value of PEEQ above zero indicates yielding in multiaxial strain space. It can be seen that at this load level, most of the pull plate had yielded and localized yielding occurred at the column flange underneath the pull plate and in the web near the k-line region. For example, Figure 4.3 shows the deformed shape of specimen 1-DP at 3% specimen elongation (corresponding to the ultimate load level in the experiments). Necking of the pull plate was observed from the deformed shape.

4.2 Local Flange Bending (LFB)

A parameter study of all possible girder-to-column combinations indicated that for commonly used connections, local web yielding always controls the need for the column stiffeners (Dexter et al., 1999). In other words, an unstiffened column will almost always fail by local web yielding before failure by local flange bending or local web crippling. It was observed from the analyses that the stress and strain patterns became even more complicated when there were interactions between local web yielding and local flange bending. To minimize the influence of local web yielding, two specimens (1-LFB and 2-LFB) were tested with strengthened webs. Two 0.5 inches doubler plates were attached to the web in each specimen. The ratios of flange strength (ϕR_n) to the required strength from the girder flange (R_u) are 0.80 and 0.89, respectively for non-seismic design.

The column flanges exhibited two-way bending: both along the column stub length and along the column flange width. Shown in Figures 4.4 and 4.5 are the vertical displacement (in the pulling direction) along the column length and transverse to the column length at 2% of specimen elongation (which corresponds to Equation (2.12b), approximately 1.2 times the nominal pull plate yield strength). As may be expected, the flange displacement concentrated around the center, where the pull plates were welded to the column flange. The column flange displacement decayed quickly with the increase of the distance from the pull plate. At 6 inches away from the centerline of the pull plate, the vertical displacement dropped 50%. The displacement along the width of the column flange was also not uniformly distributed. The column flange is highly restrained at the center due to the stiff web. The displacement due to the web elongation at the center of the flange was 0.13 inches at this elongation for both specimens. The analyses showed that at this specimen elongation level, most of the web was elastic due to the strengthened detail with doubler plates. The displacement increased towards the free edge, where less restraint was present. The maximum column flange displacement relative to the web is 0.1 inches and 0.078 inches for specimens 1-LFB and 2-LFB, respectively. A decrease of 22% in this displacement was observed when the column size changed from a W14x132 (t_{cf}=1.03) to a W14x145 (t_{cf}=1.09).

Figure 4.6 shows the deformed shape from the finite element analysis at 5% specimen elongation for specimen 1-LFB, which corresponds to the approximate pull plate ultimate strength of 520 kips. Figure 4.7 shows the deformed shape of the actual specimen (1-LFB) after the experiment. Both specimens failed in the pull plate at an ultimate load around 520 kips. From the deformed shape, it was observed that flange bending was noticeable at this high load level. However, no weld cracking was noticed in the experiment. Thus, in these cases, the mild deformation of the flanges did not cause immediate damage in the weld.

The stress and strain distributions in the column flanges under the pull plate were a result of the combination of both two-way bending and material possion effect. Additional stress and strain were introduced in the highly restrained region (e.g., the column flange center) where deformation due to the bending was restricted. Shown in Figure 4.8 is the longitudinal strain (E11) distribution near the inside surface of the column flange near the web. The quantities are plotted along the length of the column at 0.8% and 2% specimen elongation, corresponding to the load level of the nominal pull plate yield strength and 1.2 times the nominal yield strength, respectively. Highly concentrated strains were observed at the column flange center underneath the pull plate. Due to the reversed flange bending curvature, the longitudinal strain changed sign along the length. Compressive strain developed in the center and tensile strain developed at 1.5 inches from the centerline. The strain decayed towards the ends of the column. At approximately 6 inches from the centerline, the strain in the column flange was negligible. The longitudinal strain in specimen 1-LFB at 2% specimen elongation was only 0.04% at this location. Comparisons of the transverse (not shown) and longitudinal strains also showed that the column flange bending was more significant in the longitudinal direction.

Comparison between the two specimens showed that the strain in the center was approximately the same at 0.8% specimen elongation (0.2% strain in compressive). However, a much higher difference was observed at 2% specimen elongation. A compressive strain of 0.8% developed in specimen 1-LFB as opposed to 0.3% strain observed in specimen 2-LFB. Also shown in the figures are the experimental results from the strain gages at the same locations. The comparisons indicated that the finite element model predicted the strain distribution pattern well. However, the analyses over predicted the strain values in the center. The strain values obtained from the experiments were only approximately 50%-60% of that obtained from the finite analyses at the center.

Both the experimental and computational results indicate that the amplitude of the displacement and strains were not significant for these two specimens. Both specimens failed in the pull plate and no visible cracks developed in the weld connecting the pull plate to the column flange. The column flange underneath the pull plate was not yielded until significant yielding of the pull plate had occurred. Although only 80%-90% of the required strength was provided according to the design calculations, the experimental data indicates that there is no immediate damage to the connections. However it should be noted that the out-of-plane deformation in the column flanges will degrade the axial strength and flexural strength of the column. In addition, the presence of the cyclic loading will further influence the stress and strain in the connection region. Prochnow et al. (2000) and Cotton et al. (2001) study these phenomena further.

4.3 Local Web Yielding (LWY) and Interaction with Local Flange Bending (LFB)

Three unstiffened specimens were tested to investigate local web yielding behavior and the interaction of local web yielding with local flange bending. As shown in Table 3.1, the ratio of the resistance for the local web yielding (ϕR_n) to the required strength (R_u) is 0.79, 0.86, and 1.0, respectively, for design for specimens 1-LWY, 2-LWY, and 3-UNST.

Shown in Figure 4.9 are the equivalent plastic strain contour plot of specimen 1-LWY (W14x132) at 0.8% and 5% specimen elongation (corresponding to the nominal yielding strength of the pull plate and ultimate load) as well as the maximum principal stress contour plot and a plot of the maximum and minimum stress directions in the column flange at 5% specimen elongation. For the unstiffened sections, significant local web yielding and local flange bending occurred. Most strain concentrated in the column web along k-lines. The yielded area in column web initiated directly under the pull plate in the k-line region. With the increase of applied displacement, the inelastic zone progressed into the web and developed a semicircle pattern horizontally. The high stress and strain in the column flange occurred in the center, where pull plate intersected the column flange. The inelastic zone in the flange first occurred in the center of the flange directly under the pull plate. It then developed towards the flange tip along the pull plate welds, as well as perpendicular to the plate along the column web. The column flange was highly restrained at the center due to the stiffer column web.

Shown in Figure 4.10 is the vertical strain (E22) distribution along the web k-line at the 0.8% and 2% elongation levels. It can be seen that much higher strain concentrated in the middle directly under the pull plate. At 0.8% specimen elongation, the strain in the middle for specimen 1-LWY was approximately 10 times the nominal yield strain. At 2% specimen elongation, it was approximately 16 times the yield strain. A decrease in strain of 60% and 90% was observed at these load levels at this location from specimens 1-LWY to 3-UNST, respectively. The concentration of the strain decayed as the distance from the web center increased. At five inches from the center, the difference between specimens and elongation levels were not significant.

Current local web yielding criteria assumes that the concentrated stress and strain are undertaken within a distance of 5k+N along the k-line in the web. The limit state is assumed to be reached when this entire length is yielded. The analyses showed that at 0.8% specimen elongation, all specimens were not yielded in the 5k+N region. At 2% of specimen elongation, specimen 1-LWY was just yielded within this length. For specimen 2-LWY, where only 86% of the required strength was provided according to the design calculation, the analysis showed that the specimen can still provide adequate strength. Further comparison to experiments for this limit state may be found in Prochnow et al. (2000).

It was recognized that the strain component at the web center near the k-line is somewhat sensitive to the material properties. A brief parametric study was conducted to study the effect of different material models on the web strain around the k-line, where high stress and strain concentration occurred.

Shown in Figure 4.11 are the comparisons of the finite element analyses with the experimental results at different load levels. The load level *P* equal to 385 kips corresponds to the nominal yield strength of the pull plate (approximately 0.8% specimen elongation). The load level *P* equal to 450 kips corresponding to the 1.2 times the nominal yield strength of the pull plate (approximately 2.0% specimen elongation). The load level P equal to 520 kips corresponds to the ultimate load observed in the experiments (approximately 5.0% specimen elongation). Three different material model were used in the column web. As outlined in Chapter 3, Case 1 (FEM, stiffer web and k-line) is the standard model used throughout the analyses. Case 2 (FEM, stiffer k-line), different material models from the column flanges were only used for elements near the k-line region in the web. The ultimate stress was the same as in other parts, however, the yield stress was increased to 95% of the ultimate strength and the yield plateau was eliminated. Case 3 (FEM, constant properties) used the same material model throughout the cross section. The analyses showed that the material properties do not affect the results at larger distances away from the center. Similar results were obtained beyond approximately 3 inches and 5 inches from the center for the first two load levels and the ultimate load levels, respectively. In general, the web was stiffer for Case 1. Comparisons with the experimental results suggested that at lower specimen elongation levels, all models overestimated the strains at the center. At the intermediate load level (P=450 kips), Case 2 gave better predictions. At the specimen ultimate load level, however, the three cases underestimated the strains and Case 3 seemed to be a better prediction. This study shows that although the finite element model could predict well the global behavior and stress and strain distribution pattern in the highly concentrated area, it is difficult to predict exactly the magnitude of the strains at those locations due to the localized inhomogeneity of the material of the steel shapes.

For the unstiffened specimens, the flange displacement was influenced by both local web yielding and local flange bending. Figure 4.12 shows the deformed shape of 1-LWB at 5% specimen elongation from the finite element model, and the deformed shape of the actual specimen after the experiment. Compared with specimen 1-LFB, where the web was strengthened by the doubler plates, specimen 1-LWY had more significant two-way bending in the flanges. For the unstiffened specimen (1-LWY), most of the web was yielded, and a larger part of the flanges were yielded near the pull plate and along the column web as shown in Figure 4.9(a), (b). The shaded areas in the column web and the flange indicate the general yield pattern. However, in the experiments, a somewhat different yield line pattern developed in the flanges from the pull plate center and spread diagonally towards the flange edge (Figure 4.12(b)). By further comparing the yield pattern in the experiments to the principal stress flow (Figures 4.9(c) and 4.9(d)), a similar diagonal stress flow pattern was observed. However, the stress in the flange was somewhat under-predicted in the analyses and thus the flange had not yielded diagonally at this load level. Shown in Figure 4.12(c) is the flange displacement at 2% of specimen elongation. The flange displacements were amplified by the web yielding at the center. The interaction of the LFB and LWY had a more significant effect on the column flange deformation.

4.4 Continuity Plate Behavior

For the W14x132 column tested, the unstiffened section can provide only 86% of the required strength according to the design calculation. Two specimens with continuity plates were analyzed to study the stiffened section behavior, including one specimen with a continuity plate thickness equal to half the pull plate thickness (1B-HCP) and fillet-welded to the column flanges, and another with a continuity plate thickness equal to the pull plate thickness (1-FCP) and welded to the column flanges with CJP welds. The half thickness continuity plate had a tensile strength (F_yA_g) of approximately 62% of the non-seismic required strength, 385 kips.

As seen in Figure 4.1, the specimen load-deformation behavior was similar for both cases with continuity plates of different thicknesses. The specimen load capacity was not affected by the stiffener details. The same observation was obtained in parametric studies.

Comparison with the unstiffened specimen (1-LWY) showed that when the continuity plates were added, the strains both in the column web and the column flange were reduced substantially, as expected. Shown in Figures 4.13 and 4.14 are the equivalent plastic strain contour plots in the continuity plates at 2% specimen elongation. In both specimens, no inelasticity developed in the column and significant yielding had occurred in the pull plate at this load level. For specimen 1B-HCP, the continuity plate yielded underneath the pull plate (approximately to a depth of 1.2 inches away from the column flange face). The inelastic region was not uniform across the width of the continuity plate, but rather focused under the pull plate tip. At this location, the continuity plate resisted the vertical pulling stress as well as the bending stress due to the flange bending. For specimen 1-FCP, with a continuity plate having the full thickness of the pull plate, most parts of the continuity plate remained elastic. Only a small region at the edge under the pull plate yielded.

Comparing the strains in the continuity plate of these two specimens showed that the strains were reduced when the thickness of the continuity plate increased. However, it was observed that the highest strain in 1B-HCP was only approximately seven times the yield strain at the continuity plate edge when significant yielding had developed in the pull plate at 2% specimen elongation. Both the analysis and experimental results suggested that for specimen 1-HCP, the specimen still continued to carry load even after part of the continuity plate had yielded. The specimen failed in the pull plate and no visible cracks or distortions were observed in the continuity plates or the welds connecting the continuity plate to the web and flanges at the ultimate load. The continuity plate having a half thickness of the pull plate seemed adequate in providing resistance for the column flange and column web.

4.5 Box Detail

Most commonly used doubler plates are welded directly to the column web and near the k-line are assumed to be fully effective in design. In the 1997 AISC seismic provisions, doubler plates placed away from the column web (box detail) were shown in the commentary. These plates also replace any required continuity plates. One pull plate test with a box detail was tested to further explore the behavior of this kind of doubler plate detail. Specimen 1-DP was a W14x132 column section with a 0.75 inch thick doubler plate placed two inches away from the column web on both sides of the web.

Experimental and computational results showed that both the stress and strain in the column flange and in the web were reduced in the box detail. Most of the column and the doubler plates remained elastic when significant yielding occurred in the pull plate (1.5% elongation). At the ultimate load (P=520 kips), only a small part of the inside flange surface yielded at the tip.

Shown in Figure 4.15 and Figure 4.16 are the strain in the direction of pulling (E22) near the k-line region in the doubler plate and in the web at 0.2%, 1.5%, and 3% specimen elongation (corresponding to 385 kips, 450 kips, and 520 kips). Higher strain occurred in the center under the pull plate. Compared with the unstiffened specimens (e.g., Figure 4.11), much less strain occurred in the web. The doubler plate performed effectively to share the load from the column web. The same strain distribution patterns were observed in the doubler plates as in the web. The E22 strain in the doubler plate near the CJP welds was higher than that in the web k-line region. For specimen (1-DP), the doubler plates (two each at 0.75 inches) were thicker than the column web (0.645 inches). The doubler plate absorbed more force since it was stiffer than the web. A comparison to the experimental data showed that the strains in the web were over predicted in the finite model, while the strains in the doubler plate were under predicted. The strains in the doubler plate were approximately 16% lower than the experimental data. This indicated that the web was stiffer in the finite element model than that in the actual specimen, but also that the doubler plates were highly effective in the box detail.

In addition, when the doubler plates were placed away from the web, the cantilever distance of the flanges was reduced as compared to that of doubler plates attached to the column web. The maximum flange separation was less than 0.06 inches when the specimen failed in the pull plate. These results indicated that when the doubler plates were placed away from the web, the doubler plates successfully acted simultaneously as the continuity plates and provided support to the column flanges.

A brief parametric study was performed to study the behavior of the box detail. The nominal yield stress (50 ksi) was used for throughout the column section, for all three cases: Case A: Doubler plate with thickness of 0.75 inches, placed at the edge of the pull plate; Case B: Doubler plate with thickness of 0.625 inches, placed at the edge of the pull plate; Case C: Doubler plate with thickness of 0.75 inches, placed 1.75 inches from the edge of the pull plate (similar to specimen 1-DP). The analyses showed that when the doubler plates were added to the connection, no yielding occurred in the column flange or the doubler plates even when significant yielding occurred in the pull plate (at 1.5% elongation). However, the flange stress and strain distribution was sensitive to the location of doubler plate. The distribution patterns changed at the location of the doubler plate and in the web. The flange displacement across the column width was also sensitive to the location of the doubler plate.

Shown in Figure 4.17 (a) is comparison of the E22 strain distributions in the column web at 0.2% of specimen elongation between three cases. The quantities are plotted along a vertical line in the web center underneath the pull plate. The distance is measured from the intersection of the column web and flange downwards to the middle of the web. Most parts of the pull plate had yielded at this load level. When the doubler plate moved towards the column web, it helped to reduce the stress and strain in the column web. For both cases A and B, there was a small region in the web around the center, at the height of the k-line, with a total length less than 3 inches that yielded. For case C, there were no yielded regions in the column web. Comparing cases A and C, the stress in the web for case C was about 13%-20% less than that of case A. However, the analysis showed that the doubler plate thickness did not significantly affect the stress and strain in the column web.

Shown in Figure 4.17 (b) are the E22 strain distributions in the doubler plates along the vertical line (in the pulling direction) in the center. It can be seen that stress and strain in the doubler plate increased when doubler plates were moved towards the column web. The stress and strain in the doubler plates for case C was approximately 55% higher than that in case A.

The parametric study of the doubler plate showed that when the doubler plates were moved further away from the column web, the share of the load carried by the doubler plate was reduced. It should be noted that for the pull plate tests, only monotonic tensile force was applied to the column and no panel zone yielding effect was involved in the models. With the shear yielding occurring in the full connection, the difference of the doubler plates on the strain distribution of the panel zone might be less. In addition, the stress and strain patterns in the flange changed as a result of different locations of the doubler plate. Peak stress occurred at the location of the doubler plate, due to the change in the stiffness distribution. This indicated that when the doubler plates were placed away from the web, doubler plates effectively provided support to the column flanges. Similar box details have been investigated by Bertero et al. (1973). They concluded that the doubler plates were effective in the reinforced column web when attached directly to the web. The doubler plates were less effective as they were attached beyond a certain distance from the web. No specific recommendations were made regarding the location of the doubler details in their study. However, this research shows little loss in effectiveness with the box detail. Further experimental study may be needed.

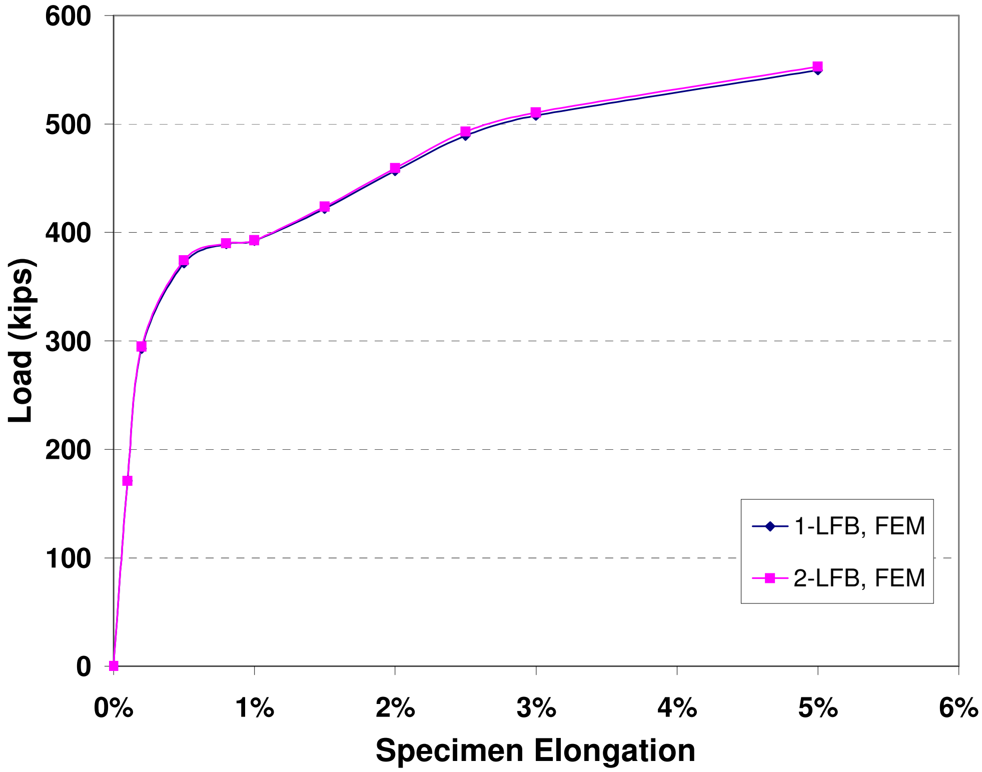

Load (kips)
Specimen Elongation
1-LFB, FEM
2-LFB, FEM
0
100
200
300
400
500
600
0%
1%
2%
3%
4%
5%
6%

(a)

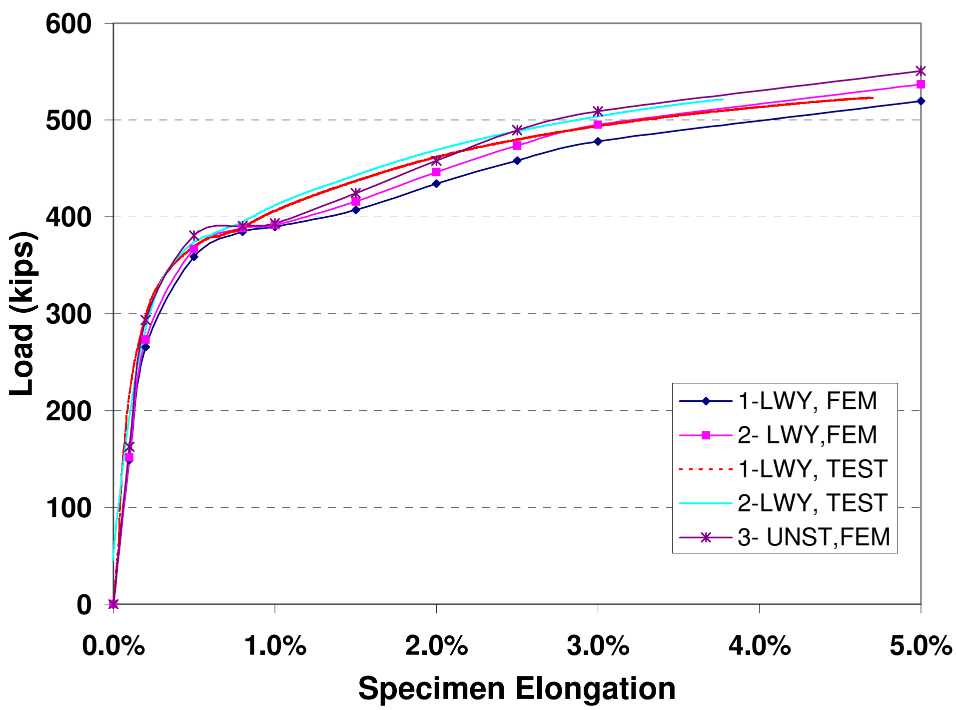

Load (kips)
Specimen Elongation
1-LWY, FEM
2- LWY,FEM
1-LWY, TEST
2-LWY, TEST
3- UNST,FEM
0
100
200
300
400
500
600
0.0%
1.0%
2.0%
3.0%
4.0%
5.0%

(b)

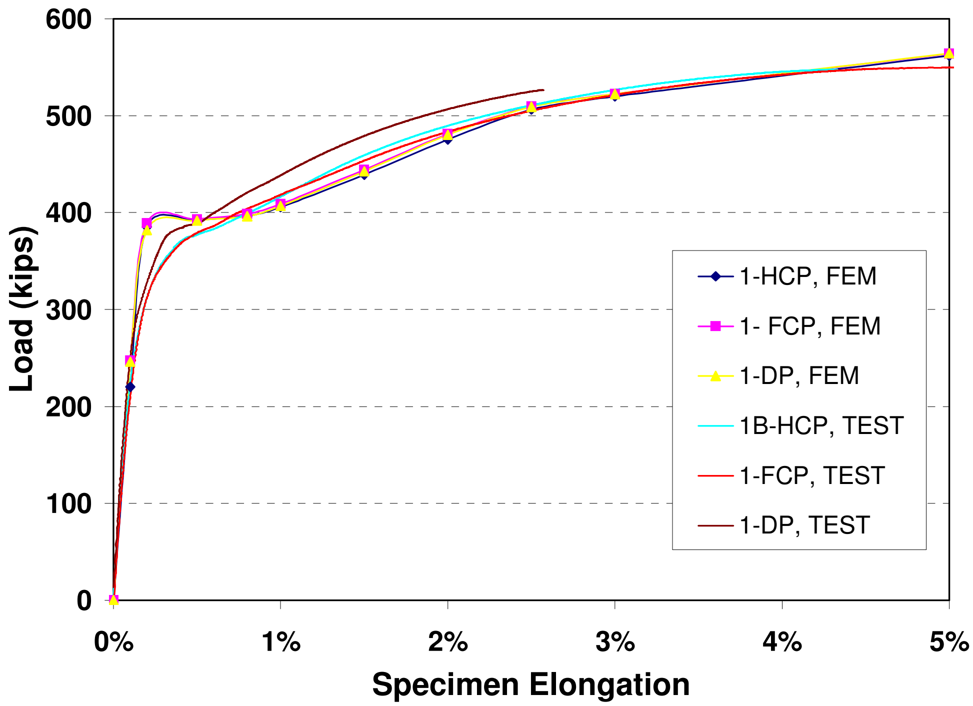

(c)

Figure 4.1: Specimen Load versus Deformation Behavior

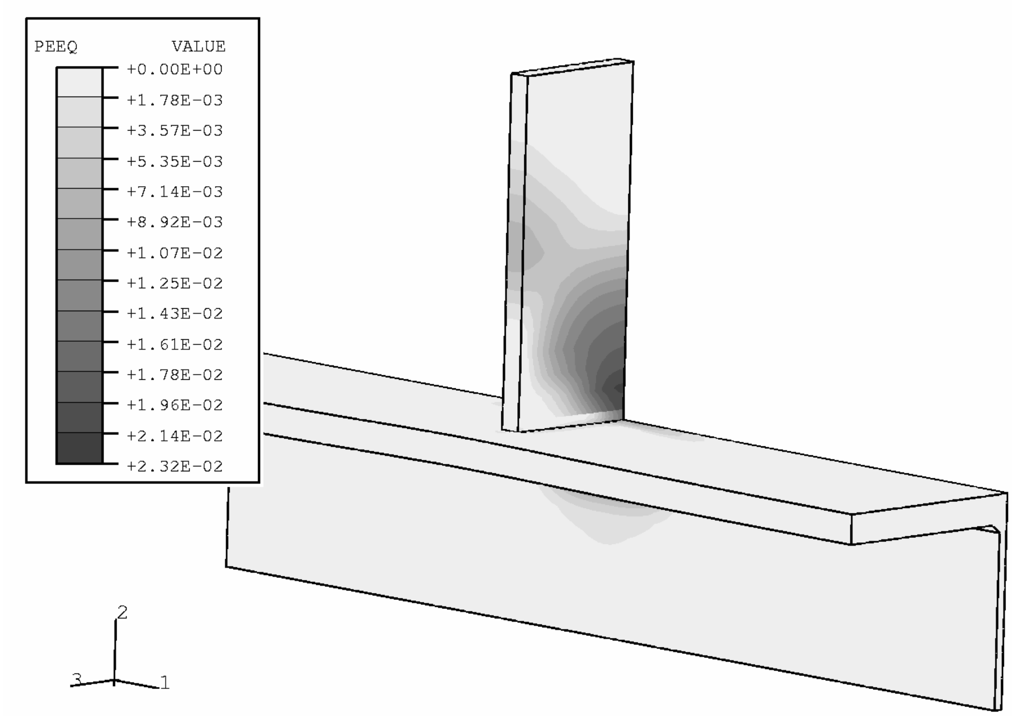

Figure 4.2: PEEQ Contour for 1-LWY at 0.8% Specimen Elongation

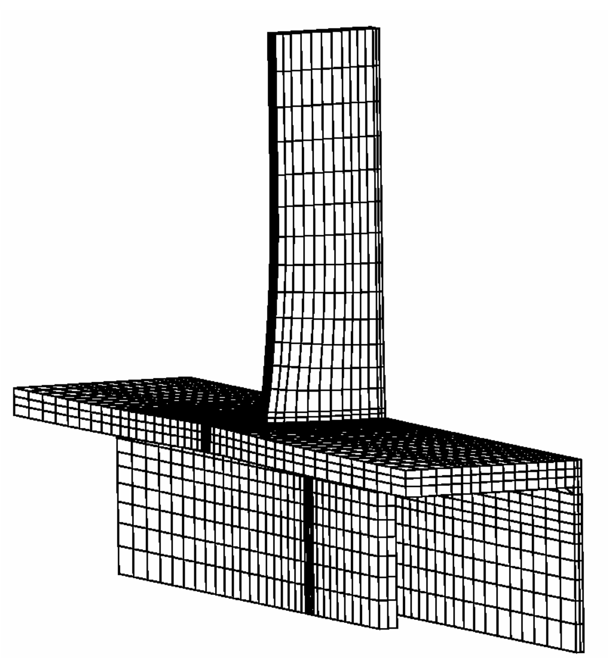

Figure 4.3: Deformed Shape for 1-DP at 3% Specimen Elongation (magnification factor=3)

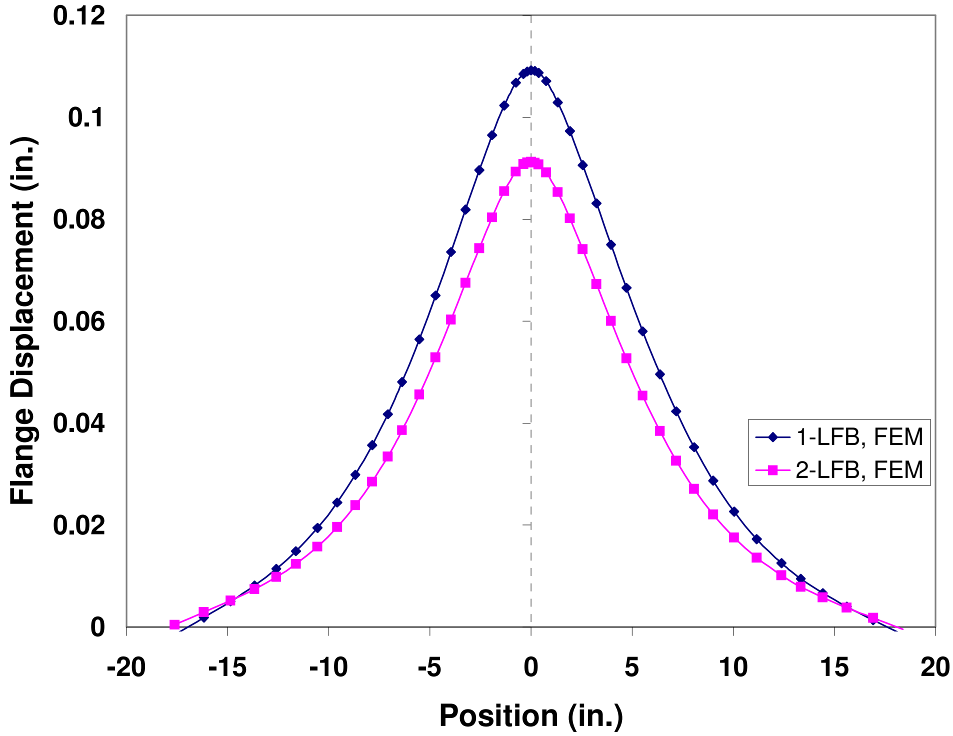

Figure 4.4: Specimens 1-LFB and 2-LFB Flange Displacement at 2% Specimen Elongation along Column Length

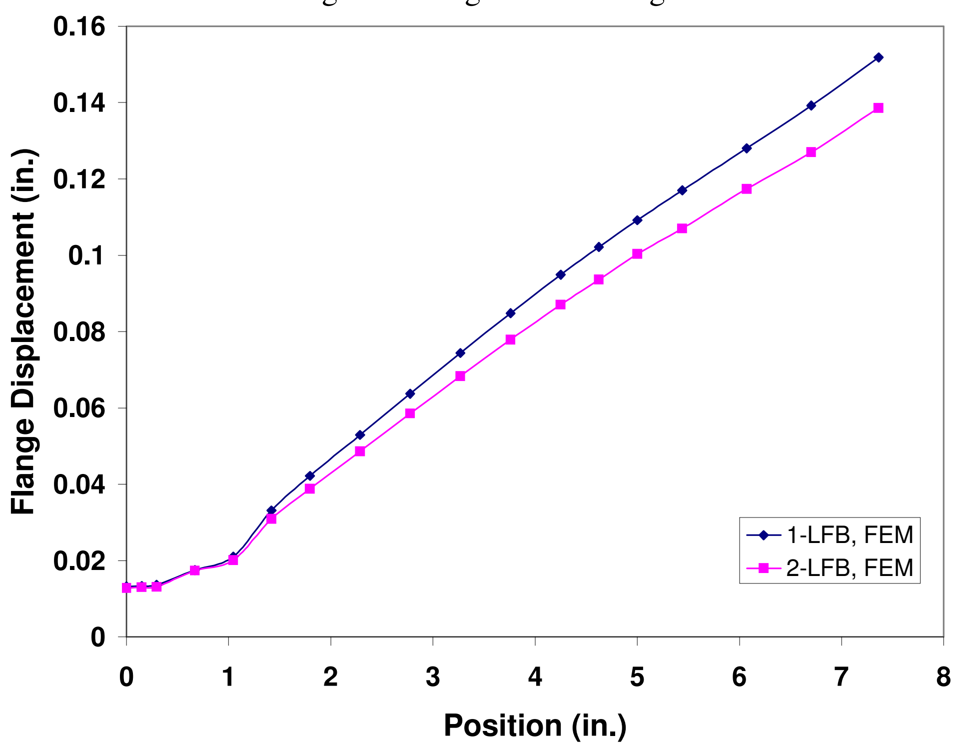

Figure 4.5: Specimens 1-LFB and 2-LFB Flange Displacement at 2% Specimen Elongation along Column Flange Width

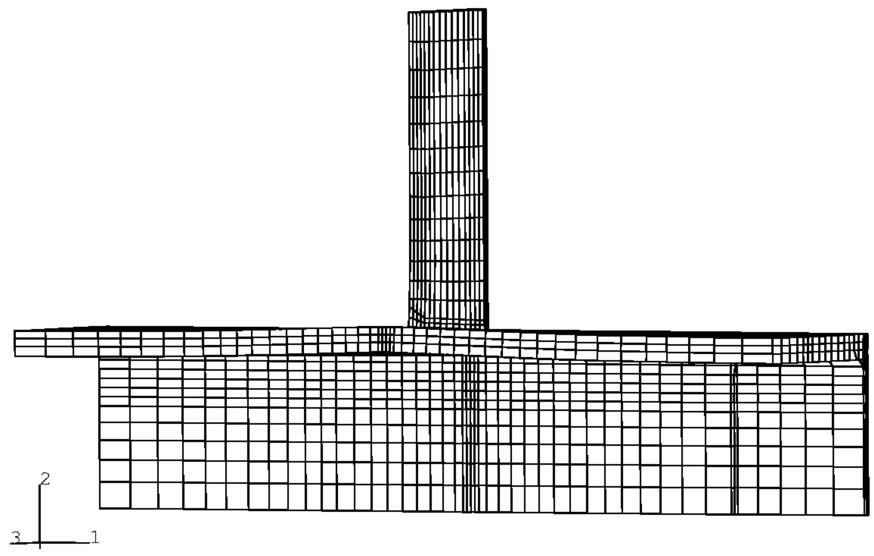

Figure 4.6: Deformed Shape for 1-LFB at 5% Specimen Elongation (magnification factor=1.0)

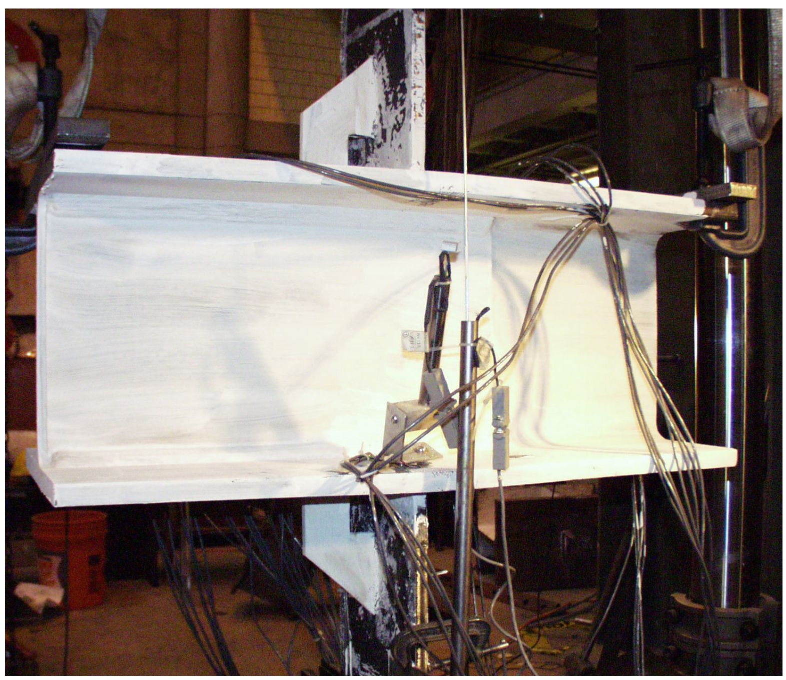

Figure 4.7: Deformed Shape for 1-LFB after experiment

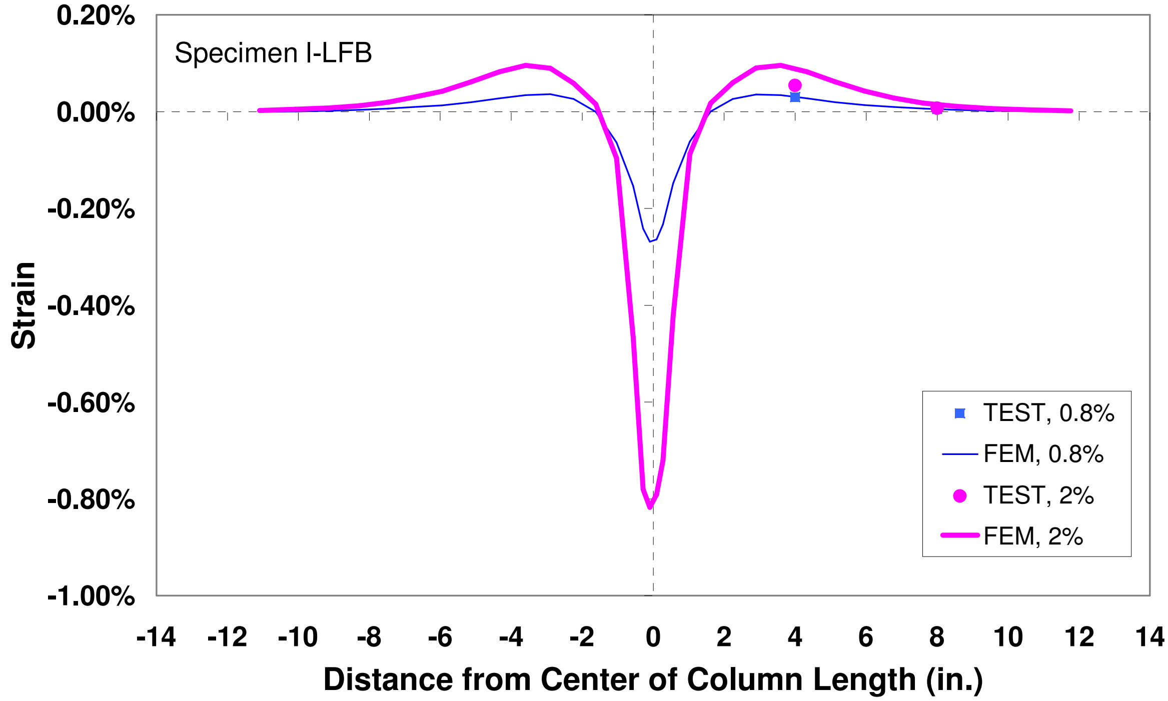

(a) Specimen 1-LFB

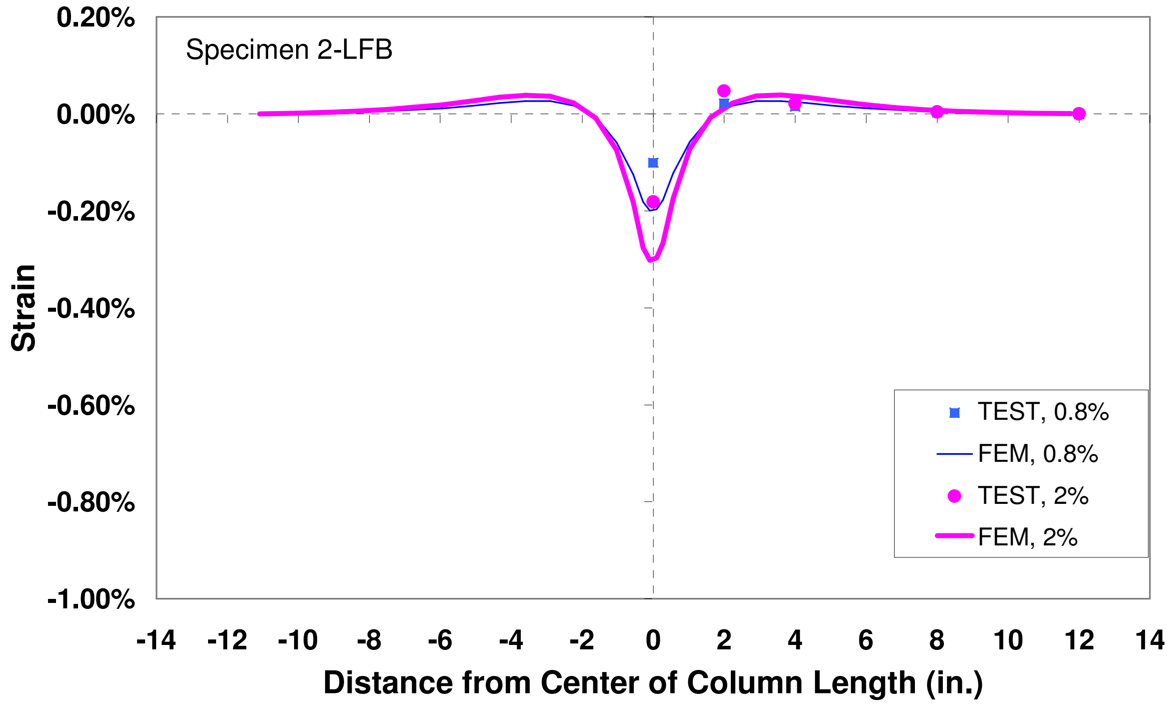

(b) Specimen 2-LFB

Figure 4.8: Specimens 1-LFB and 2-LFB Longitudinal Strain (E11) in Column Flange

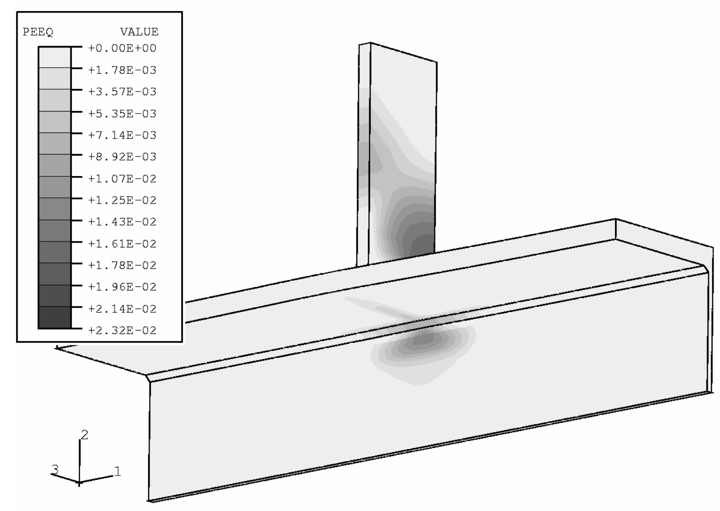

(a) PEEQ contour at 0.8% elongation

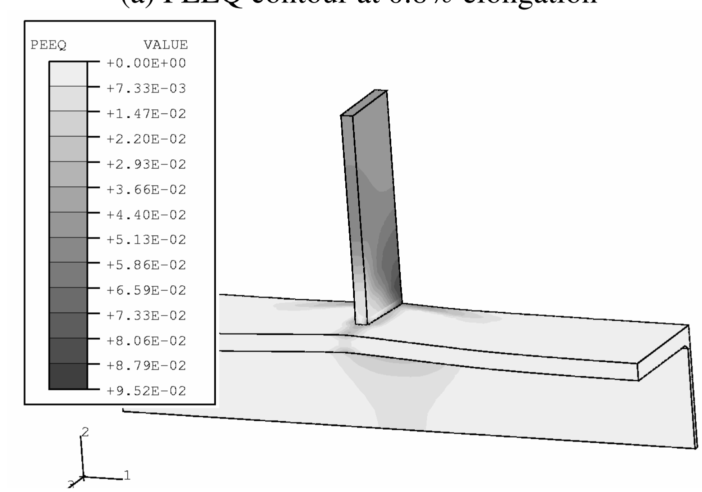

(b) PEEQ contour at 5% elongation

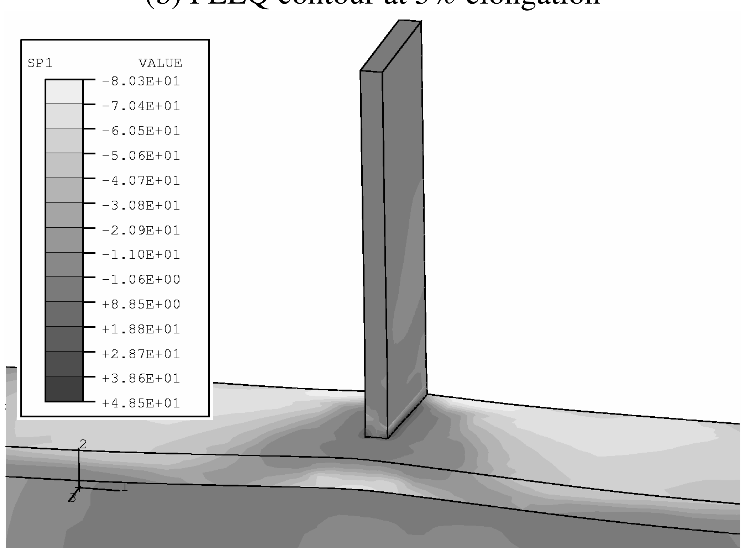

(c) Maximum principal stress contour at 5% elongation

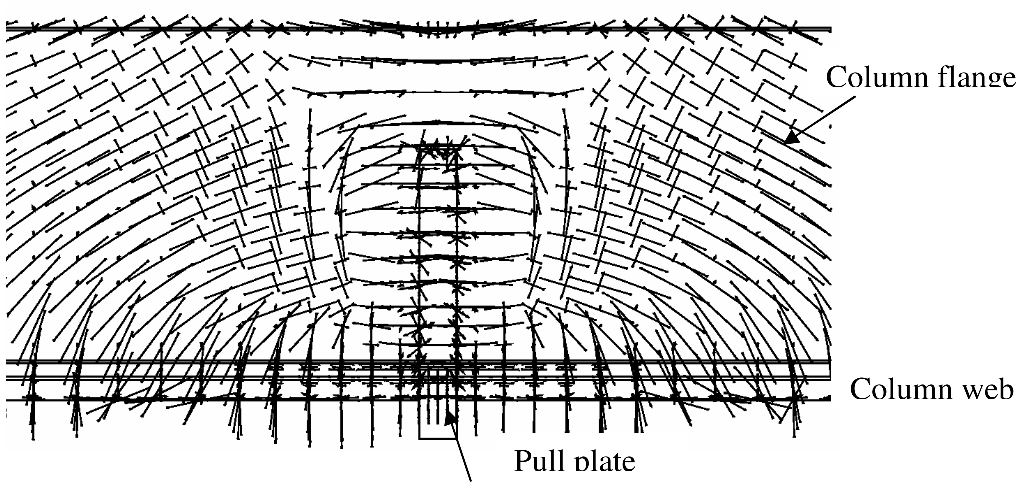

(d) Principal stress directions at 5% elongation (top view)

Figure 4.9: PEEQ and Principal Stress Plots for Specimen 1-LWY

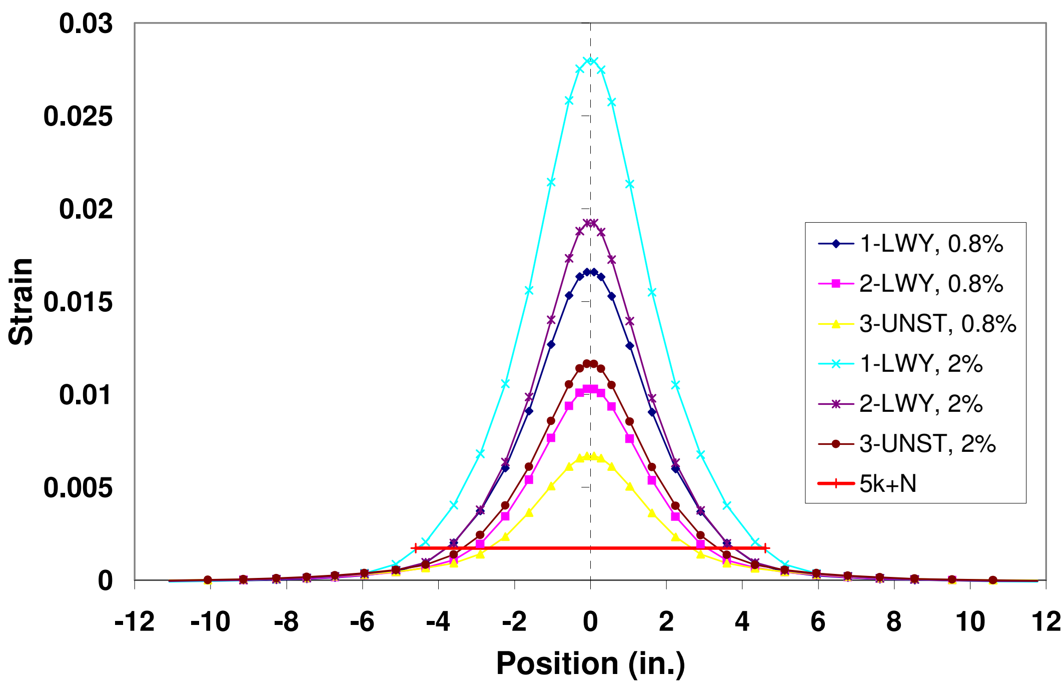

Figure 4.10: Strain (E22) in the Web k-line at 0.8% and 2% Specimen Elongation

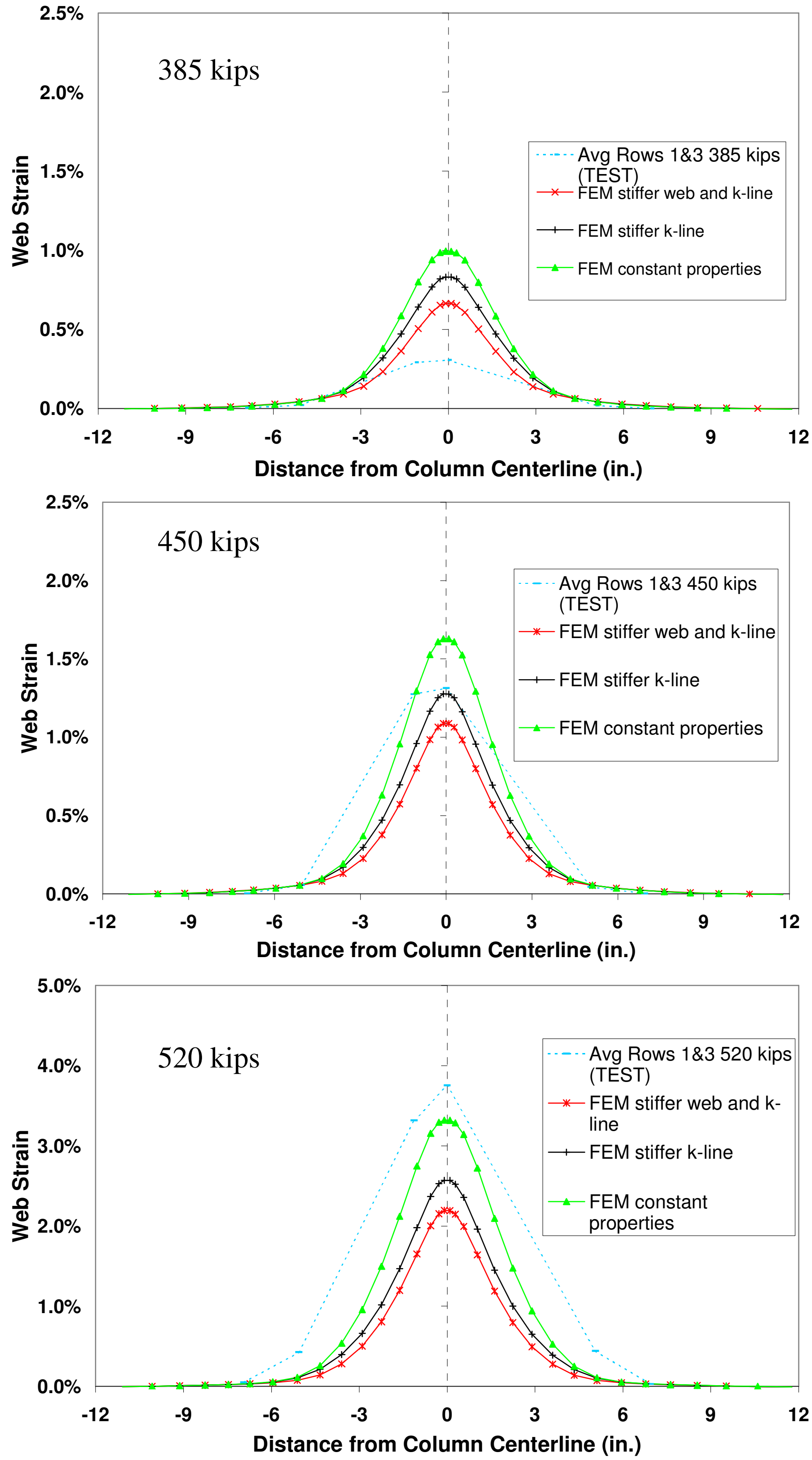

Figure 4.11: Comparison of Different Material Models in Column Web

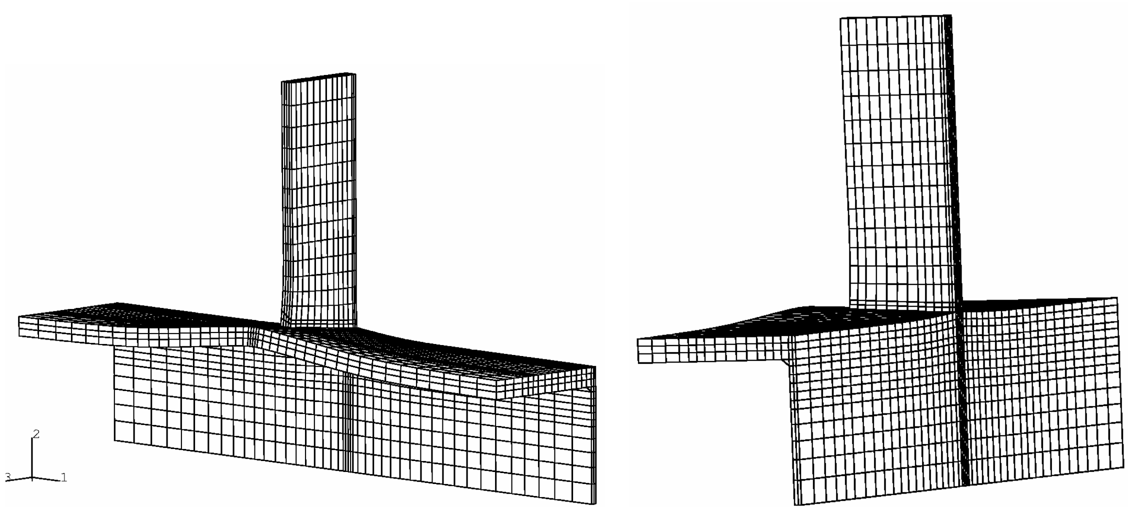

(a) Deformed Shape for 1-LWY at 5% Specimen Elongation
(magnification factor=1)

(b) Permanent Deformation of Specimen 1-LWY after Experiment

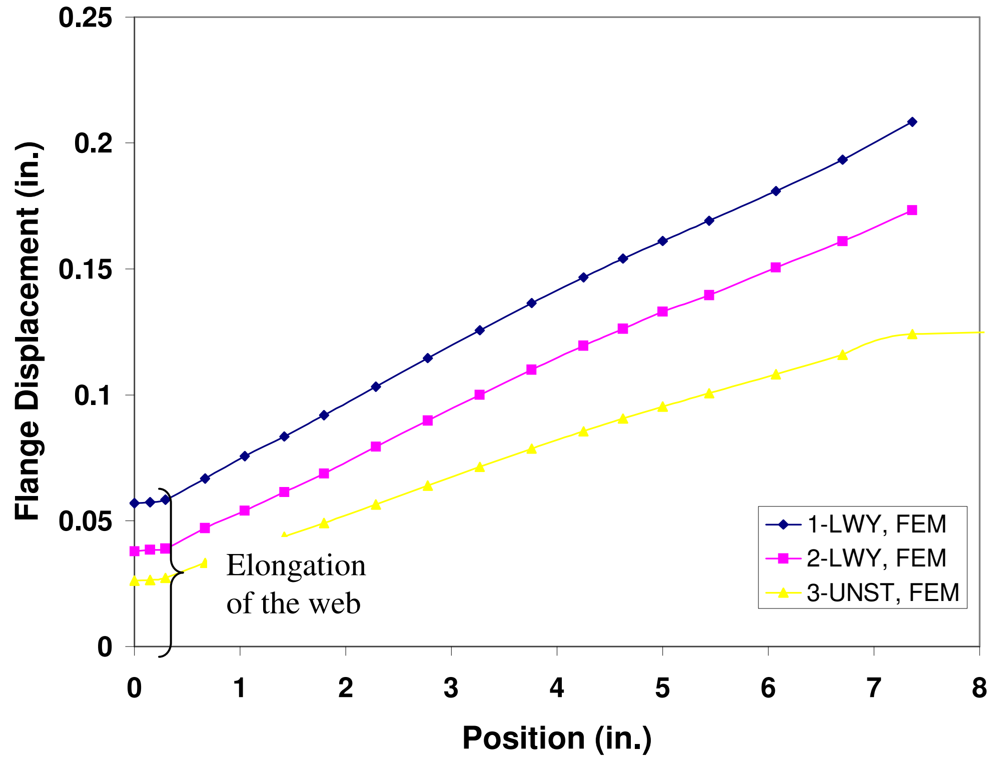

(c) Flange displacement at 2% specimen elongation along column flange width

Figure 4.12: Deformation of Specimen (1-LWY)

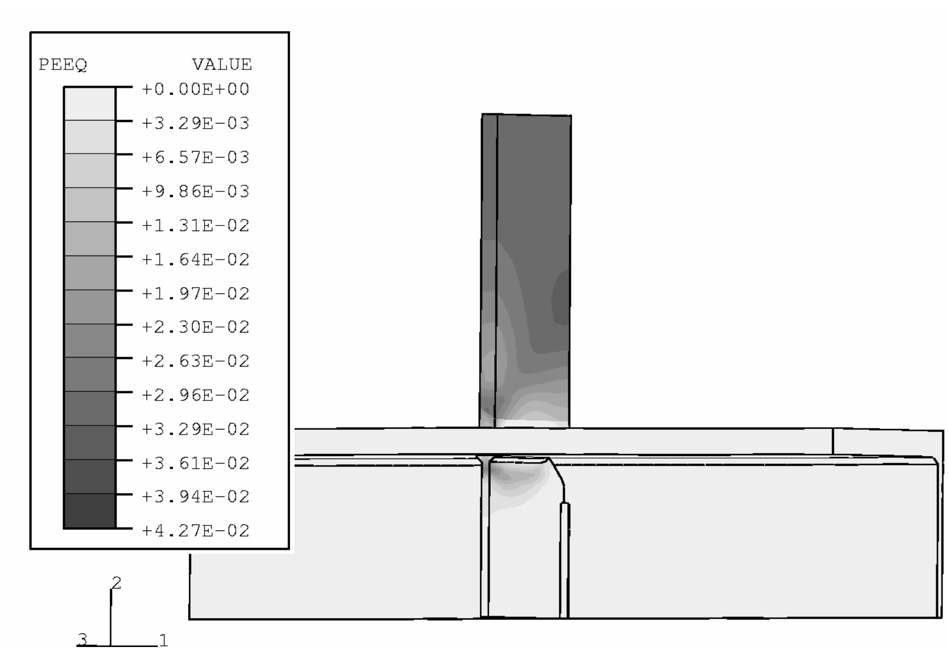

Figure 4.13: PEEQ Contour Plot for 1B-HCP at 2% Specimen Elongation

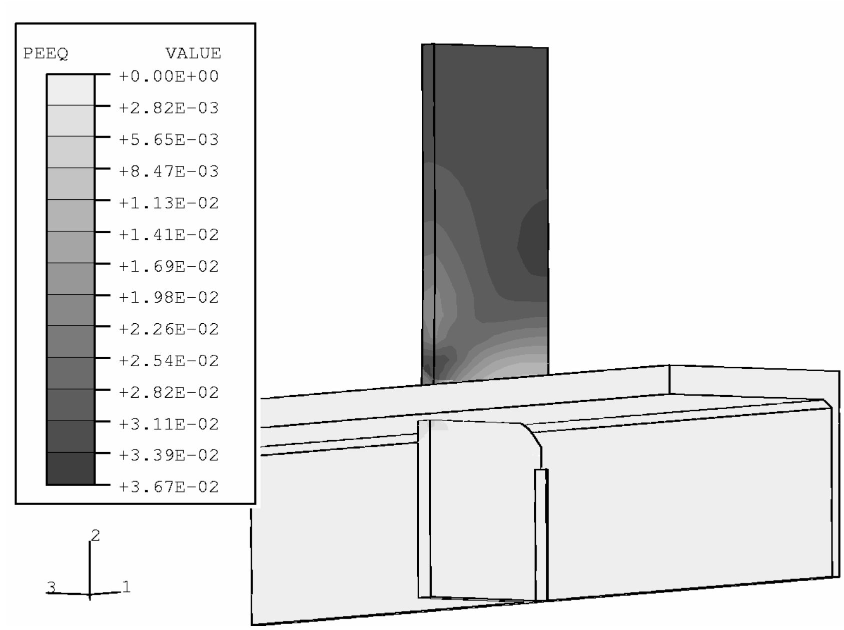

Figure 4.14: PEEQ Contour Plot for 1-FCP at 2% Specimen Elongation

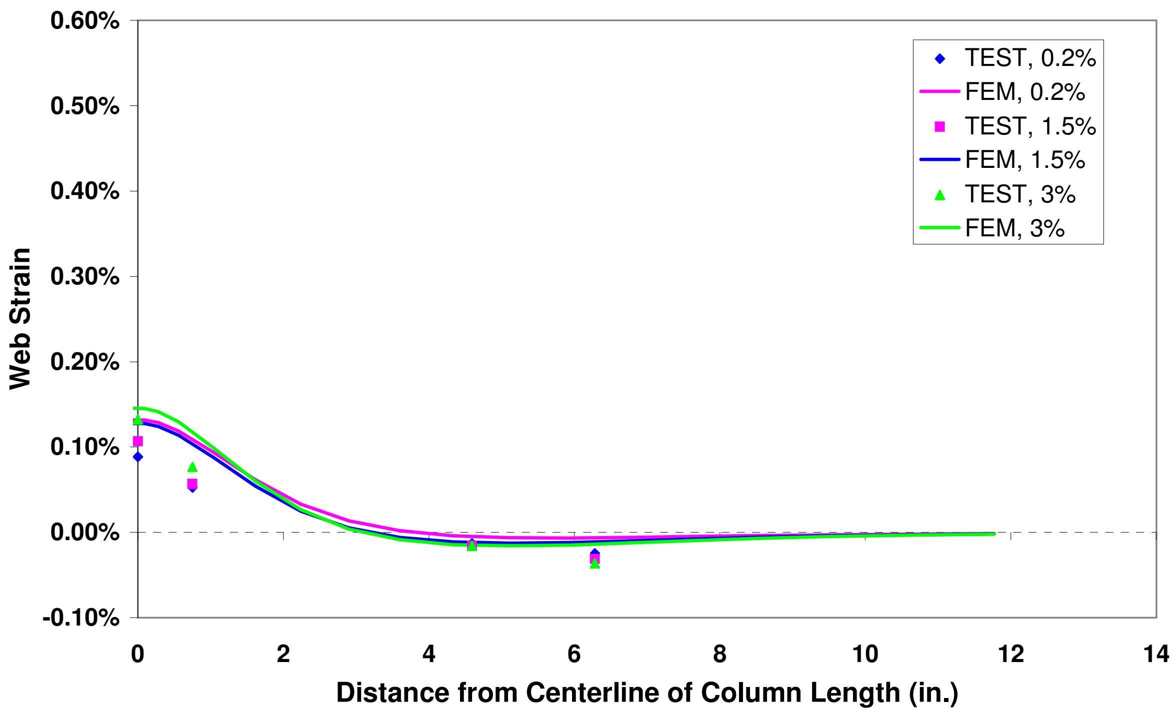

Figure 4.15: Strain Distribution along Column Web k-Line (1-DP)

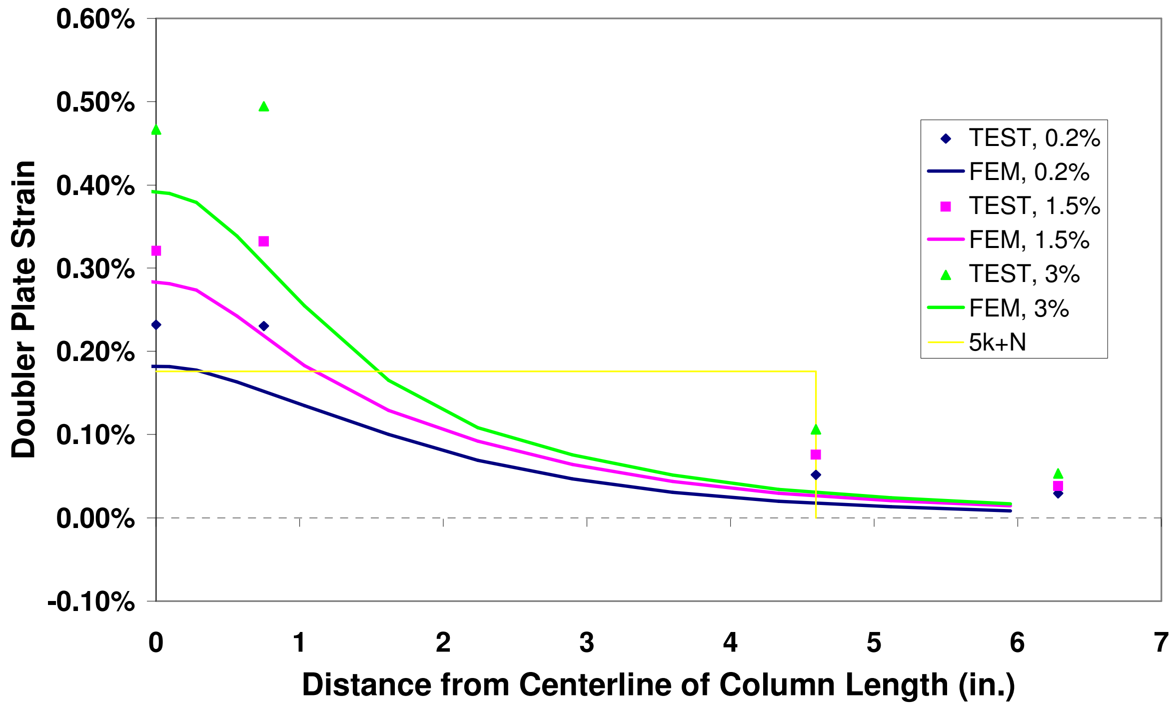

Figure 4.16: Strain Distribution in the Center of the Doubler Plate (1-DP)

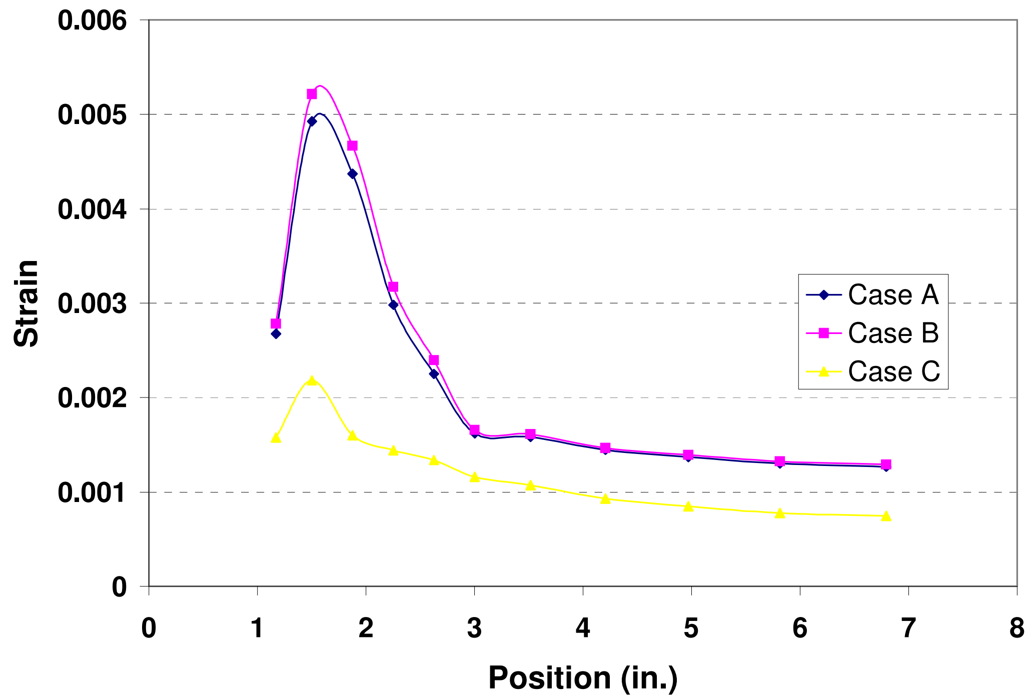

(a) Strain (E22) in the column Web

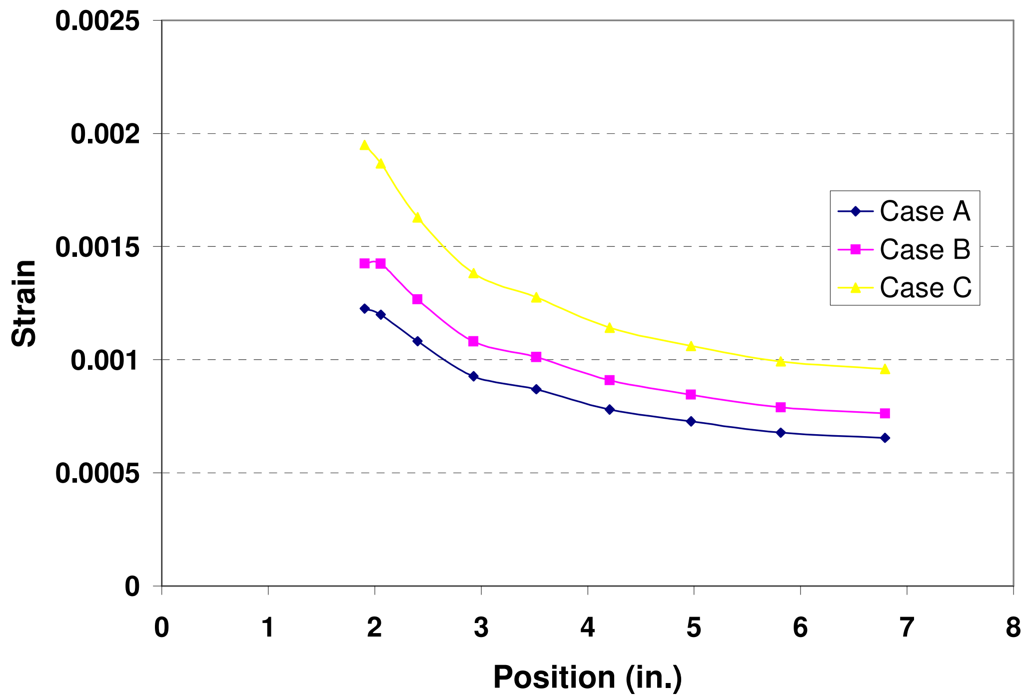

(b) Strain (E22) in the Doubler Plate

Figure 4.17: Comparison of Doubler Plate Location and Thickness
(at 0.2% specimens elongation)

Chapter 5

Analyses of Cruciform Specimens

To study the connection stiffener behavior under seismic load, five interior connection assemblies were tested. The girder size of all sections was a W24x94 and four W14 sections (W14x145, W14x176, W14x193, W14x283) were used for the columns. The test matrix for the cruciform specimens is summarized in Table 3.4. The typical test set up of the cruciform experiments is also shown in Chapter 3. Analysis results of the cruciform test specimens are discussed in this chapter. The connection global behavior, such as load versus deflection and moment versus rotation, are discussed first, followed by a discussion of localized behavior to assess the stiffener behavior. Details of the experiments including loading history, gage locations, and data reduction may be found in Cotton et al. (2001).

5.1 Global Connection Behavior

5.1.1 Load versus Deformation Behavior

Shown in Figure 5.1 are the analysis results of the applied girder end load versus interstory drift response of the specimens. As discussed in Chapter 3, the girder end displacement was increased monotonically to a peak value in the finite element model while quasi-static cyclic displacement was used in the experimental program. It is believed that the results from the monotonic loading analyses represent fairly well the envelope of the cyclic results (Leon et al., 1998). A displacement-controlled loading history was applied for all five finite element models. The applied girder end load *P* was calculated as the reaction force at the beam element node where the displacement was applied. The interstory drift, Δ_{story}, was related to the girder end displacement, Δ_{tip}, as follows:

$$\Delta_{story} = \frac{\Delta_{tip}}{(L_g + d_c / 2)} \tag{5.1}$$

where:

L_g = length between the column face and girder end

d_c = column depth

All five specimens were loaded to an interstory drift of 5%. It is shown in Figure 5.1 that specimens CR1, CR2, CR3, CR5 had similar girder end load response while specimen CR4 (the box detail) had a higher load capacity than the other four specimens at 5% interstory drift. The load increase after the initiation of significant inelastic response (i.e., the point at which the load-deformation response deviates substantially from linear response) of the five specimens was 42%, 44%, 19%, 17.5%, and 21.7%, respectively. Figure 5.2 shows the deformed shape of specimen CR3 at 5% interstory drift. Specimen CR4 has the least load increase after inelasticity occurred. Examination of the results showed that specimens CR1 and CR2 remained elastic up to approximately 1% interstory drift, (corresponding to a girder end displacement Δ_{tip}=1.4 inches) and that specimens CR3, CR4, and CR5 remained elastic up to approximately 1.5% interstory drift (corresponding to a girder end displacement Δ_{tip}=2.1 inches). Inelasticity first developed in the girder flange center at the interface and near the access hole. With an increase in load, the inelastic region spread to the girder flange-to-column flange interface. All five curves have approximately the same applied load capacity up to 1% interstory drift. Specimen CR5 had the lowest load capacity of approximately 55.4 kips and specimen CR1 had the highest load capacity of approximately 64.5 kips. All specimens remained largely elastic at this interstory drift level and the initial stiffness of the specimen could be determined from the slope of load-deformation curve.

5.1.2 Moment versus Plastic Rotation Behavior

Moment versus plastic rotation behavior for all five specimens was also examined to gain insight into the connection moment strength and rotation behavior. Figure 5.3 shows the girder moment versus connection plastic rotation curves. The moment has been normalized by the girder plastic moment (M_p). The girder moments were calculated by:

$$M = P * Lg \tag{5.2}$$

where:

P= girder end load

The connection plastic rotation, $\theta_{plastic}$, is calculated as the plastic tip displacement, $\Delta_{plastic}$, divided by the girder length:

$$\theta_{plastic} = \frac{\Delta_{plastic}}{L_g} \tag{5.3}$$

The plastic tip displacement is the total girder tip displacement, Δ_{total}, minus the elastic tip displacement, $\Delta_{elastic}$:

$$\Delta_{plastic} = \Delta_{total} - \Delta_{elastic} \tag{5.4}$$

$$\Delta_{elastic} = \frac{P}{k} \tag{5.5}$$

where:

k = initial stiffness, taken as the initial slope of the load-deformation curve determined from Figure 5.1

The analysis results showed that all connections had plastic rotations greater than 0.03 radians at 5% interstory drift. Plastic rotation occurred at approximately 1%-1.5% interstory drift. Thus, throughout this chapter, results are often shown at 5% interstory drift to show behavior beyond 0.03 radians of plastic rotation for all specimens. Specimen CR4 had the highest moment capacity (approximately 14,208 kip-in at 5% inter-story drift) among the five specimens and specimen CR2 had the lowest moment capacity (approximately 11,504 kip-in at 5% interstory drift). Specimens CR1, CR2, and CR5 had a moment capacity slightly lower than the girder plastic moment capacity. However, it should be recognized that the analysis results were based on models where only monotonically increasing loadings were applied. In the actual experiments, it is expected that the cyclic strain-hardening behavior of the material would further increase the connection moment capacity due to load reversal. In addition, it was observed from the analyses that at higher interstory drift levels, all the girder flanges were yielded. The connection regions were still subjected to the concentrated force developed by the girder strength capacity even though the whole girder section was not yielded.

The analyses showed that in specimens CR1, CR2, CR3 and CR5, the longitudinal stress near the extreme fiber at the center of the tensile girder flanges (normal bending stress S11) reached the yield stress, F_y, at approximately 0.75% interstory drift and at 1.0% interstory drift for specimen CR4. The corresponding moment when the maximum normal stress (S11) in the girder flange reached the yield stress for the five specimens was 6824 kip-in, 6021 kip-in, 6079 kip-in, 8550 kip-in and 5529 kip-in, respectively. From beam theory, the maximum moment when the extreme fiber reaches the yield stress is:

$$My = F_y * S_x = 50 * 222 = 11100 \text{ kip-in} \tag{5.6}$$

As discussed in the next section, even though the web was welded to the column flange, this discrepancy was due to focusing of the girder longitudinal stresses into the girder flanges near the connection region.

5.2 Boundary Effects in the Connection Region

For welded moment resisting frame connections using wide-flange sections, two assumptions are usually made in current design regarding stress transfer in the connection: (1) the couple produced by the girder flanges transmits the majority of the girder moments; (2) the girder web transmits the majority of the girder shear force. Finite element analyses of cruciform specimen models showed that the stress distribution patterns near the girder-to-column interface were not consistent with the above assumptions. Figure 5.4 shows the shear stress distribution in the girder web at 5% inter-story drift for specimen CR1. The shear stress along the girder web height is plotted at several locations along the girder length. The shear stress was not parabolically distributed along the girder height and the stress in the girder flanges is much higher. At the interface, the shear stress was highest near the top and bottom; while at the middle of the cross section, the shear stress changed sign. At approximately one and a half girder depths away from the interface, the boundary effect decayed quickly and the distribution pattern was consistent with beam theory. Shown in Figure 5.5 is the shear stress contour plot near the interface. It can be seen that the shear stress was not uniformly distributed along the web height and it changed sign along the height of the girder web near the interface. A similar distribution pattern was also observed at earlier load levels and for all specimens.

The boundary constraint also influences the stress flow pattern near the connection region. Figure 5.6 shows the principal stress contour plot near the connection region for specimen CR1 at 5% interstory drift. The arrows in the plot show the direction of the principal stress and the size of the arrows is proportional to the stress values. At this load level, the finite element analyses predicted that local kinking occurred at the boundary of the panel zone and that an inelastic region developed at the interface.

While these analyses are focused on welded flange-welded web connections, similar observations have been obtained in related research. Both experimental and computational research of pre-Northridge steel moment connections (welded flange-bolted web) has shown that the load transfer in the vicinity of the connection region is affected by the boundary restraints. Computational work by Goel et al. (1997), Hajjar et al. (1998), and El-Tawil et al. (1998) indicates that due to the boundary effect in welded steel moment connections, the girder flange force couple is transmitted diagonally near the interface of the girder-to-column flange.

5.3 Analysis Results in Girder Flange

To further examine the girder flange behavior near the interface, the stress and strain distributions in the girder flanges are plotted in Figures 5.7 to 5.11. The quantities are plotted near the extreme fiber in the bottom girder flange (tensile flange), near the girder-to-column CJP weld. The plots show quantities at increasing levels of interstory drift corresponding to the nine levels itemized in Table 3.5. Shown in the figures are the longitudinal stress (S11) and strain (E11) distributions across the girder flange width at different levels of interstory drift. The longitudinal bending stress (S11) was always highest at the center of the girder flange. The high stress concentration at the center was caused by high restraint from the column and the girder web. The inelastic region in the girder flange first occurred at the center. Also shown in the figures are the Mises Index and PEEQ index distribution across the girder flange width at the tensile flange. The Mises index is defined as the Von-Mises stress divided by the yield stress. The PEEQ index is the equivalent plastic strain divided by the yield strain:

$$Von\ Mises\ Index = \sqrt{\frac{3}{2} S_{ij} * S_{ij}} \,/\, F_y \tag{5.7}$$

$$PEEQ\ Index = \sqrt{\frac{2}{3} * \varepsilon_{ij}{}^{pl} \varepsilon_{ij}{}^{pl}} \,/\, \varepsilon_y \tag{5.8}$$

It can be seen that higher Von-Mises stress occurred at the girder flange center. First yielding of the girder flange began at the center at approximately 0.75% of interstory drift for connections CR1, CR2, CR3 and CR5 and began at approximately1% interstory drift for connection CR4. The flange generally yielded all across its width after 1% interstory drift. The whole girder flange was yielded at 5% of interstory drift for each of the specimens.

The center of the girder flange-to-column flange interface is seen to be the location of high constraint. Weld tearing may occur in the region if excessive plastic strain occurs at this location. The finite element analyses showed that the plastic strain was higher in the girder flange near the interface. A similar distribution pattern was observed for the longitudinal strain (E11) and the equivalent plastic strain index (PEEQ index). Comparisons of the PEEQ index across the girder flange width showed that the plastic strain demand at the interface was sensitive to the connection stiffener detail. For specimens CR2 and CR5, no continuity plates were present. A higher plastic strain gradient was observed. The peak PEEQ index occurred at the center, and then dropped quickly towards the girder flange edges. When continuity plates having a thickness of half of the girder flange thickness were added to the connection, as in specimen CR3, a somewhat more moderate PEEQ index gradient and magnitude were obtained. Similar results were observed for specimen CR1 (W14x283). Although no continuity plates were present in this connection, the PEEQ index distribution was more evenly distributed than those for unstiffened columns of W14x193 (specimen CR2) and W14x145 (specimen CR5). This suggested that either thick column flanges or continuity plates can effectively reduce the plastic strain demand at the girder-to-column interface at a given displacement level. For specimen CR4, the box detail, the analysis results showed that this detail also performed well by providing support to the column flanges. The plastic strain at the center was reduced compared to the unstiffened sections of specimens CR2 and CR5. It is noted that the plastic strain was a little higher at the tips of the girder flanges in specimen CR4. This was primarily caused by the higher stiffness towards the tip of the girder flange. When the doubler plates were moved towards the tip, more stress flowed to the stiffer region.

Comparison of the analysis results in the girder flange of the five cruciform specimens showed that the connection stiffeners and the column flanges affect the stress and strain distribution pattern and that the highest plastic strain demand occurred at the center of the girder flange-to-column flange interface. However, the analyses indicated that the plastic strains were still less than 0.04 at 5% interstory drift. Experimental results with the unstiffened pull plate specimens showed that, provided welds have minimum required toughness, these non-uniform stress and strain fields do not cause weld fractures (Prochnow et al., 2000). Therefore that, the practical significance of those stress and strain concentrations is limited.

Shown in Figure 5.11(b) is a comparison of strain (parallel to the pull plate or girder flange) near the girder-to-column CJP welds at several load levels for pull plate specimen 2-LFB and cruciform specimen CR5, both of which are W14x145 A992 columns with doubler plates. The pull plate analysis has a pull plate that is a little larger than the W24x94 girder in specimen CR5. Otherwise, the models are similar in the localized region shown in the plots. The different levels shown in the plots correspond to those itemized in Tables 3.2 and 3.5. The highest load levels shown are approximately similar in magnitude and thus similar forces are being applied to the column flanges at this stage. The quantities are plotted across the pull plate or girder width. The comparison shows that similar strain distribution patterns were observed in both models, which indicated that the strains in the pull plate provide a similar representation of strain distribution to that in the actual girder flange in the cruciform models. Deierlein and Chi (1999) provide further discussion comparing pull plate and cruciform results.

5.4 Panel Zone Behavior

5.4.1 Panel Zone Deformation

For steel moment frame connections, panel zone behavior can significantly influence the whole connection behavior. Figure 5.6 shows the principal stress directions of the panel zone for specimen CR1 at 5% interstory drift. The principal stresses in the panel zones were all oriented at approximately 45 degrees with respect to the horizontal axis, which indicates a dominant pure shear stress state. The maximum normal stress values from the analyses were only 2 ksi. The analyses for the other four specimens showed similar results. Furthermore, the analyses showed that the shear stress and strain were relatively uniformly distributed within the panel zone, with a somewhat higher magnitude near the fillet welds connecting the doubler plates to the column flange. Figure 5.12 shows the panel zone plastic strain contours at 1% and 5% interstory drift for specimen CR1. Panel zone yielding first occurred at the center. With an increase of the girder tip load, the plastic zone developed towards the edge of the panel zone. Almost the whole panel zone was yielded when 5% interstory drift was reached in all five specimens.

Panel zone deformation was calculated from the diagonal displacement within the panel zone. The diagonal deformation was measured by two LVDTs placed diagonally in the test. The finite element analysis results were obtained from the nodal displacement in the corresponding locations (see Appendix E). The deformation in the panel zone γ is taken as the average of the two diagonal deformations:

$$\gamma^{ave} = \frac{|\Delta_1| + |\Delta_2|}{2} * \frac{\sqrt{b^2 + h^2}}{bh} \tag{5.9}$$

where:

Δ_1, Δ_2 are the diagonal displacements in the panel zone

b, h are panel zone width and heights respectively

The deformation at yield, γ_y, is defined as:

$$\gamma_y = \frac{F_y}{\sqrt{3} * G} \tag{5.10}$$

where:

F_y =yield stress of the panel zone

G = shear modulus

Shown in Figure 5.13 are the analysis results of the girder end load versus panel zone deformation for the cruciform specimens. Both the initial stiffness and the post-yield panel zone deformation differred for the five specimens. Specimen CR1 (W14x283, P_z/P_g=1.1, see Table 3.4) had the highest initial joint stiffness as can been seen from the initial slope of the load-deformation curve. However, the inelastic deformation in the panel zone initiated relatively early in CR1, at about 0.005 radians of panel zone deformation, with a girder tip load of 65 kips. Specimen CR2 (W14x193, P_z/P_g=1.01) had a slightly smaller initial joint stiffness than CR1, but the inelastic panel zone deformation initiated at about the same level as CR1 (i.e., at a panel zone deformation of 0.005 radians and girder tip load of 60 kips). Specimens CR3, CR4, and CR5 all had a smaller initial stiffness than specimen CR1, but the inelastic panel zone deformation initiated at a larger load level and higher panel zone deformation. Inelastic panel zone deformation began at about 0.008 radians for these three connections, which correspond to a girder tip load of 82 kips, 92 kips, and 77.2 kips for specimens CR3 to CR5, respectively. The total panel zone deformation reached at 5% interstory drift was 0.04 radians, 0.039 radians, 0.036 radians, 0.018 radians, and 0.035 radians for specimens CR1 to CR5, respectively.

Figure 5.14 shows the panel zone plastic rotation compared with the total connection plastic rotation at each load level. It can be seen that panel zone deformation contributed greater than 50% to the total connection plastic rotation for specimens CR1, CR2, CR3, and CR5. Listed in Table 5.1 is the percentage of total connection plastic rotation contributed from the panel zone deformation at 5% interstory drift. For specimens CR1, CR2, CR3, and CR5 with a P_z/P_g ratio range from 1.0 to 1.2, the panel zone deformation contributed more than 75% of the total plastic rotation. In specimen CR1, 85% of the connection plastic rotation occurred in the panel zone. For specimen

CR4 with a stronger panel zone (P_z/P_g=1.49), the panel zone plastic rotation was greatly reduced. A total connection plastic rotation of 0.035 radians was reached at 5% interstory drift for specimen CR4, 29% of which was contributed from the panel zone shear deformation. The analysis results indicated that the box detail performed approximately as effectively as those doubler plates attached directly to column web to strengthen the panel zone region, thus reducing the panel zone deformation.

5.4.2 Panel Zone Shear

The AISC (1997) seismic design equation for panel zone shear includes both the shear resistance from the column web and the boundary members (i.e., the column flanges). The post-yielding strength of the panel zone was thought to provide additional shear resistance after initial yielding. It is generally considered that the panel zone shear strength should be reached when the panel zone deformation of $4\gamma_y$ is reached (Krawinkler et al., 1978). The AISC (1997) shear strength of the panel zone, R_v, is calculated from Equation 2.7. The required panel zone shear, V_u, is generally calculated from force equilibrium of the connection:

$$V_u = \frac{\sum M}{d_g} - V_c \qquad (5.11)$$

where:

M=moment at the column face

V_c=column shear force, calculated from the column support reaction force

Figure 5.15 shows the analysis results of the panel zone shear versus panel zone deformation of the cruciform specimens. The panel zone shear has been normalized by the nominal shear capacity R_v (Equation (2.7)) and the panel zone deformation has been normalized by the deformation at yield γ_y (Equation (5.10)). It was observed that shear yielding began at approximately $2\gamma_y$ for specimens CR1 and CR2, and at approximately 3-3.5 γ_y for other three specimens. At a panel zone deformation of $4\gamma_y$, the shear strength for all five specimens did not reach the AISC (1997) design values. Table 5.2 shows the comparison of the shear force in the panel zone obtained from the finite element analysis at a panel zone deformation of $4\gamma_y$ and from the AISC (1997) design equations. For specimen CR1, CR2, CR3 and CR5, an average V/V_n ratio of 0.8 was observed. It can be seen that significant panel zone deformation would develop before the specimens could reach the shear capacity.

In FEMA (2000a), the check of panel strength (Equation (2.7)) has been removed. Instead, the panel zone thickness is based on the concept of balanced yielding of the panel zone and the girder (FEMA, 2000a). The panel zone strength is limited to the elastic shear yielding strength so as to control the total deformation of the panel zone. The required panel zone strength is based on the flexural strength of the adjoining girder:

$$t = \frac{M_{yg} \dfrac{h - d_g}{h}}{(0.9)0.55 F_{yc} d_c (d_b - t_{gb})} \tag{5.12}$$

Shown in Figure 5.16 is the comparison of the panel zone shear strength versus the girder moment. The panel zone shear was normalized by the panel zone strength ($R_v = 0.55 F_{yc} d_c t_p$) proposed in FEMA (2000a), where t_p is the thickness of the panel zone. The moments have been normalized by the girder yield moment ($M_y = F_y * S_g$, where S_g is the elastic section modulus). It was observed that for specimens CR4, with a stronger panel zone (P_z/P_g=1.49), the flexural yielding of the girder occurred before the panel zone strength was reached. For specimens CR1 and CR2 (P_z/P_g<1.1), with relatively smaller panel zone strength, more yielding occurred in the panel zone region. For specimens CR3 and CR5 (P_z/P_g=1.2), the analysis showed that the shear strength of the panel zone and the flexural strength of the girder were reached at approximately the same time. This conclusion is consistent with the analysis results obtained from the panel zone deformation. More yielding occurred in the panel zone when a higher percentage of the plastic deformation came from the panel zone region.

The post-yielding strength of the panel zone comes from the strain hardening of the material in this region. Furthermore, the boundary elements of the panel zone (i.e., the column flanges) provide the confinement which contributes to the panel zone achieving a strength increase after first yielding. This increase of post-yielding strength of the panel zone is based on the analysis results of Krawinkler et al. (1978) and is reflected in the last term (K-term) of Equation (2.7), which is defined as:

$$K\ term = \frac{3b_{cf} {t_{cf}}^2}{d_g d_c t_p} \tag{5.13}$$

where:

b_{cf} = column flange width

t_{cf} = column flange thickness

d_c = column depth

d_g = girder depth

Table 5.2 shows the post-elastic shear strength for five specimens. The finite element analysis results agreed well with the current design provisions for specimens CR2 to CR5. However, a larger difference was observed for connection CR1 with thicker column flanges. (t_{cf}=2.07 in.). The predicted increase is 39%, while only 16% is calculated from finite element analysis. This is consistent with the computational results obtained by El-Tawil et al. (1998). Their study showed that Equation (5.13) slightly overestimates the strength of a one-sided connection with a thicker column flange (t_{cf}=3.2 inches).

5.5 Analysis Results in Column Flange

The concentrated force imparted on the column flanges by the girder flanges leads to the inelastic deformation of column flange. Figure 5.17 shows the longitudinal strain (E22) and transverse strain (E33) distribution near the inside surface of column flange opposite to the tensile girder flange tip at 5% interstory drift. The quantities are plotted along the length of the column. The plots indicate that the peak stress and strain occurred at the girder flange location. Stress and strain quickly decayed away from that region. The column flange exhibited two way bending, both along the length and transverse to the column flange width, as observed in the pull plate experiments. The analyses showed that bending along the column length (longitudinal direction) was more significant compared to that in the transverse direction.

Shown in Figure 5.18(a) is the longitudinal strain (E22) near the inside surface of the column flange at the tensile girder flange location. The quantities were plotted along the width of the column flange at 5% interstory drift. The longitudinal strains in the column flange were influenced both by the flange bending and the material Possion effect, where additional strains developed by the deformation in the other two directions. For specimen CR1, with a thicker column flange, all the longitudinal strain is compressive and the peak value of approximately 0.004 occurred at the flange tip. The other four specimens all had tensile strain near the web and compressive strain developed at approximately 1.5 inches from the web centerline. A higher strain gradient was observed in specimens CR2 and CR5. Also shown in the figure is the strain distribution in the same location of pull plate specimen 2-LFB (W14x145 column) at 2% specimen elongation, which corresponds to approximately the same load level in the girder flange. Compared with the specimen having the same column size, specimen CR5, a similar strain distribution pattern was observed in both models.

Shown in Figure 5.18(b) is the PEEQ index at the same location. The analysis results showed that at 5% intersorty drift, the plastic strain at the column flange was not significant. The highest plastic strain at the flange tip of specimen CR1 was only 1.3 times of the yield strain. Comparison of these quantities with those obtained at the girder flange indicated that much higher strain developed in the girder flange near the interface. The stress and strain distributions in the girder flanges were thus generally more critical to the connection behavior.

Comparisons between the five specimens showed that the relative column flange stiffness and connection details such as the continuity plate and doubler plate affect the stress and strain distribution in the column flange, as expected. For specimen CR1, which had a relatively thicker flange, the analyses showed that the flange performed well without continuity plate. The column flange was adequate to provide resistance to the force delivered by the girder flange. Higher stress was absorbed in the column flange due to the relatively high stiffness of the column flange (W14x283). Thus, higher strain (E22) occurred in specimen CR1. For connections with continuity plates and box detail doubler plates, most of the stresses were transferred directly to the stiffeners. The stress and strain in the column flanges were reduced.

For the cruciform specimens, the girders were subjected to opposite loading at each side. The column flanges were subjected tensile force on one side, while compressive force was applied on the opposite side. Unlike in the pull plate tests, the column flanges at each side moved together instead of separating as seen in the pull plate tests. Figure 5.19 shows the column flange displacement (in the 1-1 direction) along the width at 5% interstory drift. The quantities plotted here are the displacement relative to the column web. It can be seen that the out-of-plane column flange displacement for all specimens at this load level were all less than 1/8 inches. For specimens CR1, CR3, and CR4, the relative displacements were reduced due to the presence of a thicker column flange (CR1) and column stiffeners (CR3 and CR4). From the AISC (1997) design provisions regarding local flange bending, specimen CR5 (W14x145 column) could only provide 52% of the required strength. However, the finite element analysis showed that the maximum flange displacement relative to the column web was only approximately 0.1 inches for specimen CR5. In addition, the separation of the column flange at the bottom girder level was only about 0.016 inches at 5% interstory drift. It is expected that this magnitude of column flange deformation will not significantly deteriorate the column axial strength. The deformation in the panel zone may have more influence on the column axial strength. To compare the flange displacement in pull plate model 2-LFB (W14x145 column) and cruciform model CR5, the flange displacement of the pull plate specimen is also plotted in the same figure. A similar flange displaced shape is observed in the pull plate and cruciform models.

Table 5.1: Comparison of Panel Zone Deformation at 5% Interstory Drift

	CR1	**CR2**	**CR3**	**CR4**	**CR5**
P_z/P_g	1.1	1.01	1.2	1.49	1.20
Total Plastic Rotation	0.0397	0.0377	0.0361	0.0353	0.0350
PZ Plastic Rotation	0.0335	0.0320	0.0279	0.0101	0.0263
% of Total Connection Rotation	85.71%	84.96%	77.29%	28.75%	75.03%

Table 5.2: Comparison of Panel Zone Shear

	CR1	**CR2**	**CR3**	**CR4**	**CR5**
R_v **(AISC,1997) (kips)**	903	824.17	935.01	1163.31	923.94
***V* @ First Yield (kips)**	580	550	700	834.00	693.00
***V* at** $4\gamma_y$ **(kips)**	673.47	655.16	756.96	906.64	725.13
V/R_v **(kips)**	0.75	0.79	0.81	0.78	0.78
***K* term (AISC, 1997)**	0.39	0.17	0.12	0.09	0.08
***K* term (Analysis)**	0.16	0.19	0.08	0.10	0.05

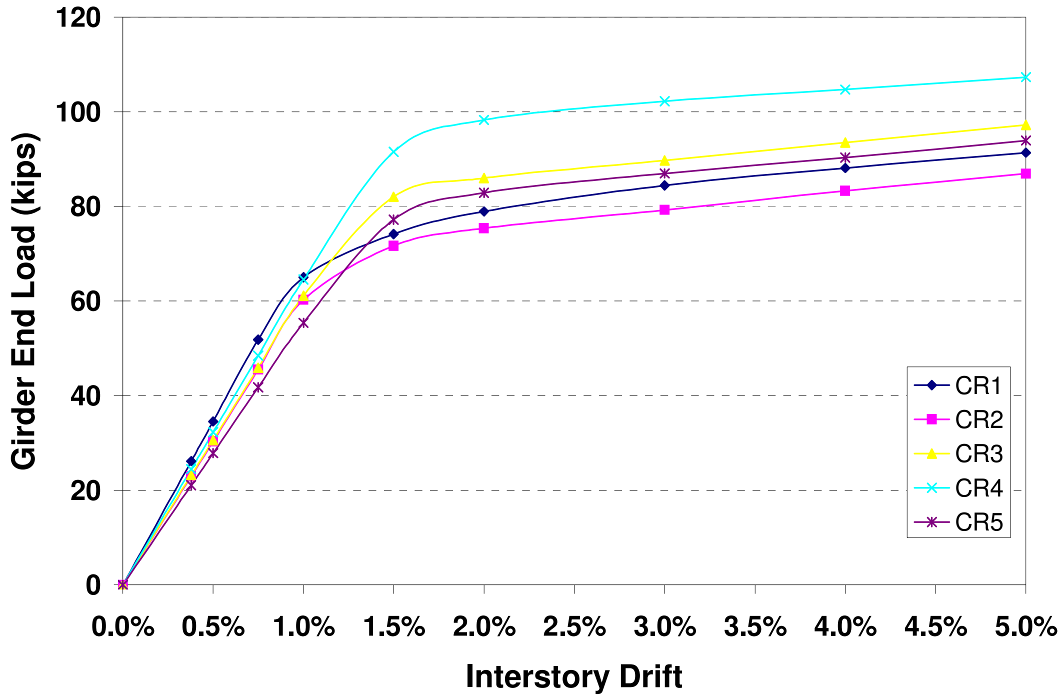

Figure 5.1: Girder End Load versus Interstory Drift

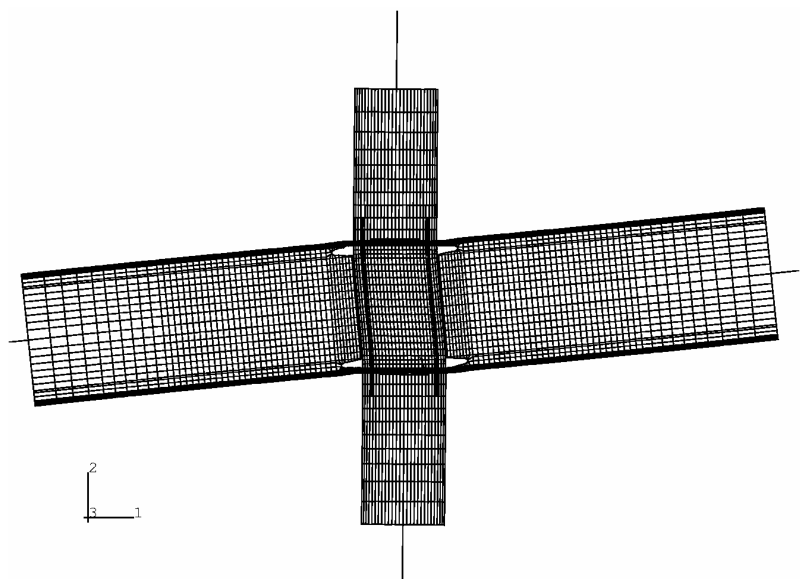

Figure 5.2: Deformed Shape of Connection Region at 5% Interstory Drift for CR3 (magnification factor=2)

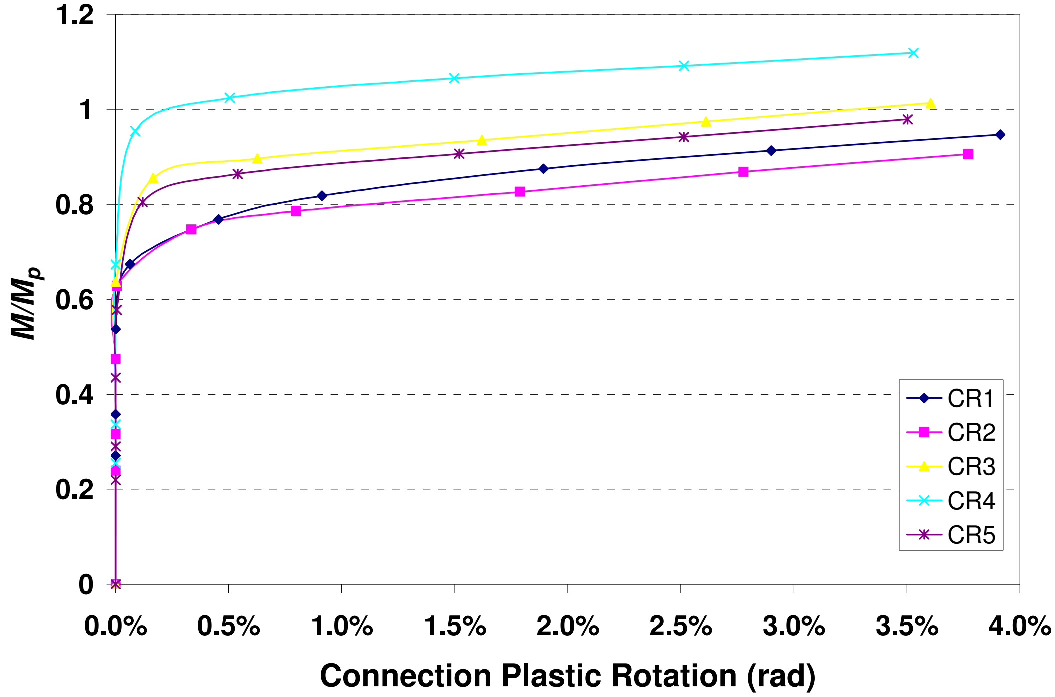

Figure 5.3: Moment Versus Connection Plastic Rotation

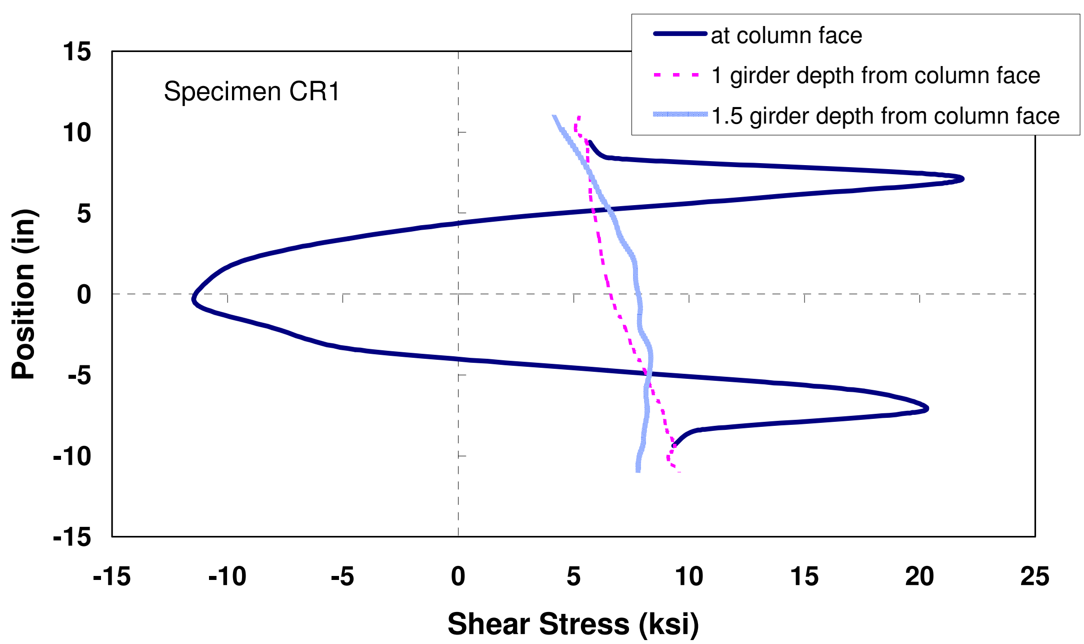

Figure 5.4: Specimen CR1 Shear Distribution in the Girder Web at 5% Interstory Drift

(Y-axis is the distance from the web center)

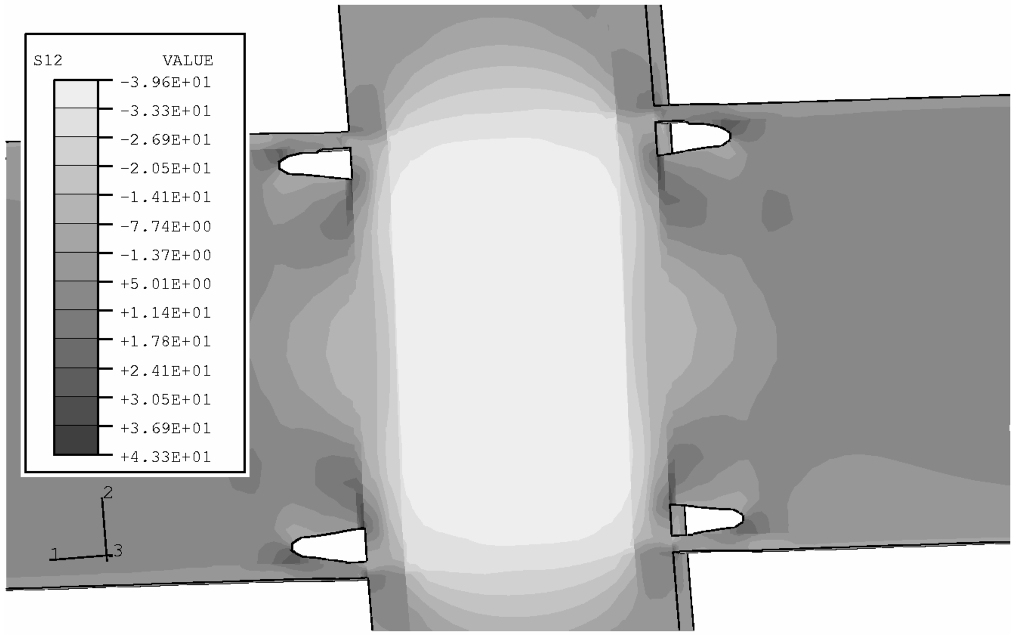

Figure 5.5: Specimen CR1 Contour of Shear Stress near the Interface at 5% Interstory Drift

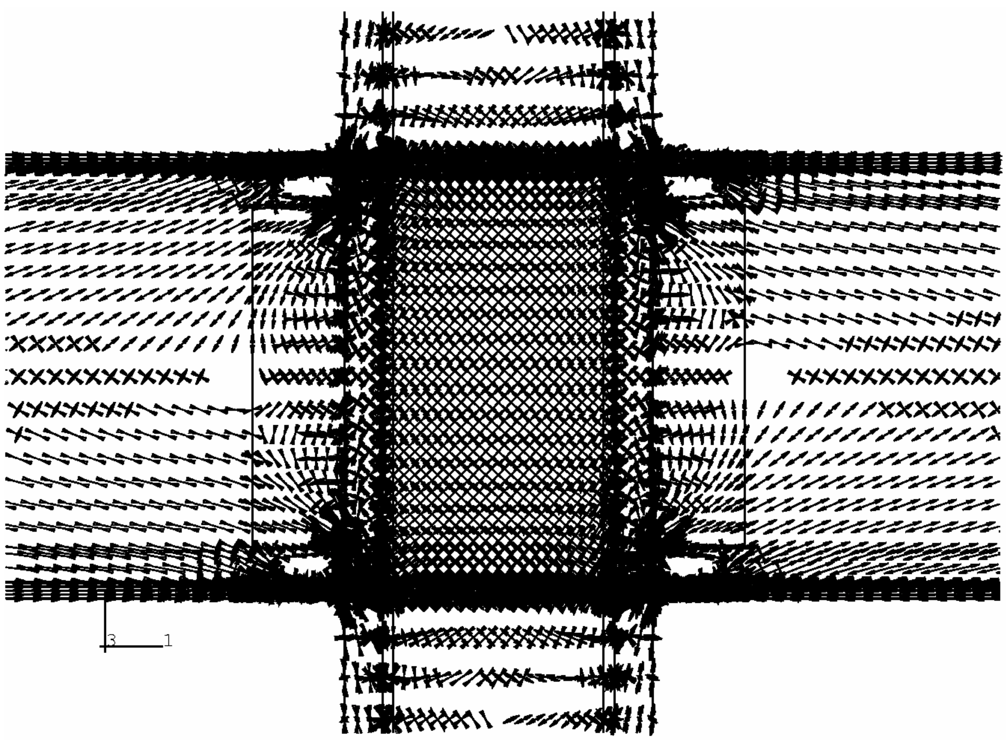

Figure 5.6: Specimen CR1 Principle Stress near the Connection Region at 5% Interstory Drift

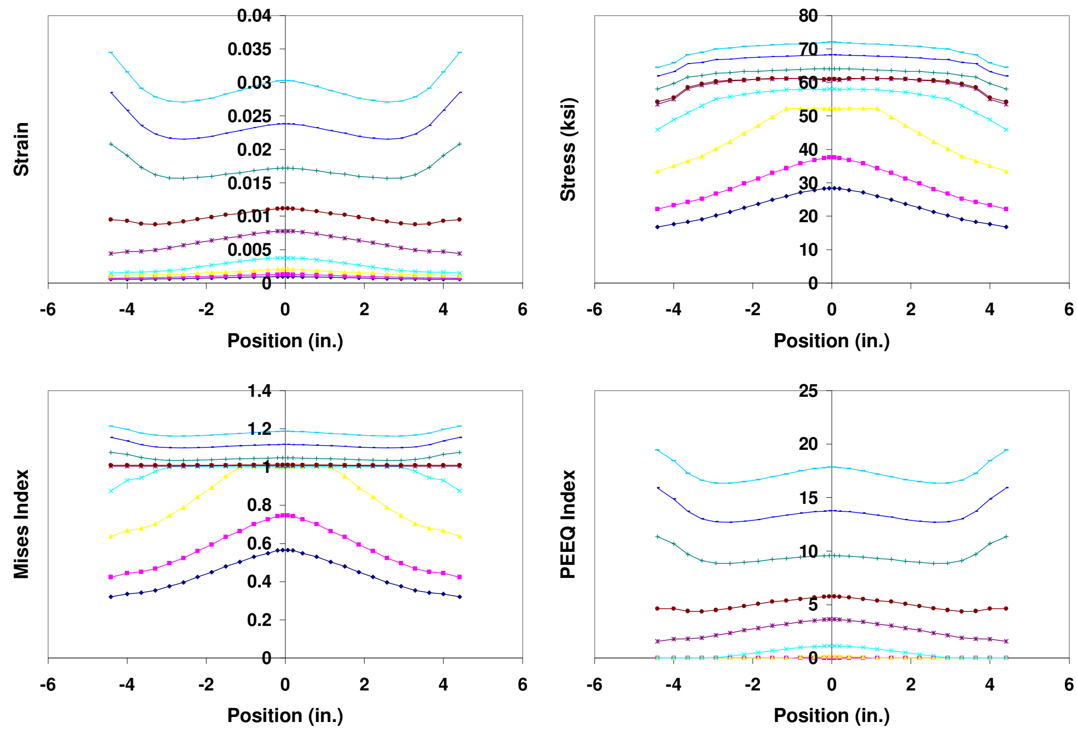

Figure 5.7: Stress and Strain Distribution in Girder Flange near the CJP Welds (CR1)

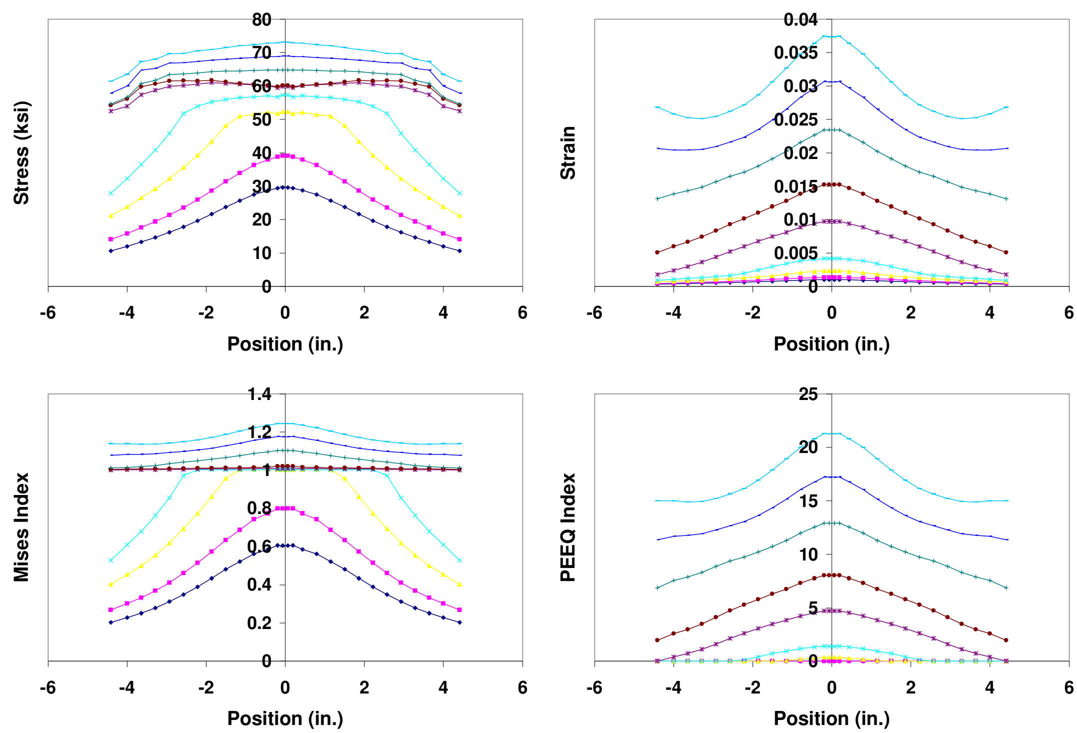

Figure 5.8: Stress and Strain Distribution in Girder Flange near the CJP Welds (CR2)

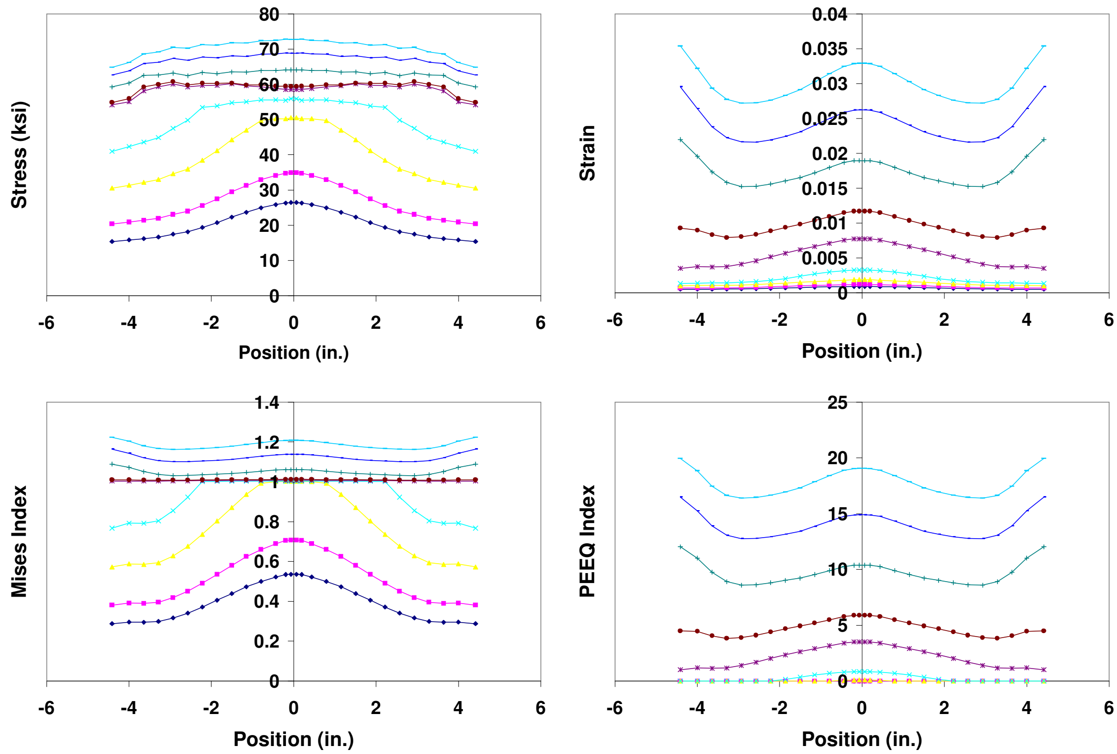

Figure 5.9: Stress and Strain Distribution in Girder Flange near the CJP (CR3)

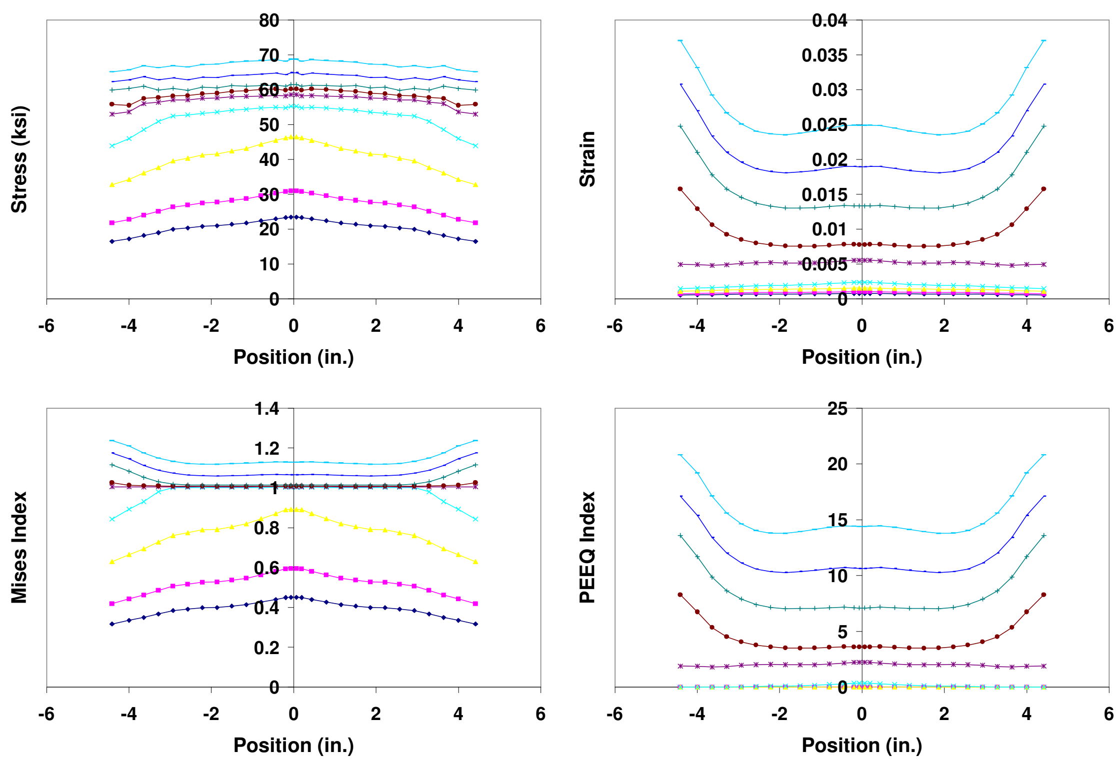

Figure 5.10: Stress and Strain Distribution in Girder Flange near the CJP Welds (CR4)

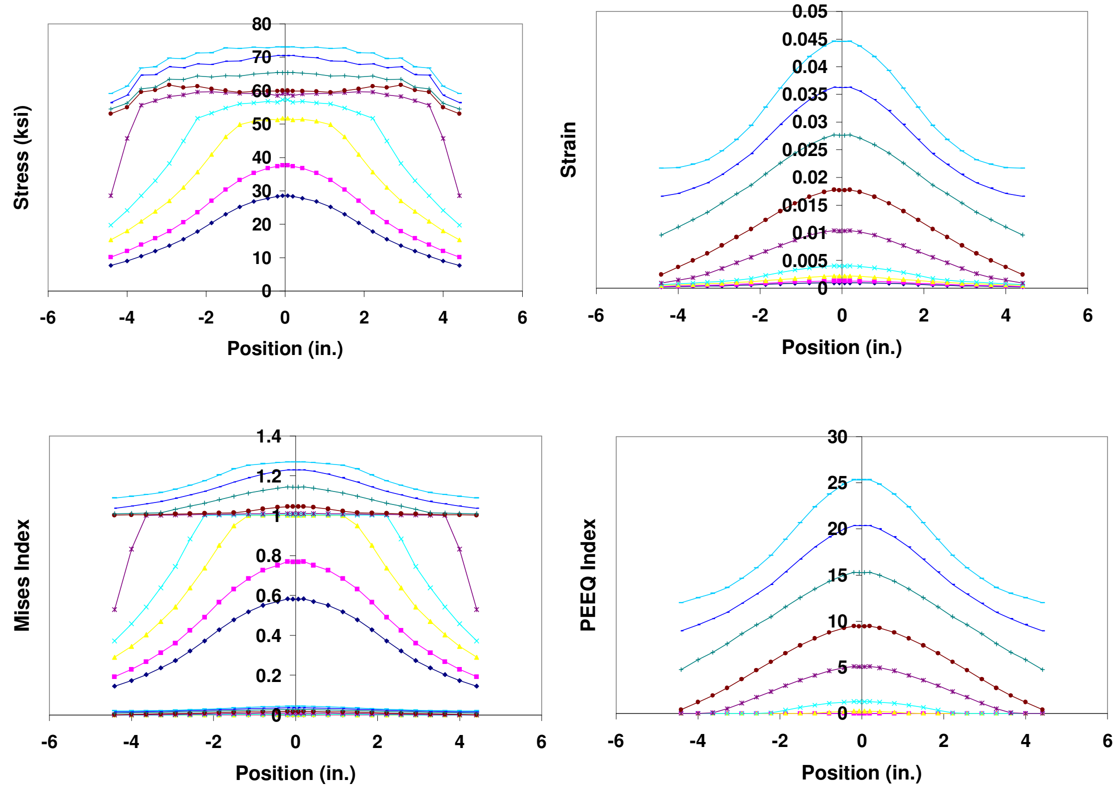

Figure 5.11(a): Stress and Strain Distribution in Girder Flange near the CJP Welds (CR5)

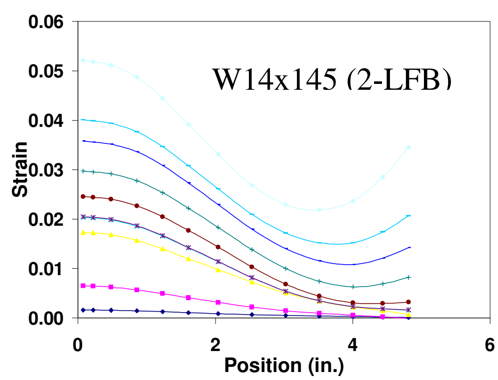

Strain in pull plate near CJP welds

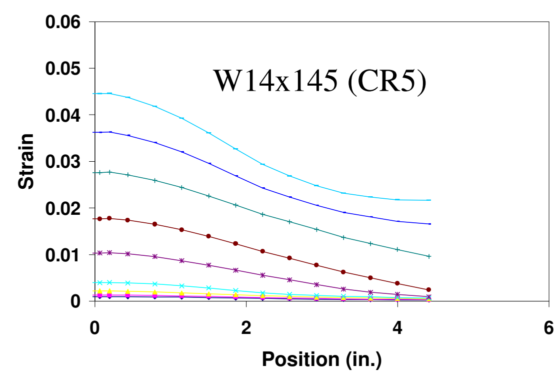

Strain in cruciform girder flange near CJP welds

Figure 5.11(b): Comparison of Girder Flange Strain in Pull Plate and Cruciform Models (x-axis is the distance from the center of the girder flange, the strains are plotted at progressive load levels)

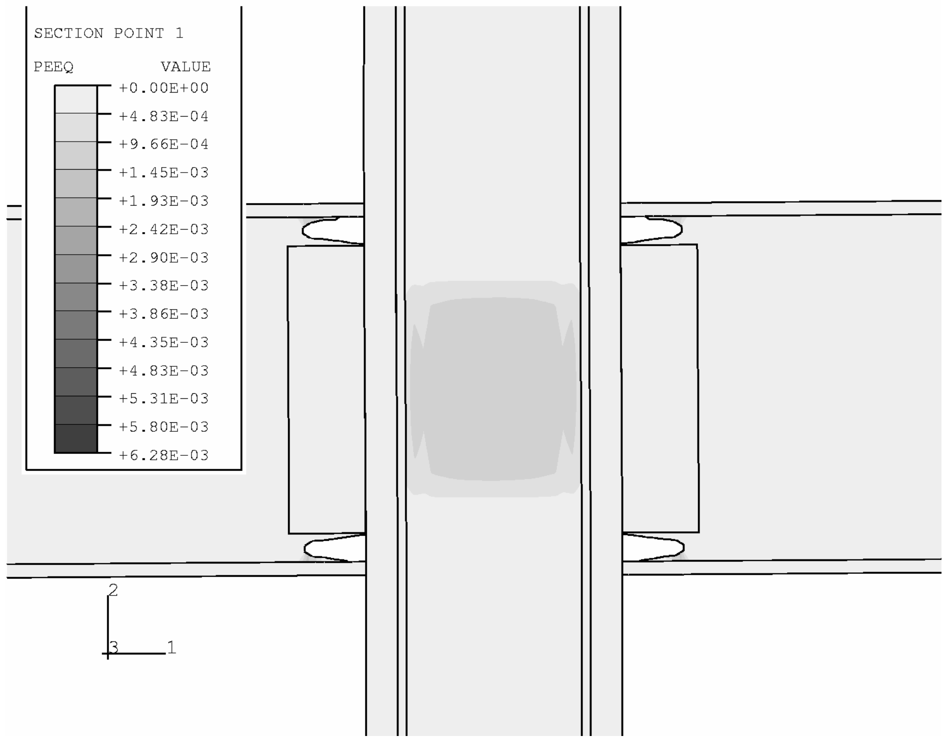

(a) 1% interstory drift

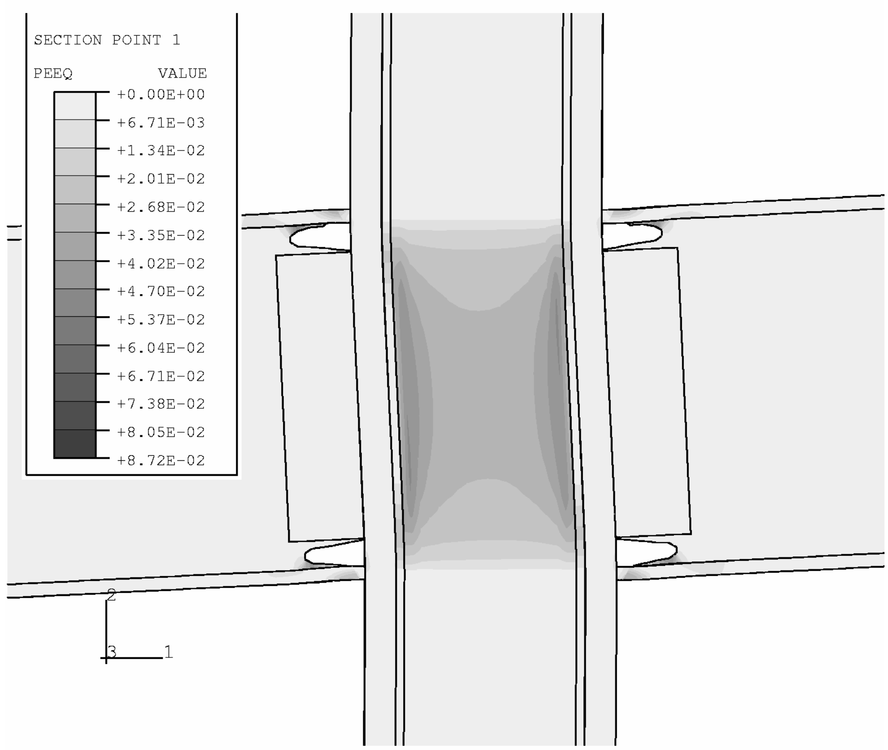

(b) 5% interstory drift

Figure 5.12: Specimen CR1 Contour of Equivalent Plastic Strain in Panel Zone

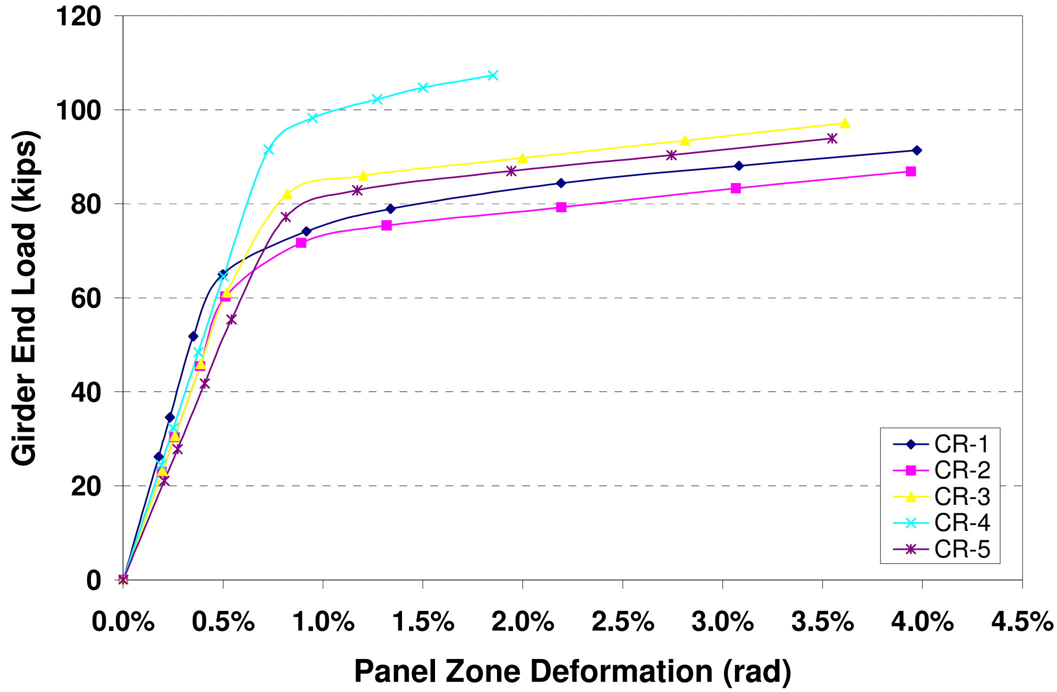

Figure 5.13: Girder End Load versus Panel Zone Deformation

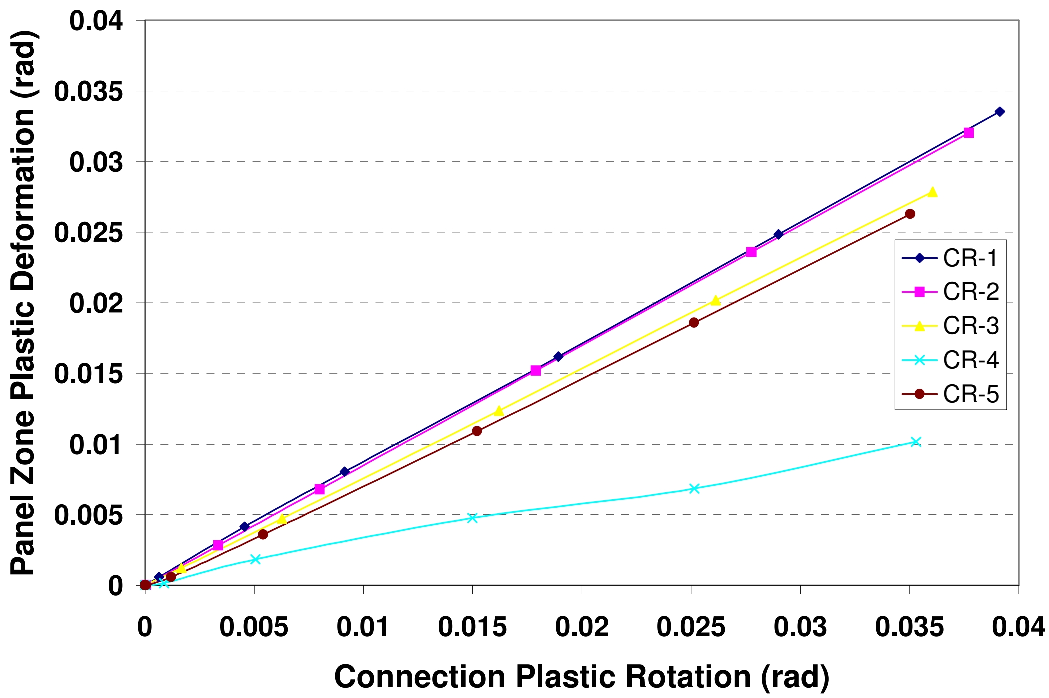

Figure 5.14: Panel Zone Plastic Deformation

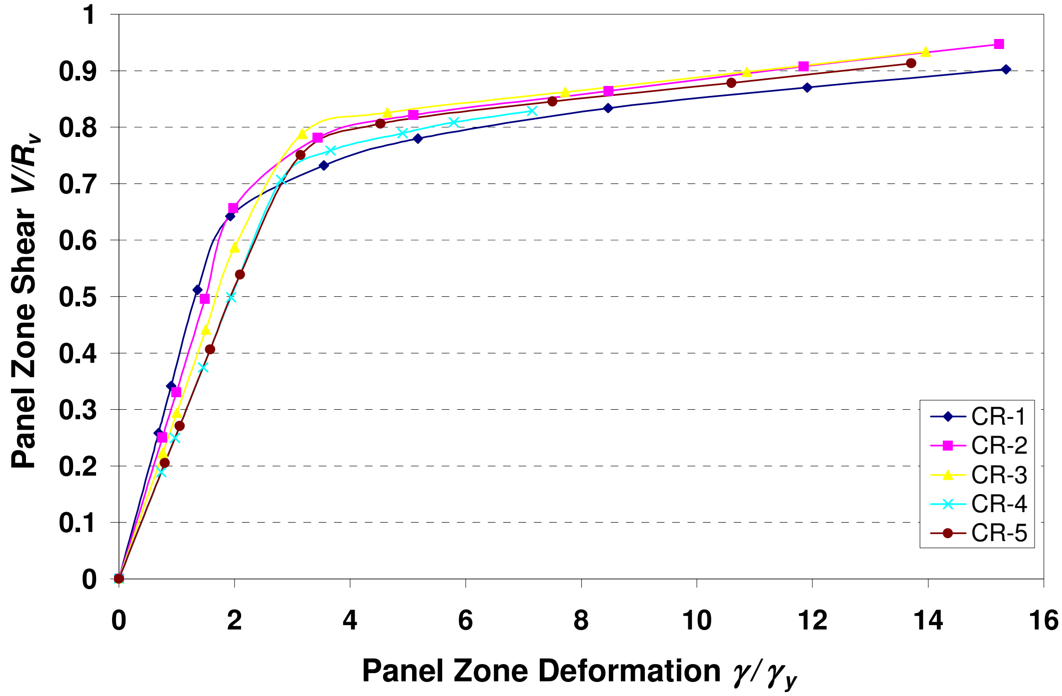

Figure 5.15: Panel Zone Shear versus Panel Zone Deformation

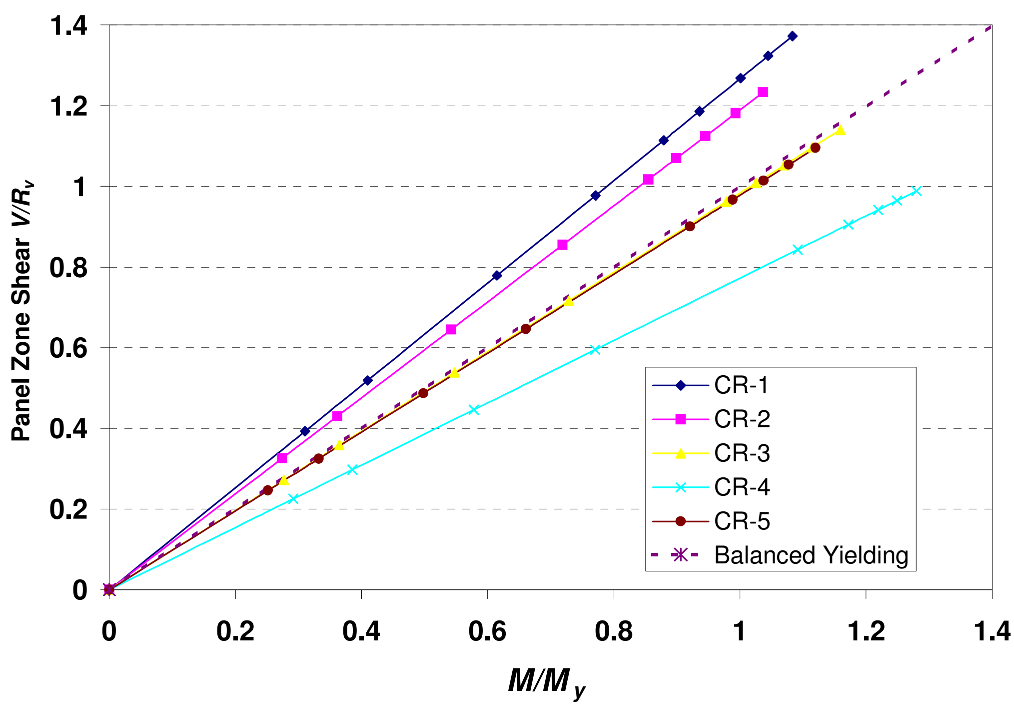

Figure 5.16: Panel Zone Shear versus Girder Moment

(Panel zone shear is normalized by FEMA (2000a) shear strength)

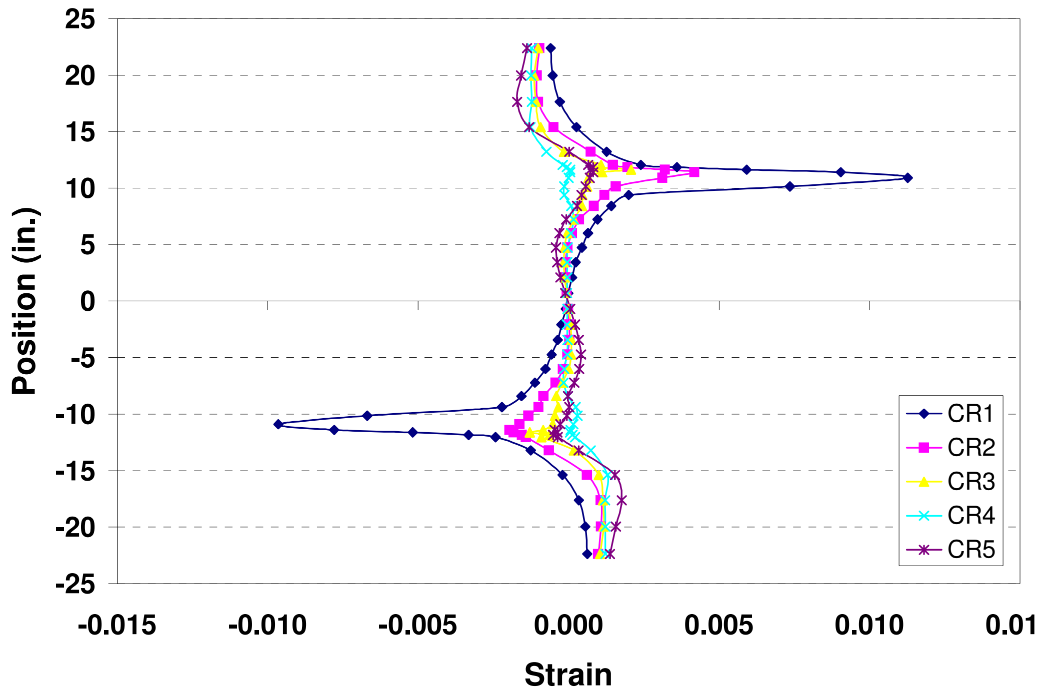

(a) Longitudinal Strain

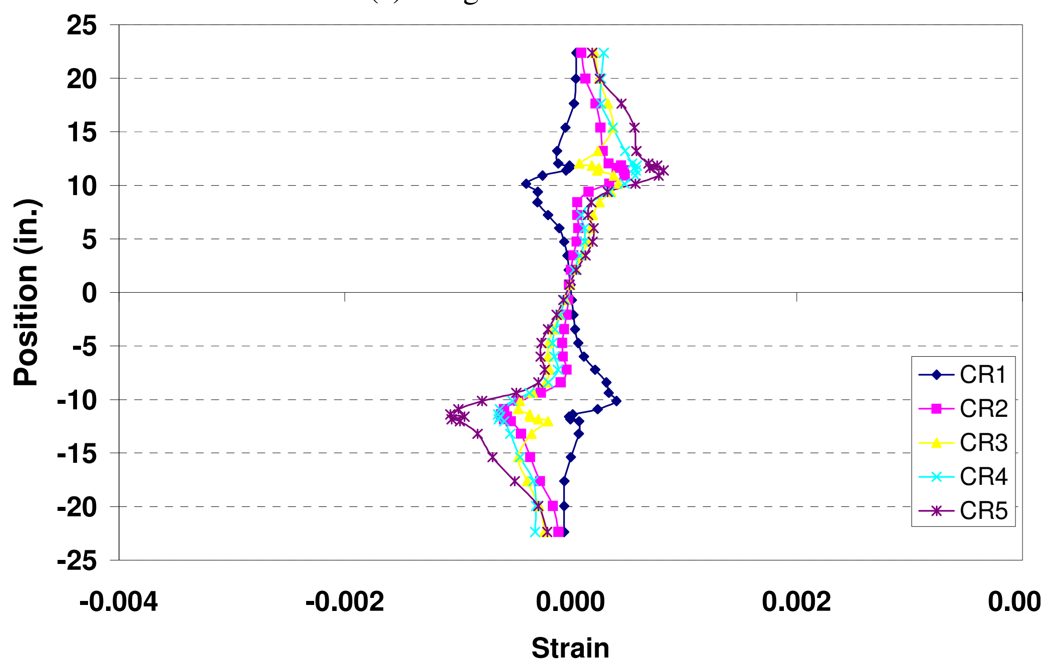

(b) Transverse Strain

Figure 5.17: Strain Distribution in Column Flange at 5% Interstory Drift

(Y-axis is the longitudinal distance along the column length from the girder flange centroid; the location is near the inner face of the column flange opposite to the tip of the girder flange)

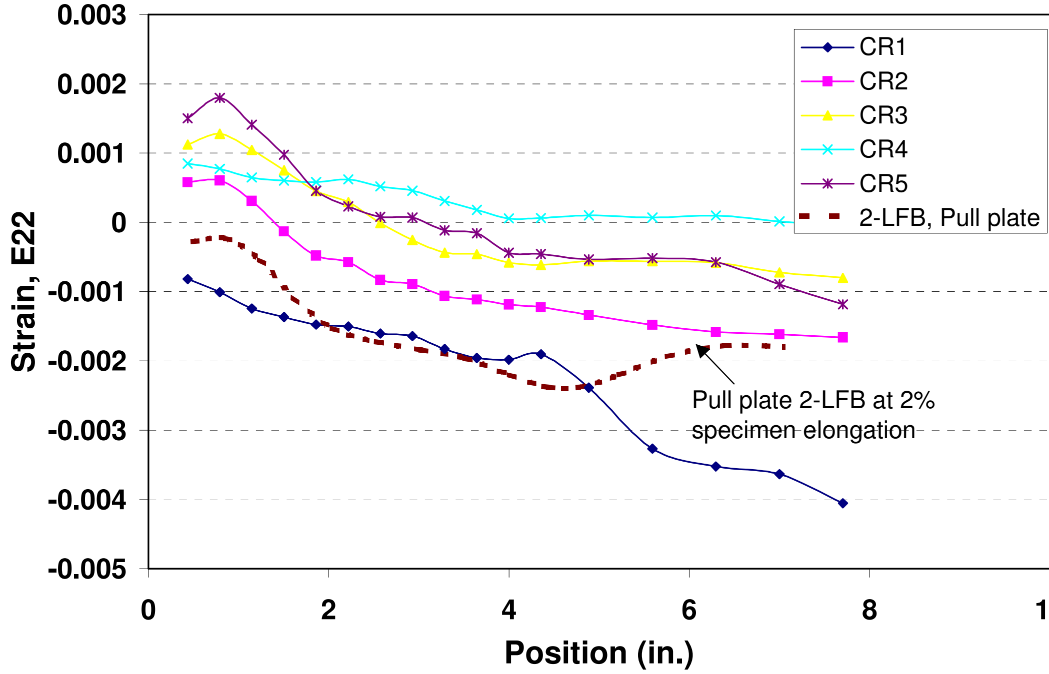

(a) Longitudinal strain

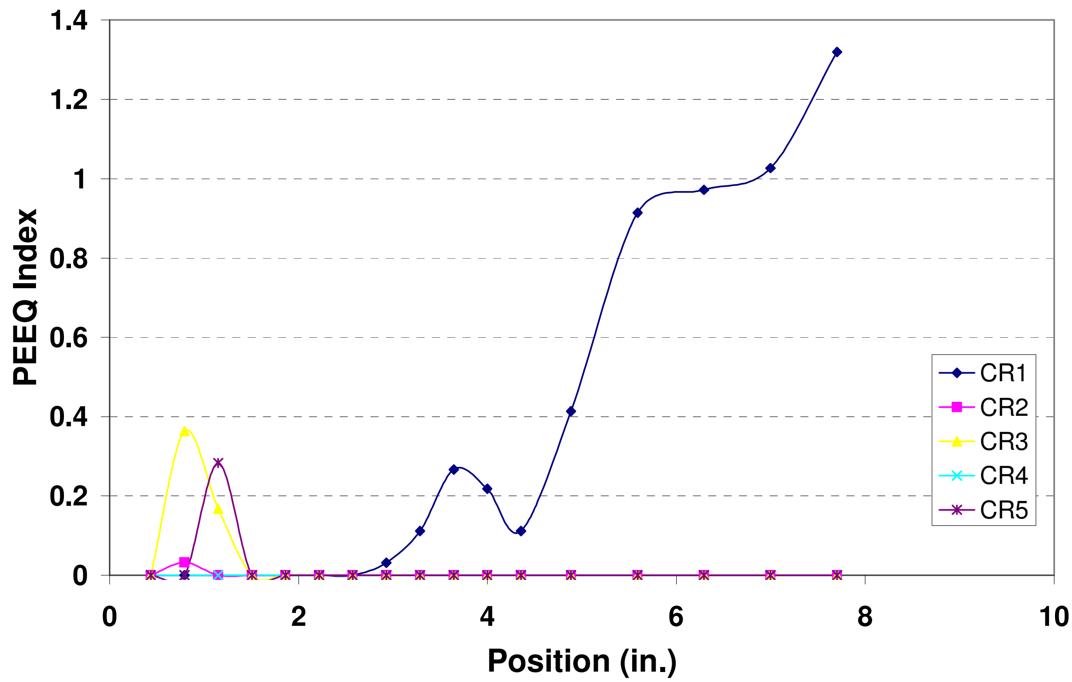

(b) PEEQ index

Figure 5.18: Longitudinal Strain (E22) and PEEQ Index in Column Flanges at 5% Interstory Drift

(along column flange width at tensile girder flange level)

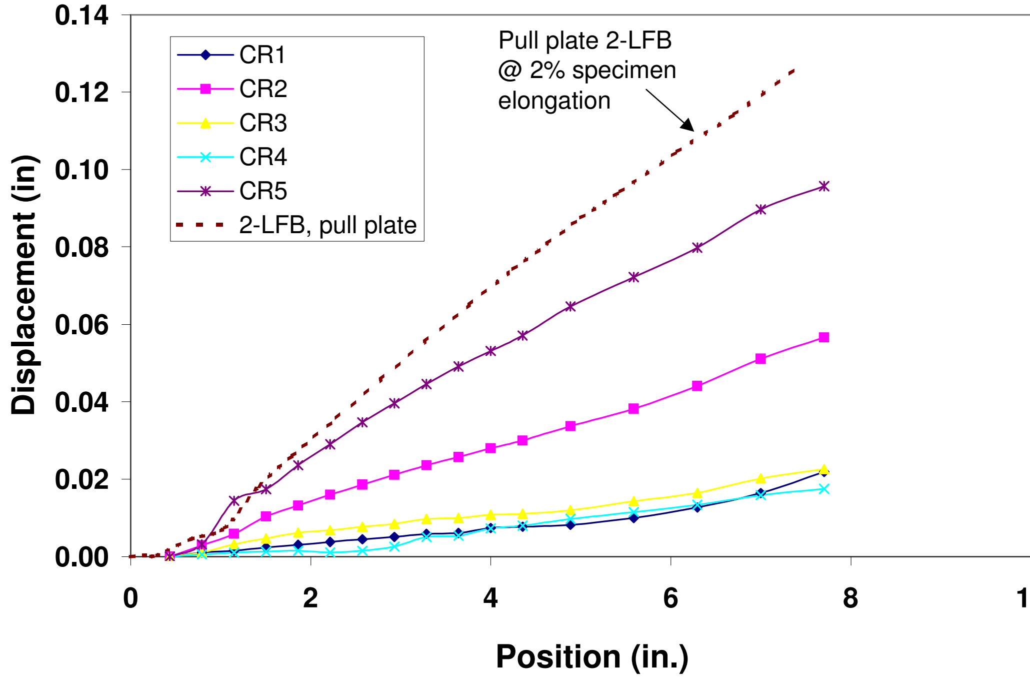

Figure 5.19: Column Flange Displacement at 5% Interstory Drift (displacement U1 is relative to the column web)

Chapter 6

Parametric Studies

Several parametric studies were conducted on the key variables of the girder-to-column connections. These studies are intended to extrapolate the test results to a wider range of parameters covered. The key variables included the continuity plate thickness, the column flange thickness, panel zone (column web and doubler plate) thickness, and the doubler plate location. The basic connection configurations were based on the cruciform test specimens. Other sections were also included for the parametric studies. Listed in Table 6.1 to Table 6.5 are the detailed connection configurations analyzed in each group. The equations used in calculating the ratios are summarized in Appendix D. The material properties used in the parametric studies are nominal stress strain properties for A992 steel based on the research by Frank (1999), and E70 weld metal. Finite element models used in the parametric study were generated in a similar method as discussed in Chapter 3. The results of parametric study are presented in this chapter.

6.1. Continuity Plate Thickness and Details (Group CP)

The parametric study on continuity plates includes nine cases (Group CP, Table 6.1) and aims to compare different continuity thickness effects on the connection behavior. The thickness of the continuity plates in the CP group varies from zero to full girder flange thickness for the various cases. A range of column flange thicknesses was analyzed in this group: from 0.99 inches to 2.07 inches. The girder flange width-to-column flange thickness ratio (b_f/t_{cf}) varied from 4.4 to 8.3.

In cases CP-1 to CP-4, the same girder and column sizes were used (girder: W24x94, column: W14x176). Note that continuity plates were required by Equation (2.2) for local flange bending for this girder and column combination. Only the thickness of continuity plate varied in each case. Shown in Figures 6.1 and 6.2 are the load-deformation behavior and the girder moment-connection plastic rotation behavior for cases CP-1 to CP-4. For case CP-1 (W14x176) without continuity plates, the load and moment capacity was a little smaller than the cases with continuity plates. However, the maximum difference was only about 2%. There was little difference for cases CP-2 to CP-4, where the thickness of the continuity plates or clip detail varied in each case. It is clear that the presence or absence of continuity plates and continuity plate thickness did not affect much the global connection behavior.

The analysis results showed that the maximum inelastic strain occurred at the column flange-to-girder flange interface. There was a significant difference between cases with continuity plates and without continuity plates. The difference was more obvious at high inelastic strain levels. Figure 6.3 shows the distribution of the PEEQ index, Pressure index (hydrostatic stress divided by the yield stress), and Mises index across the width of the girder tensile flange near the interface at 5% interstory drift. The PEEQ index at the center changed from 25.7 to 20.8 (a decrease of 20%) and the Mises index changed from 1.24 to 1.20 (a decrease of 3%), respectively, when continuity plates were added to the connection. Without continuity plates, the peak inelastic strain and stress occurred at the center, then dropped quickly towards the girder flange ends. Large stress and strain gradients developed across the girder flange width at the interface. With the presence of continuity plates, the stress and strain distributions were much more uniformly distributed. There was still variation of stress and strain across the girder flange width, but the gradient was much smaller. Comparisons of cases CP-2, CP-3, and CP-4, where all cases had continuity plates but the thickness and clip detail varied, showed that the PEEQ and Mises index distribution at the interface was not sensitive to the thickness plates or clip detail. Almost identical results were obtained from these three cases.

Figure 6.3 (d) shows the strain distribution (E11) at the interface at 5% interstory drift. Similar observations were obtained as with the PEEQ and Mises indices. Continuity plates effectively reduced the peak strain at the center and the strain distribution was mild when continuity plates were present. The peak strain at the center for E11, E22, and E33 reduced 21%, 13%, and 44% respectively when continuity plates were present.

To compare the connection behavior among different column sizes, three other column sizes (W14x283, W14x193, and W14x145) were analyzed. For case CP-5, a thicker column flange (W14x283) was used without continuity plate. The flange thickness is 2.07 inch, which satisfies the requirement for omitting continuity plate by Equation (2.2). In cases CP-6 and CP-7, a thinner column flange was used without continuity plates. These two column sizes require continuity plates by Equation (2.2). Case CP-6, with a column size of W14x193, is just on the cusp of requiring continuity plates as per the seismic design equations. Figures 6.3 (e) and (f) show the PEEQ index and Mises index for different column sizes at the same location. The inelastic strain demand was evenly distributed across the girder flange. Compared to the results from the W14x176 with continuity plates (CP-2), the W14x283 column without continuity plates had a smaller peak PEEQ and Mises index at the center, as expected. For a W14x145 section, much higher strain and stress gradient occurred than both W14x176 and W14x193 and an increase in the PEEQ index of approximately 45% was observed compared to case CP-5. It is noted that by Equation (2.2) and Equation (2.3), the required strength demand to column flange strength capacity for W14x145, W14x176, W14x193 and W14x283 are 0.52, 0.75, 0.91, and 1.88, respectively. The analysis results indicated that these equations gave reasonable estimations for the continuity plate requirement.

For cases CP-8 and CP-9, smaller sizes (W10x88 and W18x40) were used to expand the range of parametric study. Both connections without continuity plates (CP-8) and with continuity plate thickness equal to half girder flange thickness (CP-9) were used. This column size does not require continuity plates according to Equations (2.2) and (2.3) (with capacity to demand ratio of 1.08 and b_f/t_{cf}=6.1)). The girder end load-deformation curves and girder moment-plastic rotation curves are shown in Figure 6.4. The global connection behavior was not sensitive to the presence of continuity plates as shown from Figure 6.4. Examination of the PEEQ index in the girder tensile flange at the interface near the CJP welds at 5% interstory drift indicated that when continuity plates were present, the PEEQ index at the center changed from 15.7 to 12.3 (a decrease of 20%). A decrease of 2% of the Mises index at the same location was obtained from the two cases, which was not as significant as that of the plastic strain at this location. The stress and strain curves were flatter near the middle of the girder flange (at the web-to-flange intersection region) when continuity plates were added. Comparing these two cases to the results from the W14 sections, it is noted that the stress and strain distribution patterns were similar to the case of a W14x283 without continuity plates and a W14x176 with continuity plates, where relatively high stress and strain occurred at the tips of the girder flange instead of the center. For cases with W14x145, W14x176 and W14x193 columns without continuity plates, the peak plastic strain occurred at the center of the girder flange, then dropped sharply towards the flange end.

Continuity plates are welded to the column flanges and the web. To avoid the high restraints caused by the weld intersection at the fillet region, the continuity plates are usually cut out at the corner near the k-line region. With an enlarged clip, welds connecting the continuity plate to the column flange and web will stop outside the k-line region. For case CP-4, the same thickness is used as for case CP-2 (0.5 t_f). But CP-4 has a larger clip size (1.5 inches) compared with 1.0 inch in CP-2. In all models, the fillet welds stopped 0.5 inches short of the corner clips. This case study aims to examine the possibility of avoiding welding into the core region of the column while still providing a satisfactory load transfer between the two column flanges. Comparisons of the results of CP-2 and CP-4 showed that the global connection behavior was not affected by the enlarged clips. In addition, examination of the clip region in the continuity plates indicated that no obvious stress or strain concentration occurred with the enlarged clip details. It should be noted that fracture analysis was not included in the finite element model, and a direct conclusion of the initiation of the fracture could not be made from the analysis results.

In summary, finite element analysis of the continuity plate details showed that higher plastic strain occurs at the girder tensile flange near the CJP welds at the girder flange-to-column flange interface. Stress and strain were more uniformly distributed when continuity plates or thicker column flange were present. However, this parametric study showed that this effect was not sensitive to the thickness of continuity plate, with the smallest thickness being half the thickness of the girder flange. No significant improvement was achieved when thicker continuity plates were added. Furthermore, the analysis results also indicated that connections without continuity plates also performed well (e.g., the W14x283 and W10x88 columns). This observation agreed with the predictions from Equations (2.2) and (2.3), which do not require continuity plates for these two cases. It was also noted that with the presence of continuity plates, the tensile hydrostatic stress increased at the center of the girder flange near the groove welds (an 8% increase in this study), which indicated that the presence of continuity plates also increases the constraint at this region. While this study did not model fracture or residual stress, it could be speculated that an increase of hydrostatic stress may occur when much thicker continuity plates than needed are used. In addition, larger welds will also be needed to connect the continuity plates to the connection, thus further increasing the constraint and resulting hydrostatic stress.

6.2. Panel Zone Thickness (Group DP)

Global frame behavior is influenced by panel zone strength. In the AISC seismic design provision (1997), the panel zone strength (R_v) is assumed to be reached when the panel zone deformation reaches $4\gamma_y$ (Equation 2.7). FEMA (2000a) has proposed another approach to address this issue by adopting the concept of balanced yielding. The check of the panel zone strength is based on the ratio of the girder flexural strength to the panel zone shear strength, where only the shear yielding strength of the panel zone is included (Equation 2.9).

To evaluate the influence of the relative panel zone strength on the connection behavior, five cases were included in the parametric study of panel zone thickness (Group DP, Table 6.2). The parametric study of panel zone thickness was based on the panel zone strength (P_z) to girder strength (P_g) ratio (Appendix D). The same girder (W24x94) was used in the first three cases, with the column size and panel zone thickness varied in each case. The other two analyses included one case with larger sections (girder: W36x150, column: W14x398) and one case with smaller sections (girder: W18x40, column: W10x88). The thickness of the panel zone varied in each case, resulting in a P_z/P_g ratio from 0.93 to 1.59, which covers the typical range of this ratio in practice. A fictitious column flange thickness was used in cases DP-1 and DP-4, resulting in a post-yield strength (*K*-term) in each case of approximately 15%-20%, thus allowing comparisons for effect of different P_z/P_g ratio based on post-yield strength percentage (*K*-term) that was approximately constant.

Figure 6.5 shows the connection load-deformation behavior. It is shown that all five connections could achieve 3% plastic rotation when 5% interstory drift was reached. There was a difference in the girder moment capacity of the connections. For connections DP-1 to DP-3, where the P_z/P_g ratio was less than 1.2, the connection did not develop the full girder plastic moment capacity. The moment developed in connection DP-1 (P_z/P_g =0.93) was only 87% of the girder plastic moment even after significant yielding occurred at the connection region. For connections DP-4 and DP-5, where the P_z/P_g was 1.36 and 1.59, respectively, the full-plastic girder moment capacity was achieved. As expected, this further explains that the P_z/P_g ratio indicates what part of yielding will dominate the connection behavior.

Shown in Figure 6.5 (c) is the panel zone plastic rotation versus total connection plastic rotation. It is clear that a higher percentage of total the connection plastic rotation occurred in the panel zone for connections with a weaker panel zone (P_z/P_g<1.2), thus resulting in less deformation demand at the girder. The panel zone plastic rotation and total connection plastic rotation at 5% interstory drift are tabulated in Table 6.6. It can been from the table that for connection DP-1 (P_z/P_g =0.93), nearly 90% of the total plastic rotation came from the panel zone, while for connection DP-5 (P_z/P_g =1.59), the panel zone only contributed 36% of the total plastic rotation. Although the inelastic deformation demand in the girder was smaller for the weaker panel zones, the larger inelastic deformation that occurred at the panel zone would cause significantly higher principal stress at the middle of girder-to-column interface. This results in higher potential for cracking initiation (El-Tawil et al., 1998).

The panel zone shear strength was also examined to compare the P_z/P_g ratio. Figure 6.5 (d) shows the panel zone shear versus panel zone deformation relationship. Both the shear force and the distortion were normalized by the corresponding AISC design shear R_v (Equation 2.7) and shear yielding strain γ_y (Equation 5.10). The same observations were obtained that a smaller panel zone deformation was achieved in connection with stronger panel zone. At 5% interstory drift, a total panel zone deformation of 0.04 radians developed in connection DP-1, while only 0.02 radians of plastic deformation developed in connection DP-5.

The parametric study of the panel zone strength to girder strength ratio in group DP indicates that most of the plastic deformation develops in panel zone region for weaker panel zones (e.g., P_z/P_g <1.2 from this study) and that the predicted girder plastic moment was not achieved. The analyses showed that for all five cases in group DP, the shear force that developed in the panel zone at $4\gamma_y$ was less than the values predicted by AISC (1997) equation (Equation 2.7). The shear force that developed at a panel zone deformation of $4\gamma_y$ was approximately 65%-80% of the AISC (1997) design values for cases DP-1 to DP-5 (Table 6.7). This suggested that significant panel zone deformation would occur before the design panel zone strength could be reached.

The post elastic panel zone strength increase (K-term) is also shown in Table 6.7. In the analyses, this K-term was obtained approximately by comparing the girder tip load at 5% interstory drift with that when the specimens deviated from the linear response. The finite element results agree well with the current AISC design value for most cases. However, it is noted that for case DP-5 with a thicker column flange, the increase is 9% from finite element analysis while a 19% strength increase is predicted by AISC code.

Figure 6.5(e) shows the comparison of panel zone shear strength to the girder flexural strength using the FEMA (2000a) approach. The shear forces have been normalized by the shear strength proposed in FEMA (2000a) ($R_v=0.55F_c d_c t_p$). The moments have been normalized by the girder yielding moment (M_y). For cases DP-1 and DP-2, the panel zone shear strength was reached before the girder reached its flexural yielding strength. For cases DP-4 and DP-5, which had a relatively stronger panel zone, flexural yielding occurred in the girder. For case DP-3, where P_z/P_g=1.2, the shear yielding of the panel zone and the flexural yielding of the girder occurred at approximately the same time.

6.3. Column Flange Thickness (Group CF)

In the AISC (1997) seismic provisions, the shear strength of the panel zone comes from both the panel zone (column web and doubler plate) region as well as the column flanges, which act as boundary members for the panel zone. The relative stiffness of the flange influences the inelastic behavior of the panel zone. The parametric study of Group CF is intended to investigate the effects of column flange thickness on panel zone shear resistance. For panel zone shear resistance, the contribution from the flange thickness is reflected predominantly in the post-yield behavior of the panel zone, which is generally considered to be proportional to the square of the column flange thickness as reflected in the K-term of Equation (2.7), as is expressed in Equation (5.13).

Group CF includes four column sizes with column flange thickness of 2.07, 1.7, 1.31, and 1.09 inches, respectively (Table 6.3). The column web and doubler plates thickness varied in each case. The four cases had approximately the same of P_z/P_g ratio of 1.0. From the AISC (1997) design equation, it was expected that all four cases had approximately the same panel zone shear strength. As the flange thickness varied in each case, the post-yield strength differed. The "K-term" in this group varied from 8% to 39.4%.

The panel zone deformation versus interstory drift curves are plotted in Figure 6.6 (a) for the four connections. The four specimens had approximately the same ultimate load capacity at 5% interstory drift. The difference of the load was approximately 3.4% among the connections. Comparison of the panel zone plastic rotation showed that the connection with thicker column flanges had a larger panel zone plastic rotation than the connection with thinner flanges. Table 6.8 shows the plastic panel zone deformation reached at 5% interstory drift. A decrease of 20% in the panel zone plastic deformation was observed from CF-1 to CF-4.

The column flange thickness also affects the panel zone shear strength. Shown in Figure 6.6 (b) was the panel zone shear versus panel zone deformation relationship. The panel zone deformation has been normalized by the corresponding yield strain γ_y (Equation (5.10)) and the panel zone shear has been normalized by the AISC (1997) design strength R_v (Equation (2.7)). In spite of the fact that the four connections had approximately the same P_z/P_g ratio, the connection with thicker column flanges had higher initial joint stiffness than those with thinner column flanges. In addition, inelastic panel zone distortion occurred at lower drift levels for the connection with thicker column flanges. This could be observed from the stiffness change in the figure. Inelastic distortion in connection CF-1 occurred at approximately 0.005 radians of panel zone deformation, while inelastic distortion occurred at approximately 0.008 radians for connection CF-4. The post-yield panel zone shear strength differed in the four connections. Shown in Table 6.9 is the comparison of the panel zone shear at first yield and at $\gamma/\gamma_y=4$. Comparison of the panel zone shear at $4\gamma_y$ with the design equation value showed that the actual shear resistance of the four connections was only approximately 75% of the AISC (1997) design equation prediction.

Another difference observed was the panel zone shear increase after first yield. This strength increase was primarily attributed to the strain hardening of the material that occurred in the panel zone region after first yielding. From the AISC (1997) panel zone strength design equation, the predicted post-yield strength increase due to the K-term is 39.4%, 23.3%, 11.9% and 8.0%, respectively for connections CF-1 to CF-4. Similar results were obtained from finite element analysis. As shown in Table 6.9, an increase of 28.6%, 21.0%, 18.0%, and 3.6% was achieved for connections CF-1 to CF-4, respectively. Case CF-1, with thicker column flanges, had its post-yield strength overpredicted.

Shown in Figure 6.6(c) is the comparison of the panel zone shear and girder moment. The shear is normalized using the proposed FEMA (2000a) equation (Equation

2.12b). The moment is normalized by M_y (Equation (2.10)). The analysis results indicated that for these cases having relatively weaker panel zones (P_z/P_g=1), the panel zone reached their shear strength before the flexural strength of the girder was reached. For the connection with thicker flanges, more panel zone deformation occurred in the panel zone region relative to the other connections.

This parametric study of the effect of column flange thickness on panel zone behavior indicates that earlier and more extensive inelastic panel zone deformation occurs for connections with thicker column flanges. A higher strength increase is achieved for connections with thicker column flanges. However, the finite element analysis showed that the actually strength increase was smaller than the AISC (1997) panel zone strength equation. The shear resistance for all connections at a panel zone deformation of $4\gamma_y$ was approximately 75% of the values predicted by AISC (1997) seismic design equation. For the sake comparison, the FEMA (2000a) panel zone strengths are also shown in Table 6.9. These values have no dependence on column flange thickness, and are seen to compare better with the general peak strengths seen in the analyses.

6.4. Doubler Plate Location (Group Box)

The parametric study in this group includes four doubler plate locations to investigate the optimal location for placing the doubler plates in the box detail of Figure 3.12. These possible locations investigated here include: directly against the web, at the girder flange edge, at 2/3 of the girder half flange width from the column web, and at 1/3 of the girder half flange width from the column web (Table 6.4). This parameter is intended to study the effectiveness of the doubler plate location relative to the girder flange width. In case Box-1, the doubler plates were attached to the column flanges adjacent to the column web by fillet welds as in Figure 3.4. This configuration was used as the base line for comparison with other doubler plate locations.

Figure 6.7 (a) shows the load-deformation curves for group Box. The load capacity of four cases was almost identical up to about 1.0% interstory drift. When the doubler plates were attached directly to column flanges by fillet welds (case Box-1), the load capacity was a little smaller than for the other doublers locations. The load capacity was the highest when the doublers plates were located at approximately 2/3 of half girder flange width from the column web (case Box-3). However, the difference of load capacity was not significant (within 2-3%). Figure 6.7 (b) shows the moment-connection plastic rotation for the four cases, with the moment normalized by the girder nominal plastic moment. All four cases achieved a plastic rotation greater than 0.03 radians at 5% interstory drift and a moment capacity greater than the girder plastic moment capacity. A smaller moment capacity was achieved when doubler plates were attached directly to the column web. It was noted that the difference was still quite small (within 7%). In general, the moment capacity and load capacity was not sensitive to the relative doubler plate location.

For a W14x176 column and W24x94 beam, doubler plates were required by current AISC (1997) seismic design equation (Equation (2.2), Table 6.1). Figure 6.7 (c) shows the average panel zone shear deformation at different interstory drift levels. It is clear that all four cases showed similar results regardless of the doubler plate location. Shown in Figure 6.8(a) is the shear stress (S12) and strain (E12) at the column web center along a horizontal line at 5% interstory drift. Figure 6.8 (b) shows the shear stress (S12) and strain (E12) at the column web center along a vertical line at 5% interstory drift. Observation of the plots indicated that most of the column web was yielded at 5% interstory drift. Peak stress and strain occurred at the center and remained fairly constant within 4 inches from the center. Shear stress and strain were a little higher when doubler plates were attached to the web and at the girder flange edge than for the other two locations. The difference was usually 3-5%. Examination of the results for other load levels indicated the same conclusion. The similarity of the stress and strain distributions for these four cases studied clearly showed that the doubler plate location does not significantly affect the column web behavior.

The doubler plates themselves yielded in shear after 2% interstory drift was reached. Figure 6.9 shows the stress and strain distribution along a horizontal and vertical line at the doubler plate center sampled at 5% story drift. Most of the doubler plate yielded and the shear stress and strain were quite uniformed distributed within the doubler plate region. The comparisons among the four cases indicated that the difference of stress and strain between these cases was small, usually between 2-3%. It is noted that there was noticeable difference in strain (E12) at the far end of the doubler plates along the horizontal lines. The strain decreased toward the end for case Box-1, where the doubler plates were attached to the column flanges by fillet welds. Whereas the strain increased towards the end for the other three cases, where doubler plates were attached to the column flange by CJP welds. This difference could be attributed to the difference in welding. For doubler plates connected to the flanges by fillet welds, as in case Box-1, the stress and strain transferred to the column flange through the fillet welds near the ends, so that less restraint was present in the doubler plates. For the doubler plates connected to the flange by complete joint penetration welds, as in the other three cases, the stress and strain transferred to column flange through the highly restrained welds near the ends, so a higher strain demand resulted in the doubler plates.

To further investigate the effect of the doubler plate stress and strain, the peak stress and strain at the doubler plate center were compared at each load level. The results are tabulated in Tables 6.10 and 6.11. The stress and strain was a little smaller when the doubler plates were placed adjacent to the web and at the girder flange edge up to 1% interstory drift. However, the difference was within 10% and most of the connection region remained elastic at this load level. After inelasticity developed, the doubler plate behavior was essentially identical in all cases.

For the column and girder combinations used in this group, both doubler plates and continuity plates were required according to Equations (2.2) and (2.7). The doubler plates located away from the column web also served as continuity plates that provided support for the column flange. The effect of the doubler plate as a continuity plate was also examined. Figure 6.10 shows the comparisons of the PEEQ index and Mises index plotted across the tensile girder flange near the CJP welds at 5% interstory drift. The plots show that when the doubler plates were attached directly at the column web (case Box-1), the PEEQ index was highest at the girder flange center. When the doubler plates were moved towards the girder flange edge, the peak PEEQ index at the girder flange center reduced and the peak PEEQ index occurred at the girder flange edge. The PEEQ index at the girder flange center for the four cases was 25.3, 22.8, 19.78, and 19.5, respectively, when the doubler plates moved from the column web towards the girder flange edge. A maximum of decrease of 25% in the PEEQ index was thus observed. Meanwhile, the PEEQ index at the girder flange edges was 19.3, 21.2, 26.8, and 39.6, respectively as the doubler plates moved away from the column web. This maximum increase of the PEEQ index was nearly 100%. This could be related to the relative stiffness change of the column flange across the width. When the doubler plates were adjacent to the column web, the column flanges were stiffer at the center more than other locations and higher constraint occurred at the girder center, thus resulting in higher stress and strain at this location. The same situation occurred when the doubler plates moved towards the flange edge. Higher strain demand developed near the location where the flange was stiffer. Comparisons of the four doubler plate locations indicated that when the doubler plates were located between 1/3 to 2/3 of the half girder flange width away from the column web, both the PEEQ index at the center and at the flange tip were smaller than the other two locations. Thus the doubler plates were more effective when located at these locations when used as continuity plates as well.

Examination of the Mises stress index across the width of the girder flange near the CJP welds showed that although there were variations of the Mises stress along the flange width due to the different doubler plate locations, the difference was quite small, since the inelastic region developed at the interface and the girder flanges were all yielded across the width.

The parametric study for doubler plate locations showed that the box detail is an excellent alternative method of connection stiffener detailing. The box detail is most cost effective when it serves both as the doubler plates and continuity plates. Similar results were obtained in global connection behavior, the panel zone region, and the doubler plates regardless of the doubler plate locations. However, the doubler plates are more effective in reducing the girder flange inelastic strain demand at the flange center near the girder-to-column interface when the doubler plates are placed at approximately 1/3 to 2/3 of the girder half flange width away from the column web.

Table 6.1: Continuity Plate Thickness and Detail (Group CP)

												LFB R_n/R_u		
	Girder	Column	DP	CP	Clip	P_g	P_z	P_c	P_z/P_g	P_c/P_g	b_f/t_{cf}	Non seis.	Seis.	PZ
CP-1	W24x94	W14x176	2@0.5"	NA	NA	192.40	202.70	267.20	1.05	1.39	6.9	1.35	0.75	0.85
CP-2*	W24x94	W14x176	2@0.5"	0.5"	1.0"	192.40	202.70	267.20	1.05	1.39	6.9	1.35	0.75	0.85
CP-3	W24x94	W14x176	2@0.5"	0.875"	1.0"	192.40	202.70	267.20	1.05	1.39	6.9	1.35	0.75	0.85
CP-4	W24x94	W14x176	2@0.5"	0.5	1.5"	192.40	202.70	267.20	1.05	1.39	6.9	1.35	0.75	0.85
CP-5	W24x94	W14x283	NA	NA	NA	192.40	196.00	450.00	1.02	2.34	4.36	3.38	1.88	2.12
CP-6	W24x94	W14x193	1@ 0.625"	NA	NA	192.40	178.70	296.10	0.93	1.54	6.3	1.63	0.91	1.03
CP-7	W24x94	W14x145	2@ 0.625"	NA	NA	192.40	200.20	217.40	1.04	1.13	8.31	0.94	0.52	0.59
CP-8	W18x40	W10x88	2@ 0.4375"	NA	NA	58.07	79.14	67.06	1.36	1.15	6.1	1.94	1.08	1.16
CP-9	W18x40	W10x88	2@ 0.4375"	0.25"	1.0"	58.07	79.14	67.06	1.36	1.15	6.1	1.94	1.08	1.16

*Configurations used in the experimental investigation are highlighted

Table 6.2: Panel Zone Thickness (Group DP)

													PZ R_n/R_u		
	Girder	Column	DP	CP	t_p	t_{cf}	P_g	P_z	P_c	P_z/P_g	P_c/P_g	K-term	Non. Seis.	AISC	FEMA
DP-1	W24x94	W14x193	1@0.625"	NA	1.515	1.44	192.40	178.70	298.10	0.93	1.55	0.171	0.93	0.77	0.77
DP-2	W24x94	W14x176	2@0.5"	NA	1.83	1.5	192.40	207.79	267.20	1.08	1.39	0.156	1.09	0.90	0.94
Dp-3	W24x94	W14x211	2@0.5"	NA	1.98	1.56	192.40	231.56	296.10	1.20	1.54	0.152	1.21	0.97	1.03
DP-4	W18x40	W10x88	2@0.4375	NA	1.48	0.99	58.07	79.14	67.06	1.36	1.15	0.184	1.21	1.13	1.24
DP-5	W36x150	W14x398	2@0.75"	NA	3.27	2.2	464.80	738.57	755.51	1.59	1.63	0.188	1.58	1.31	1.38

Table 6.3: Column Flange Thickness (Group CF)

	Girder	Column	DP	CP	t_f	t_p	P_g	P_z	P_c	P_z/P_g	P_c/P_g	K term
CF-1	W24x94	W14x283	NA	NA	2.07	1.29	192.4	196.0	450.1	1.02	2.34	0.394
CF-2	W24x94	W14x233	1@0.5	NA	1.72	1.57	192.4	201.6	409.9	1.05	2.13	0.233
CF-3	W24x94	W14x176	2@0.5"	NA	1.31	1.83	192.4	202.0	267.2	1.05	1.39	0.119
CF-4	W24x94	W14x145	2@0.625"	NA	1.09	1.93	192.4	200.2	217.4	1.04	1.13	0.08

Table 6.4: Doubler Plate Location (Group Box)

	Girder	Column	DP	CP	Location	P_g	P_z	P_c	P_z/P_g	P_c/P_g
Box-1	W24x94	w14x176	2@0.75"	NA	web	192.4	252.2	267.2	1.31	1.39
Box-2	W24x94	W14x176	2@0.75"	NA	Flange edge	192.4	252.2	267.2	1.31	1.39
Box-3	W24x94	W14x176	2@0.75"	NA	2/3 half girder flange	192.4	252.2	267.2	1.31	1.39
Box-4	W24x94	W14x176	2@0.75"	NA	1/3 half girder flange	192.4	252.2	267.2	1.31	1.39

Table 6.5: Connection Configuration Summary

													SCWB		
	Girder	**Column**	Z_g	Z_c	d_g	d_c	b_{cf}	t_{cf}	t_{cw}	b_{gf}	t_{gf}	A_g	P_u= 0 ksi	P_u= 10 ksi	P_u= 20 ksi
1	W24x94	w14x283	254	542	24.31	16.7	16.11	2.07	1.29	9.065	0.88	27.7	Yes	Yes	Yes
2	W24x94	w14x233	254	409	24.31	16	15.89	1.72	1.07	9.065	0.88	27.7	Yes	Yes	No
3	W24x94	w14x211	254	390	24.31	15.7	15.8	1.56	0.98	9.065	0.88	27.7	Yes	Yes	No
4	W24x94	w14x193	254	355	24.31	15.5	15.71	1.44	0.89	9.065	0.88	27.7	Yes	No	No
5	W24x94	w14x176	254	320	24.31	15.2	15.65	1.31	0.83	9.065	0.88	27.7	Yes	No	No
6	W24x94	w14x145	254	260	24.31	14.8	15.5	1.09	0.68	9.065	0.88	27.7	No	No	No
7	W36x150	W14x398	581	801	35.85	18.3	16.59	2.845	1.77	11.98	0.94	44.2	Yes	No	No
8	W18x40	W10x88	78.4	113	17.9	10.8	10.27	0.99	0.61	6.015	0.53	11.8	Yes	No	No

SCWB is the strong column weak beam check (Appendix D)

Table 6.6: Comparison of Panel Zone Deformation (Group DP)

	DP1	DP2	DP3	DP4	DP5
P_z/P_g	0.93	1.08	1.2	1.36	1.59
Total Plastic Rotation	0.0383	0.0369	0.0374	0.0321	0.0385
PZ Plastic Rotation	0.0342	0.0300	0.0315	0.0173	0.0139
% of total plastic rotation	89.29%	81.15%	84.24%	53.95%	36.23%

Table 6.7: Comparison of Shear Strength in Panel Zone for Group DP

	DP1	DP2	DP3	DP4	DP5
R_v **(AISC, kips)**	831	966	1076	531	1995
V **@ First Yield (kips)**	540.00	650.00	630.00	370.00	1200.00
V **(FE at 4γ_y)**	645.64	759.93	717.51	370.00	1302.03
V/R_v	0.78	0.79	0.67	0.70	0.65
K term **(AISC)**	0.17	0.16	0.15	0.18	0.19
K term **(FE)**	0.20	0.17	0.14	0.14	0.09

Table 6.8: Comparison of Panel Zone Deformation (Group CF)

	CF1	CF2	CF3	CF4
P_z/P_g	1.02	1.05	1.05	1.04
Total Plastic Rotation	0.0397	0.0381	0.0368	0.0357
PZ Plastic Rotation	0.0359	0.0329	0.0304	0.0287
% of total plastic rotation	90.31%	86.39%	82.48%	80.39%

Table 6.9: Comparison of Shear Strength in Panel Zone for Group CF

	CF1	CF2	CF3	CF4
***R_v* (AISC, kips)**	903	929	935	906
***R_v* (FEMA, kips)**	594	693	766	768
***V* @ First Yield (kips)**	510.00	583.03	620	688.14
***V* (FE at $4\gamma_y$) (kips)**	655.83	705.47	730.68	713
***V/R_v* (AISC, kips)**	0.73	0.76	0.78	0.76
***K term* (AISC)**	0.39	0.23	0.12	0.08
***K term* (FE)**	0.29	0.21	0.18	0.04

Table 6.10: Shear Stress at Doubler Plate Center (Group Box) (ksi)

Interstory Drift	**Doubler Plate Location**			
	At web	**1/3 girder flange**	**2/3 girder flange**	**Flange end**
0.38%	8.353	8.923	8.816	8.309
0.05%	11.03	11.79	11.64	10.97
0.75%	16.55	17.68	17.47	16.46
1%	22.04	23.59	23.29	21.92
1.50%	31.54	31.54	31.54	31.47
2%	31.63	31.64	31.64	31.53
3%	31.82	31.83	31.83	31.66
4%	32.34	32.37	32.37	31.93
5%	33.12	33.1	33.09	32.36

Table 6.11: Shear Strain at Doubler Plate Center (Group Box)

Interstory Drift	**Doubler Plate Location**			
	At web	**1/3 beam flange**	**2/3 beam flange**	**Flange end**
0.38%	0.0007489	0.0008	0.00079041	0.00074491
0.05%	0.0009891	0.0010566	0.0010439	0.00098384
0.75%	0.0014836	0.0015849	0.0015659	0.0014757
1%	0.0019764	0.0021151	0.0020883	0.0019653
1.50%	0.0040083	0.004415	0.0043475	0.0036024
2%	0.0095612	0.0097193	0.0096651	0.0087849
3%	0.020718	0.020856	0.020803	0.01991
4%	0.031899	0.031651	0.031552	0.030862
5%	0.042841	0.041795	0.041554	0.041451

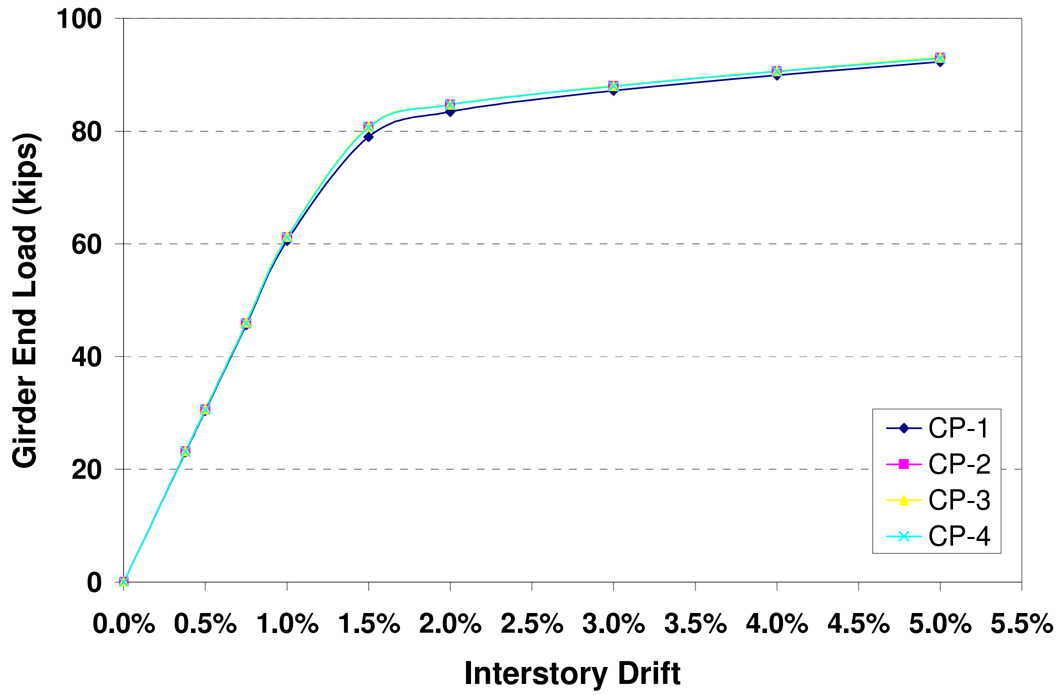

Figure 6.1: Girder End Load versus Interstory Drift (Group CP)

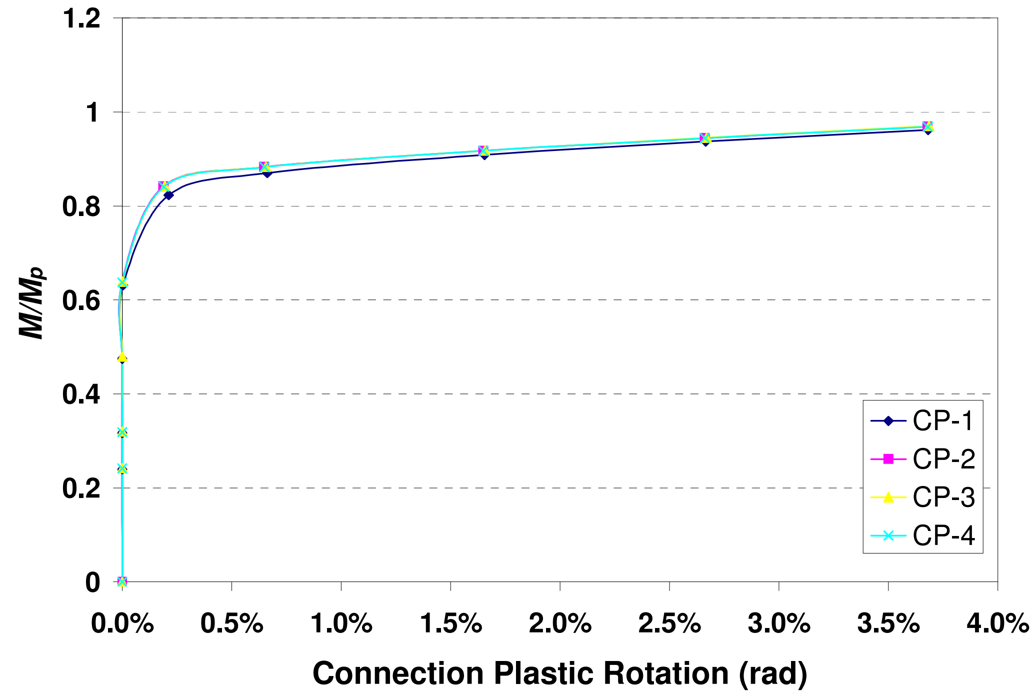

Figure 6.2: Moment versus Plastic Rotation (Group CP)

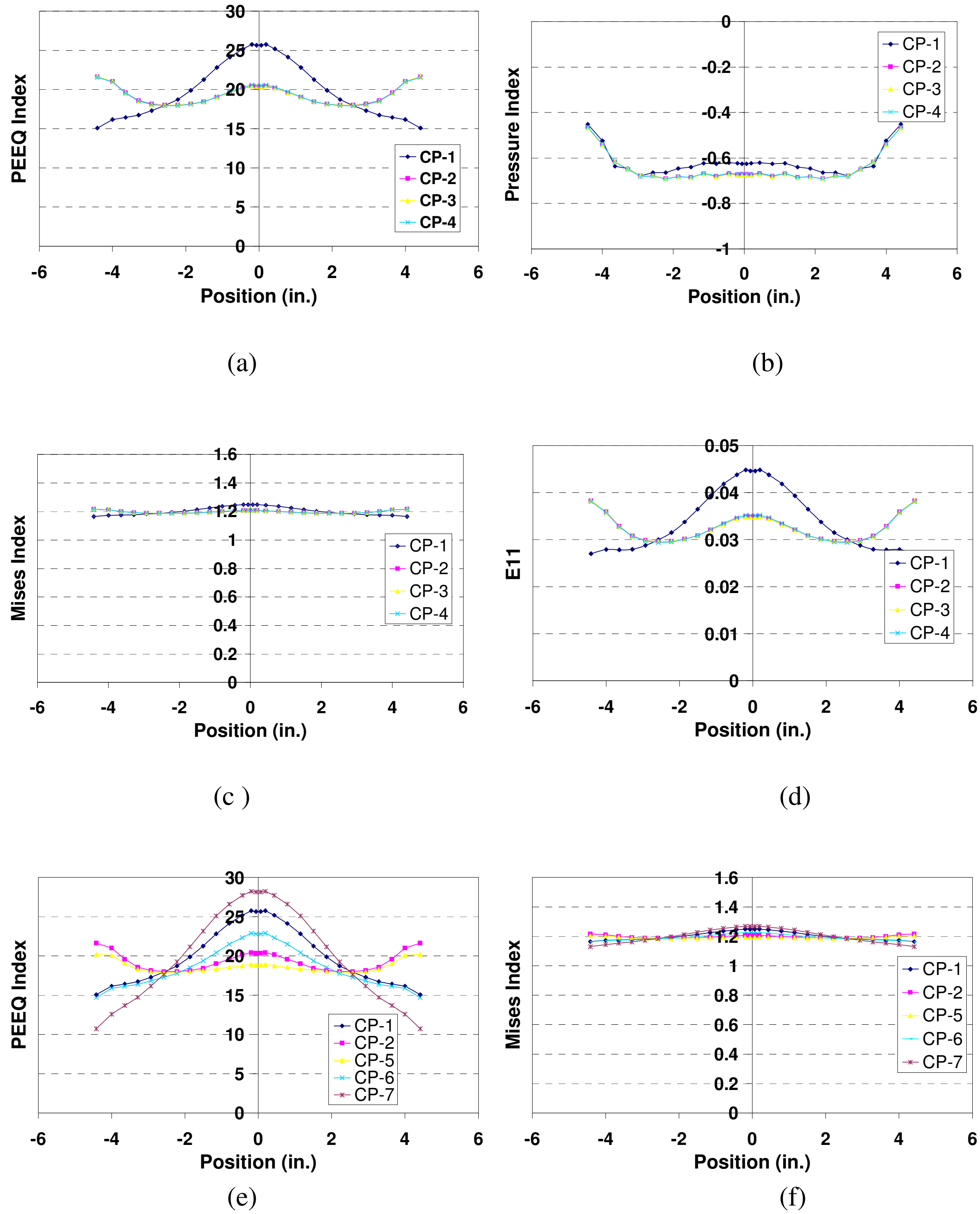

Figure 6.3: Stress and Strain Distribution along Width of Girder Flange near CJP Welds (Group CP)

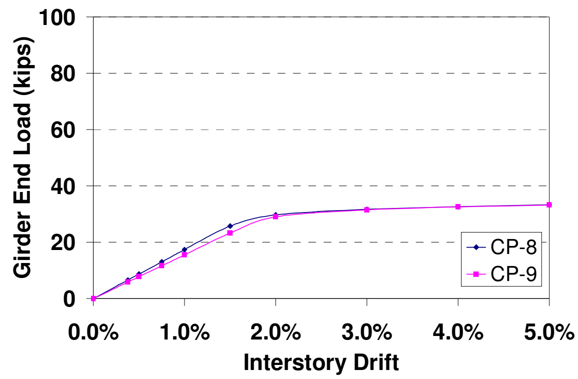

(a)

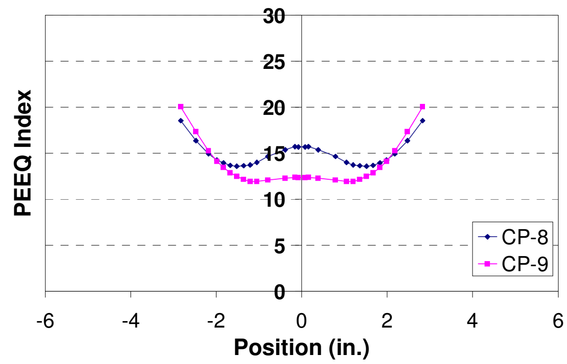

(b)

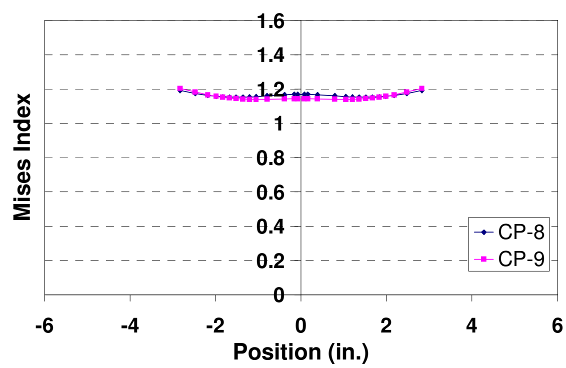

(c)

Figure 6.4: Analysis Results for Cases CP-8 and CP-9

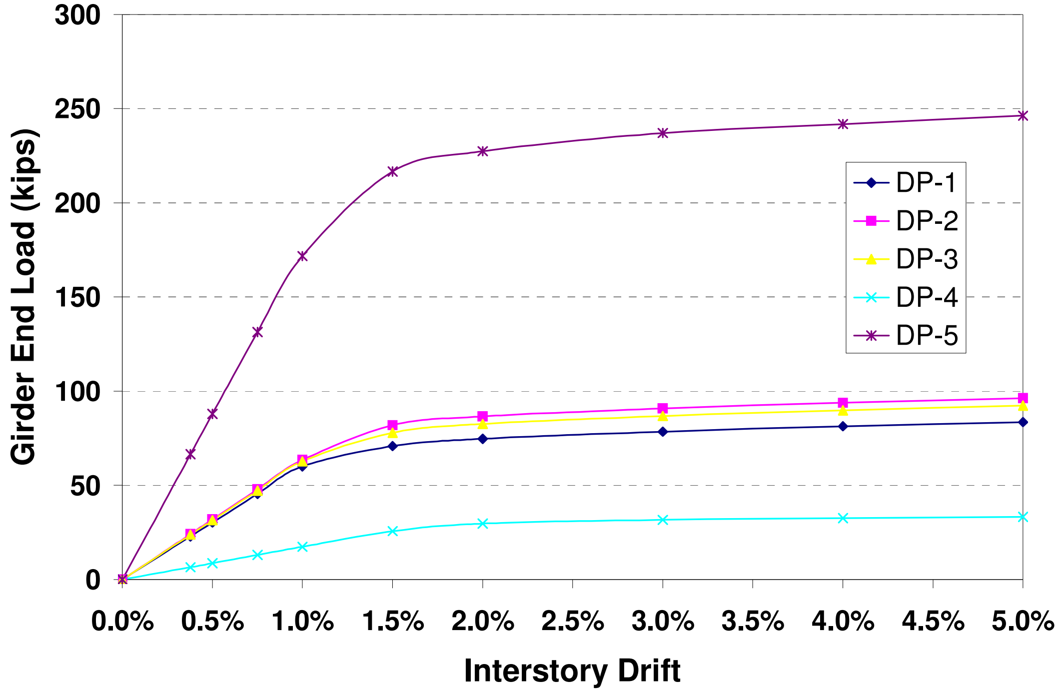

Figure 6.5(a): Load versus Deformation (Group DP)

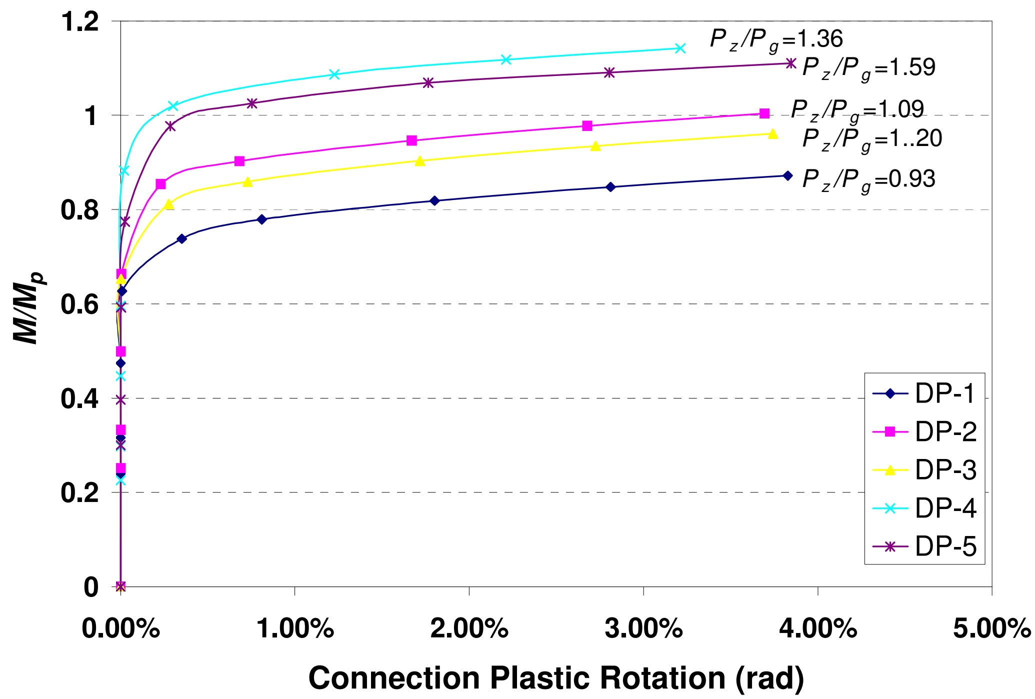

Figure 6.5(b): Moment versus Connection Plastic Rotation (Group DP)

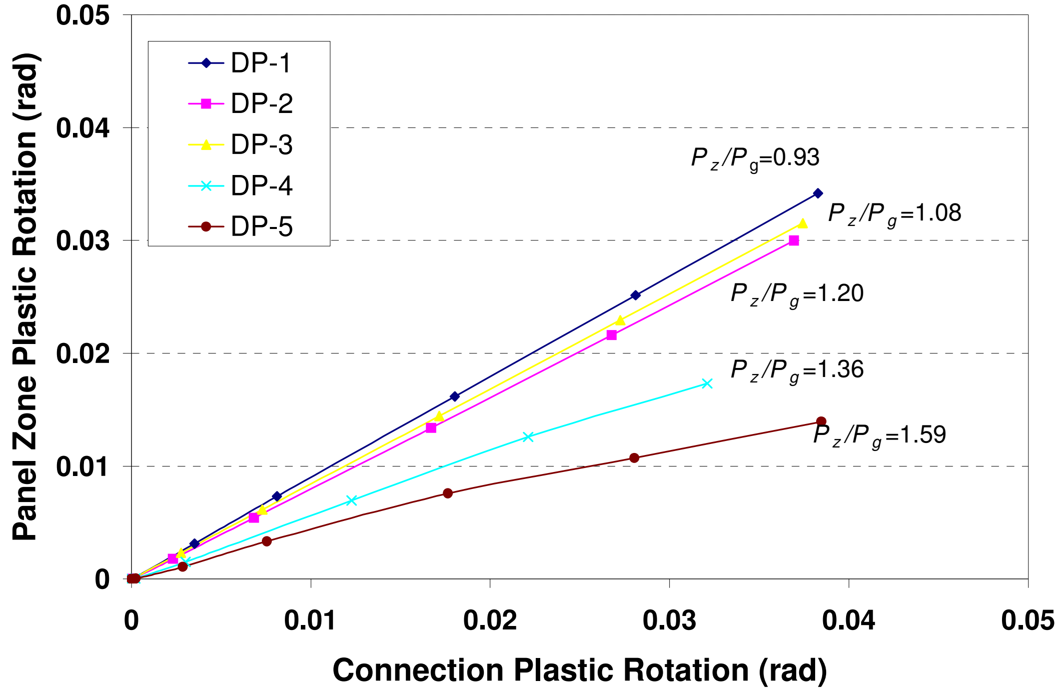

Figure 6.5(c): Panel Zone Deformation versus Connection Rotation (Group DP)

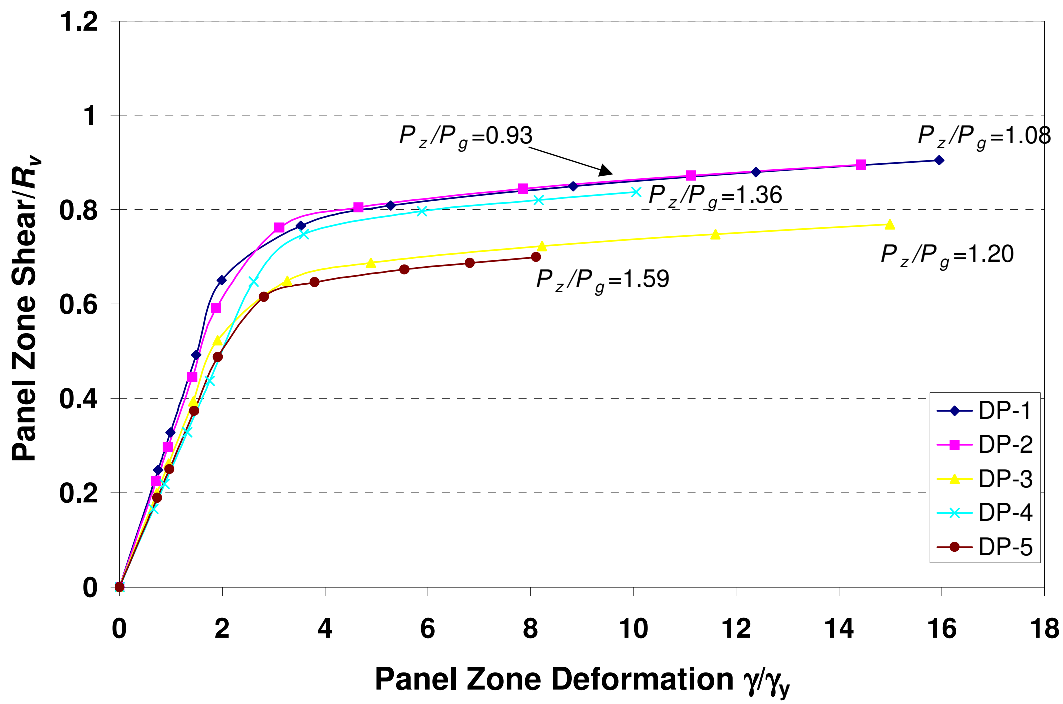

Figure 6.5(d): Panel Zone Shear versus Panel Zone Deformation (Group DP)

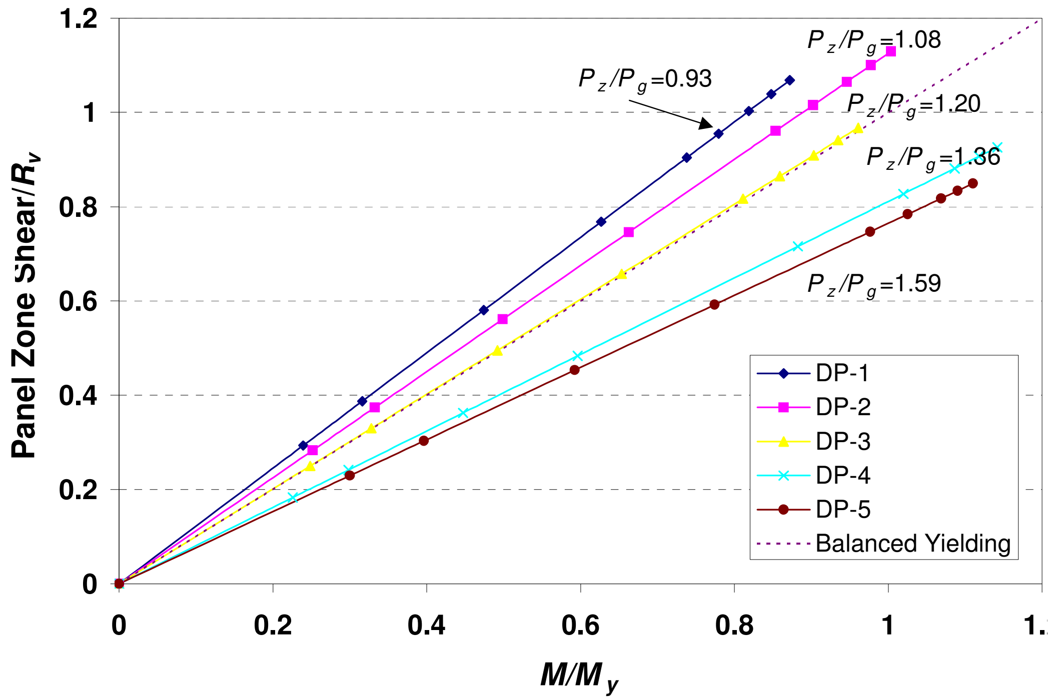

Figure 6.5(e): Panel Zone Shear versus Girder Moment (Group DP)
(panel zone shear is normalized by the FEMA (2000a) shear strength)

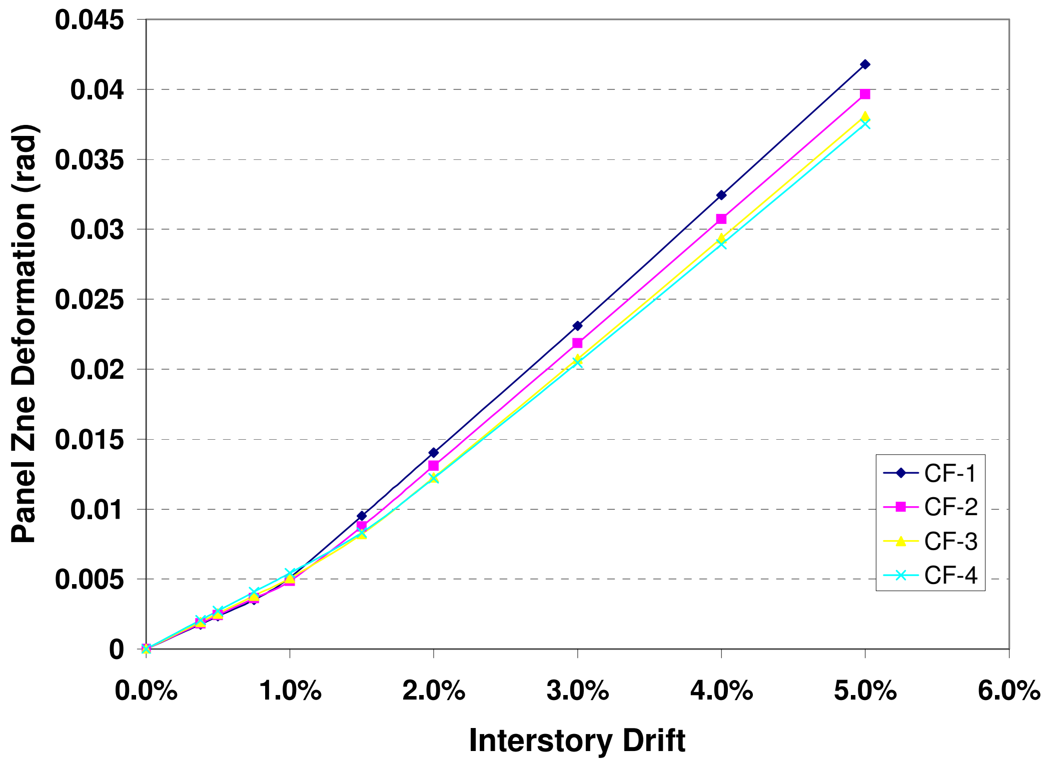

Figure 6.6(a): Panel Zone Deformation versus Interstory Drift (Group CF)

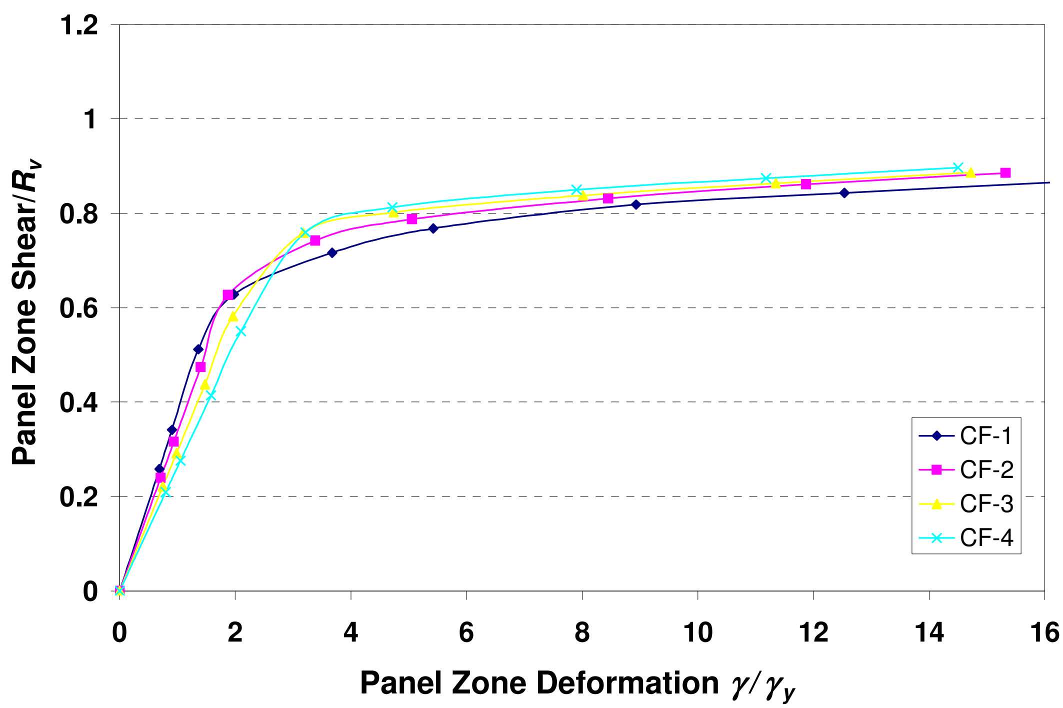

Figure 6.6(b): Panel Zone Shear versus Panel Zone Deformation (Group CF)

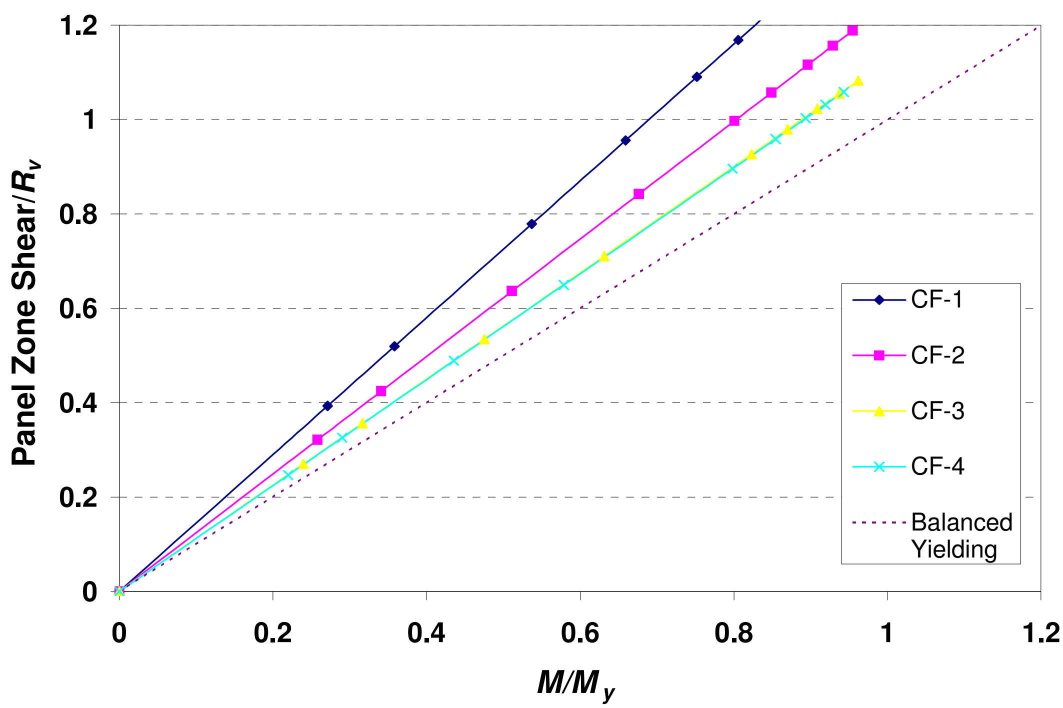

Figure 6.6(c): Panel Zone Shear versus Girder Moment (Group CF)
(panel zone shear is normalized by the FEMA (2000a) shear strength)

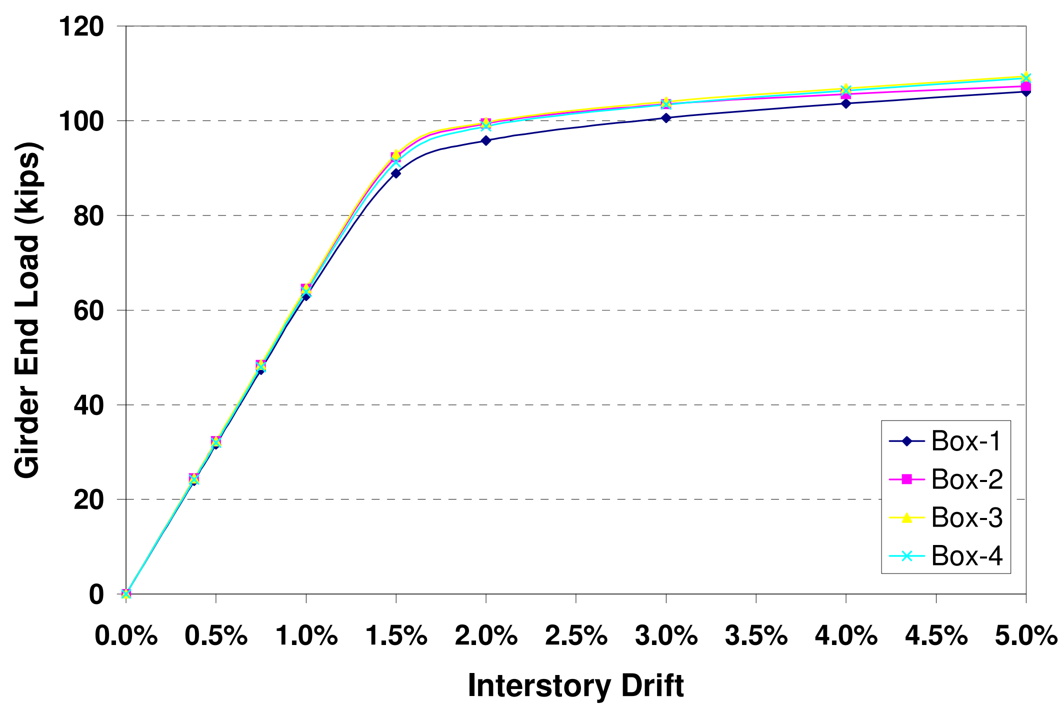

Figure 6.7(a): Load versus Deformation (Group Box)

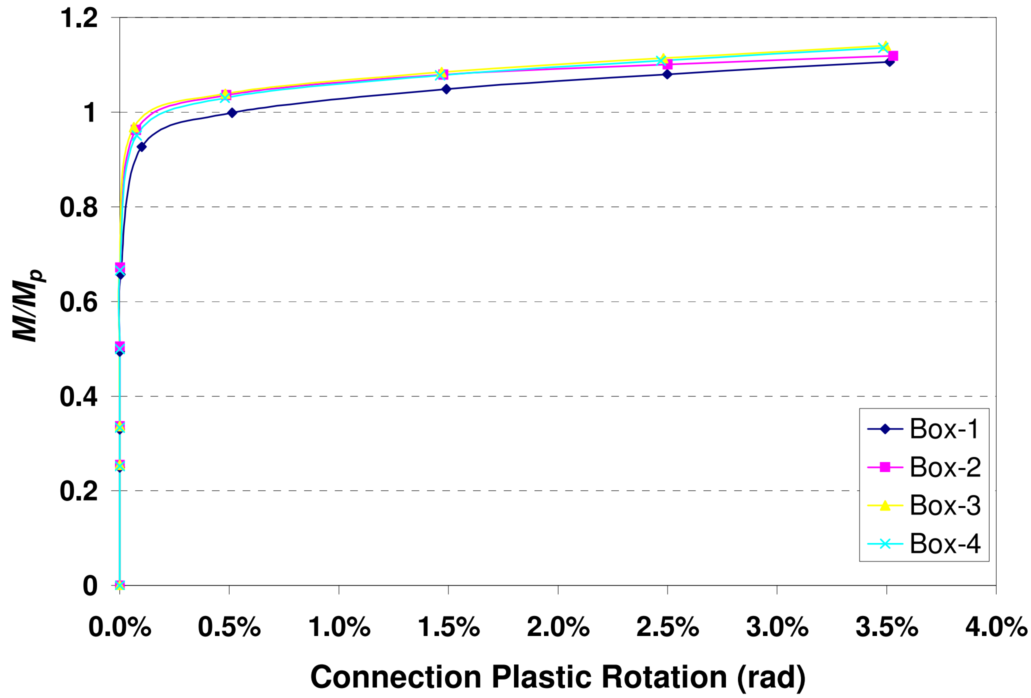

Figure 6.7(b): Girder Moment versus Connection Plastic Rotation (Group Box)

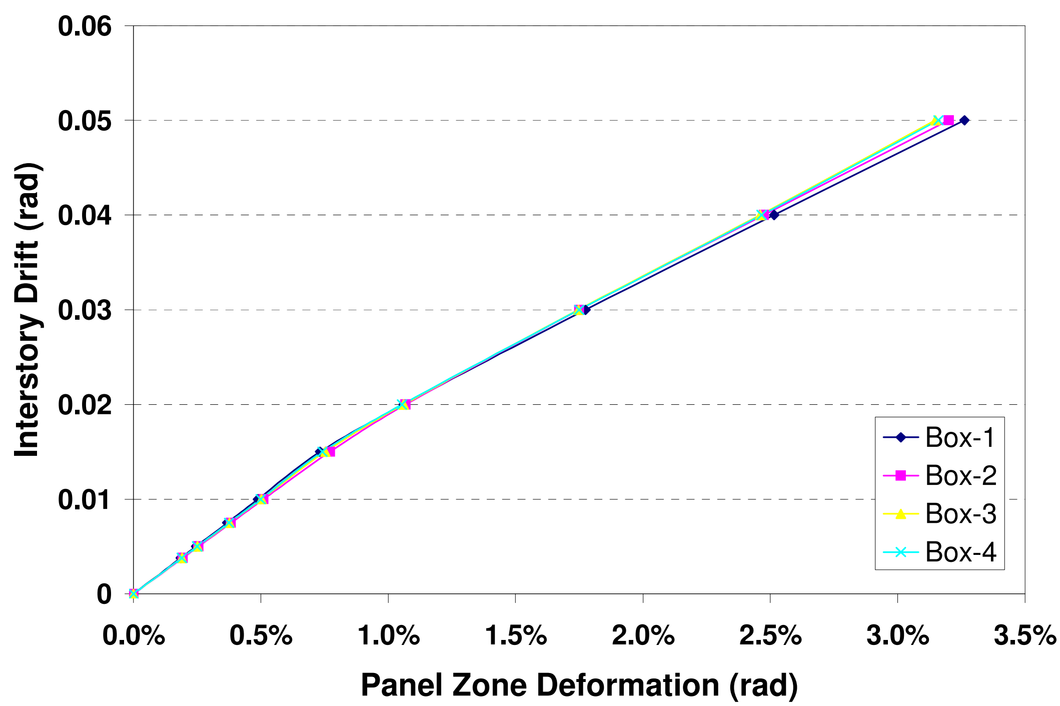

Figure 6.7(c): Panel Zone Deformation versus Interstory Drift (Group Box)

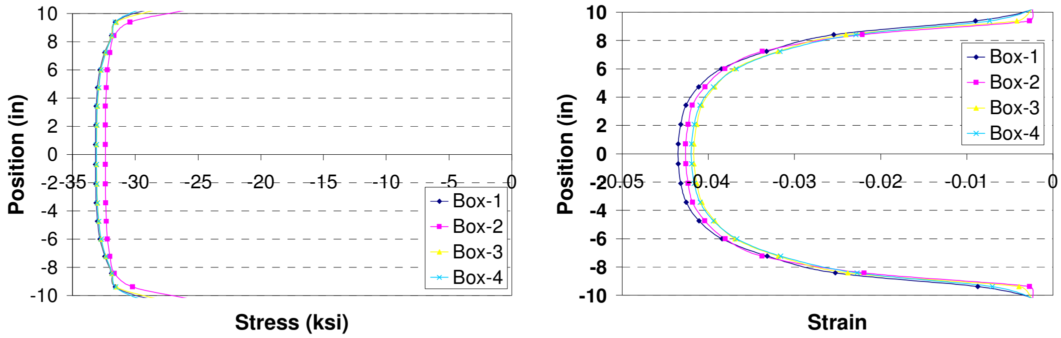

(a) Along Horizontal Line in the Center

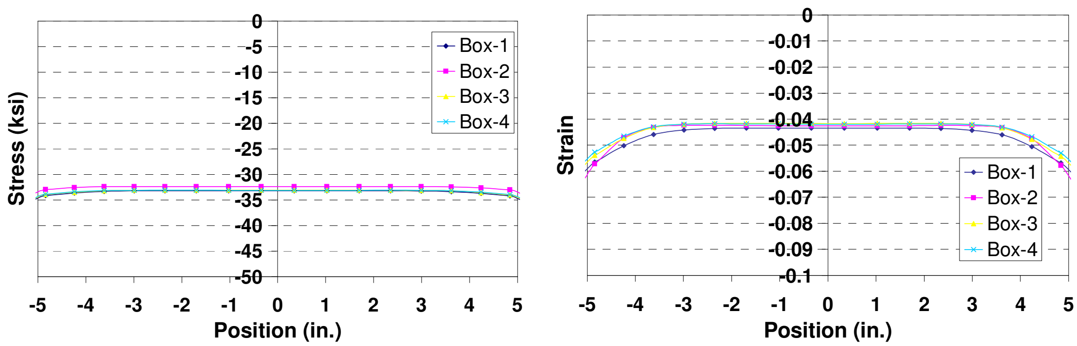

(b) Along Vertical Line in the Center

Figure 6.8: Stress and Strain Distribution in the Panel Zone (Group Box)

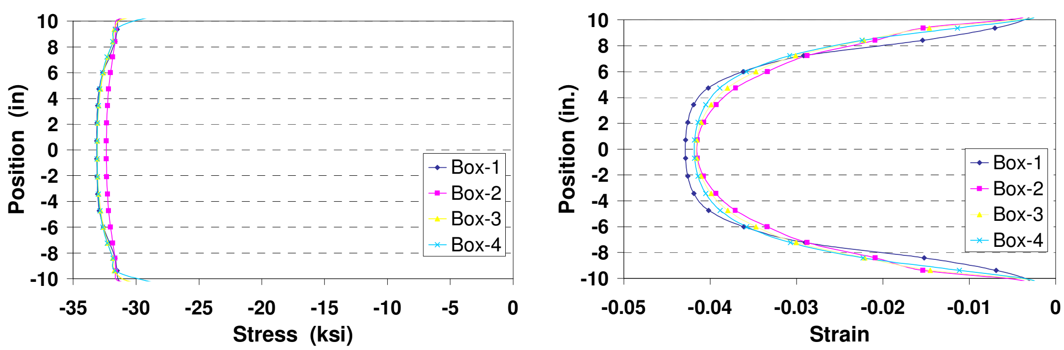

(a) Along Horizontal Line in the Center

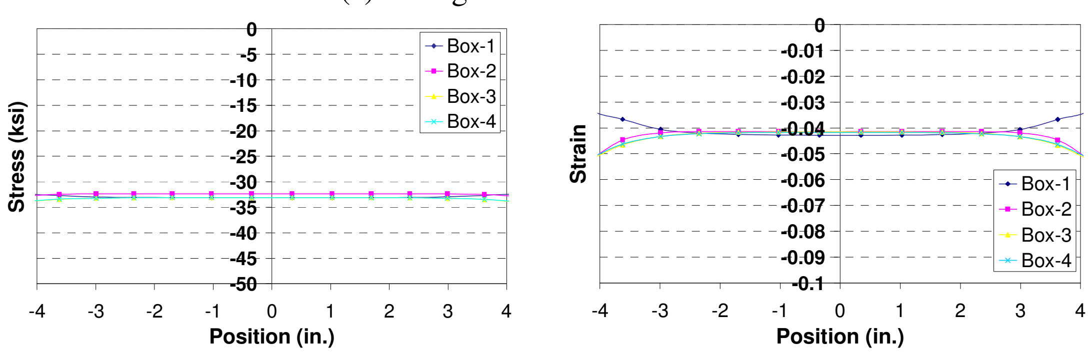

(b) Along Vertical Line in the Center

Figure 6.9: Stress and Strain Distribution in the Doubler Plate (Group Box)

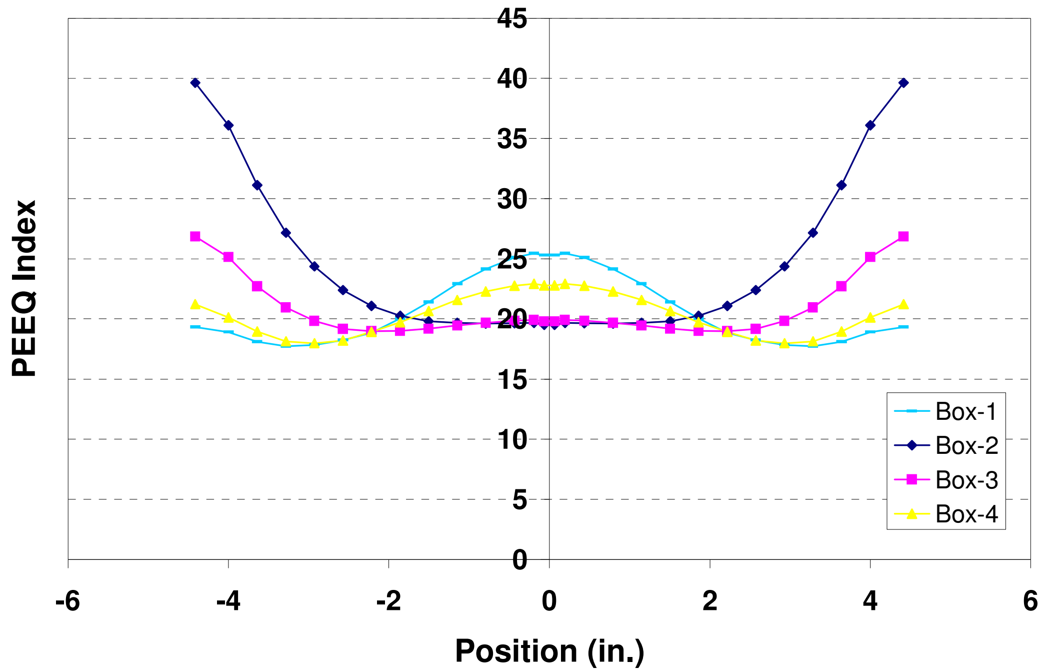

(a)

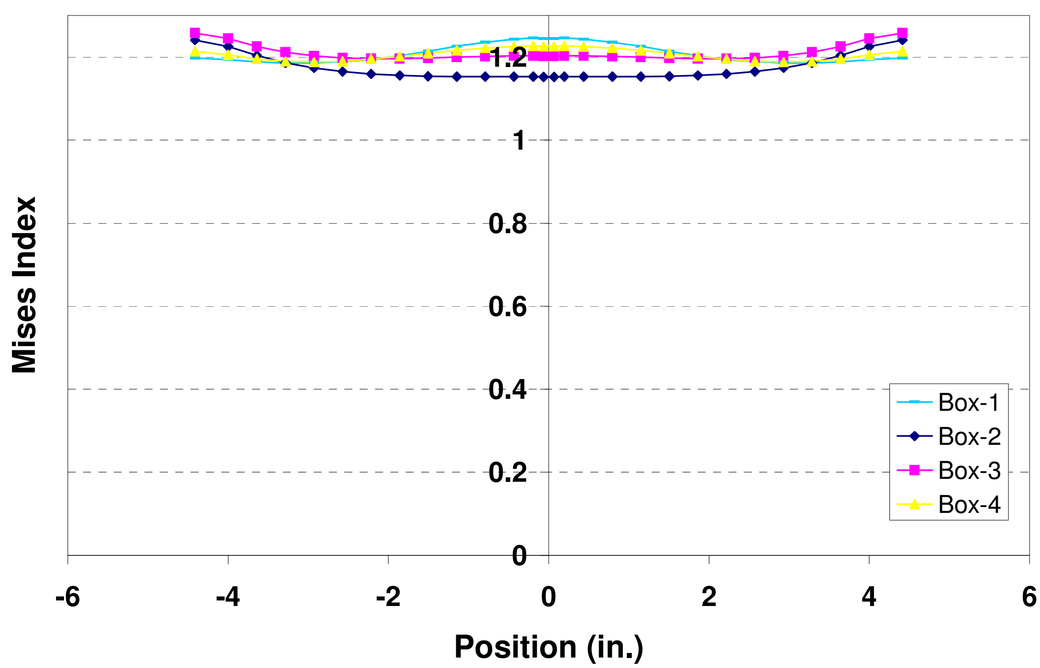

(b)

Figure 6.10: Stress and Strain in the Girder Flange (Group Box)

Chapter 7

Summary and Conclusion

7.1 Summary

This computational research is part of an ongoing project focused on the connection stiffener (continuity plate and doubler plate) behavior in steel moment frame connections. The objective of the research is to gain further knowledge of the connection stiffener behavior, clarify the need for and design of the continuity plates and doubler plates, and either reaffirm or develop new non-seismic and seismic provision for column stiffener detailing.

The research includes the following components: (1) literature review; (2) experimental research; and (3) computational research. The experimental research includes nine monotonically-loaded pull plate specimens and five cyclically-loaded cruciform specimens.

For this thesis, three-dimensional nonlinear finite element analyses have been conducted using the ABAQUS program. All the test specimens were analyzed and additional configurations were created so as to conduct a parametric study. The pull plate specimen models consisted of three-dimensional eight-node solid elements. The cruciform specimen models consisted of a combination of three-dimensional eight node solid elements and beam elements. Both material nonlinearity and geometry nonlinerity were accounted for in the analysis. Fracture and residual stresses were not modeled. Static displacement-control loading histories were applied monotonically to all the finite element models. Simulations of the cyclically-loaded cruciform tests were also loaded monotonically. The results are believed to adequately represent the envelope of the cyclic results.

The finite elements analyses of the specimens provided necessary information to corroborate the experimental work. The results were used to select specimens, to help determine the instrumentation plan and expected failure criteria, and to elucidate the test results. The parametric studies aimed to extrapolate the test results to a wider range of member sizes and to characterize the connection stiffener behavior.

7.2 Conclusions

Based on analyses of the pull plate specimens as compared to the experimental results, the analyses of the cruciform specimens, and the parametric study, the following highlights the main conclusions obtained from this research regarding connection stiffener behavior. Further detail on the experimental research and background may be found in Dexter et al.(1999), Prochnow et al.(2000), and Cotton et al.(2001). These conclusions are based on monotonically-loaded specimens and analyses and relate primarily to non-seismic detailing. Conclusions for seismic detailing are pending (Cotton et al., 2001).

Pull plates tests provided an alternative method to investigate the local web yielding (LWY) and local flange bending (LFB) near the tensile girder flange. Analyses of the pull plate specimens showed that the load capacity was governed by the pull plate strength. High stress and strain concentrated in the column underneath the pull plate. Similar stress and strain distributions were found in the cruciform models, indicating that the pull plate tests should be an adequate model to evaluate these limit states.

For the unstiffened sections tested, the localized stress and strain were influenced by a combination of both LFB and LWY. The column flange exhibited two-way bending with the bending in the column longitudinal direction more dominant than the transverse direction. Local flange bending was more significant when affected by local web yielding occurred in the column web. Stress and strain concentration, LWY, and LFB were all greatly reduced when continuity plates were used. The connections with continuity plates having half the thickness of the pull plate provided adequate resistance. The box detail performed effectively to serve both as doubler plates and continuity plates. The complications of welding the doubler plates to the column k-line and fit-up tolerance in the column fillet region could be avoided by the box detail.

Higher plastic strain occurred at the girder tensile flange near the CJP welds at the girder flange-to-column flange interface, as also observed in the cruciform models. The stress and strain were more uniformly distributed when continuity plates or thicker column flanges were present. However, the parametric study showed that this effect was relatively insensitive to the thickness of continuity plate, including use of continuity plates having a thickness equal to the thickness of the pull plate and welded to the column flanges with CJP welds. The analysis results also indicated that the connections without continuity plates also performed well if adequately sized (W14x283 and W10x88 column). In addition, with the presence of continuity plates, the tensile hydrostatic stress increased at the center of the girder flange near the girder CJP welds (an 8% increase in this study), which indicated that the presence of continuity plates also increased the constraint in this region. This study did not model fracture or residual stress. However, it could be speculated that an increase of hydrostatic stress may occur when much thicker continuity plates than needed are used. In addition, larger welds will also be needed to connect the continuity plates to the connection, thus further increasing the constraint.

The parametric study of the panel zone strength to girder strength ratio (P_z/P_g, see Appendix D for these calculations) and of the column flange thickness indicated that most of the plastic deformation developed in the panel zone region for weaker panel zones (P_z/P_g <1.2 for this study), for which the predicted girder plastic moment could not be achieved. The connection strength was controlled by the panel zone in these cases. In addition, the analysis results showed that the actual shear strength was usually 75% -80% of that predicted by the AISC (1997) design equation (Equation (2.7)) at $4\gamma_y$. Furthermore, the predicted post-yield increase in the panel zone strength was not achieved for connections with thicker column flanges. The panel zone shear strength proposed in FEMA (2000a) ($0.55F_ct_pd_g$) and the girder flexural strength were reached at approximately the same time for connections with (P_z/P_g =1.2). A higher percentage (80%) of the plastic deformation also occurred in the panel zone region for the connections with weaker panel zone (P_z/P_g <1.2).

The parametric study for the doubler plate location in the box detail showed that the box detail is an excellent alternative method of connection stiffener detailing. The box detail is most cost effective when it serves both as the doubler plates and the continuity plates. Similar results were obtained in the global connection behavior, panel zone behavior, and doubler plate behavior regardless of the doubler plate locations. However, the doubler plates were more effective in reducing the girder flange inelastic strain demand at the girder flange center near the girder-to-column interface when the doubler plates were placed approximately 1/3 to 2/3 of half girder flange width away from the column web.

Appendix A

Mesh Refinement Study of Pull Plate Specimen Model

A mesh refinement study was conducted on an unstiffened pull plate model (a W14x120 column section), focusing on where high stress and strain gradients were observed. The original unstiffened pull plate model consisted of 3272 elements and 4725 nodes (Figure A.1). The refined mesh consisted of 5758 elements and 8789 nodes. The displacements and stress and strain results were compared at several locations of interest.

A.1 Finite Element Meshing And Mesh Refinement Results

Typically there are four layers of elements through the thickness of the pull plate, the column web and the continuity plates; three layers of elements through the column flange thickness; seventeen elements along the half width of the column flange; and eleven elements along the half depth of the column web. Because local web yielding and local flange bending are a localized phenomenon, high stress and strain are expected to occur near the center. Smaller element lengths were thus used near the column flange, column web, and pull plate intersection region. To reduce the computational expense, larger elements were used towards the end of the pull plate and column stub where the stress and strain gradients were small.

The finite element meshing and deformed shape of both meshes are shown in Figure A.2. In both cases, the web had significant inelastic deformation and the column flange had two-way bending. High stress and strain concentrated at the center of the pull plate-to-column flange interface and around the column k-line region.

The global behavior of the finite element model was not sensitive to the mesh refinement. The vertical displacements (the same direction as the pulling direction) were compared. Three locations were chosen where the largest deflection occurred (Figure A.2): the column flange tip (point A), the end of the pull plate (point B), and at the center of the column flange in the core region (point C). The displacement versus total specimen elongation for three locations is shown in Figure A.3. The plot shows that converged results of the displacement were obtained from the two meshes.

For the stress and strain, two locations were compared: one line in the column flange under the pull plate along the column flange width (group FLA_Z-1), and one vertical line in the web at the column center (WEB_Y-1). These two locations were chosen based on the fact that the stress and strain gradients were relatively large.

Figures A.4 to A.8 show the stress and strain distributions from the two meshes. Analyses are compared at selected load steps (S1 to S8 correspond to load steps in Table 3.2). Generally the results from the two meshes showed good convergence results, with the largest difference being within 15%. Following are some observations from the comparison:

- Stress showed better convergence than strain, due to many material points being yielded.
- Stress in the primary direction showed better convergence than the other two directions. For group FLA_Z-1, due to the dominant flange bending along the x-axis (longitudinal direction), the primary bending stress is S11. For group WEB_Y-1, due to the large elongation in vertical direction, the primary stress is S22 (Figure A.8).
- At locations away from the center, the stress and strain showed better convergence, especially after significant inelastic behavior occurred, than at the center where high stress and strain were concentrated.

A.2 Implication of the Mesh Refinement Study

The results from both meshes reported above show that the global behavior such as nodal displacements, deformed shape, and stress and strain distributions are not sensitive to the mesh refinement. For the unstiffened section studied, the column section underwent high stress and strain concentrations at the girder flange-to-column flange interface when subjected to tensile force. The column flange is more flexible at the free edge, but is more restrained by the stiffer column web at the middle. High stress and strain concentrations occurred at the middle of column flange and in the k-line region in the web opposite to the girder flange. The analysis results in this region may in general be sensitive to the finite element meshing and element type, especially for inelastic behavior. Similar results were also reported by other research (e.g., El-Tawil et al., 1998).

The results from the stiffened connections showed that the connection stiffeners (continuity plates) provide a straight load path between the column flange and the doubler plates strengthen the column web, thus effectively reducing the stress and strain concentration in the column web and the flanges. The stress and strain gradients in the column flange and the web are much smaller than that in the unstiffened sections. It is concluded that same meshing will work even better in those stiffened models. Thus it is believed that the study on the unstiffened section is sufficiently representative of the mesh convergence study.

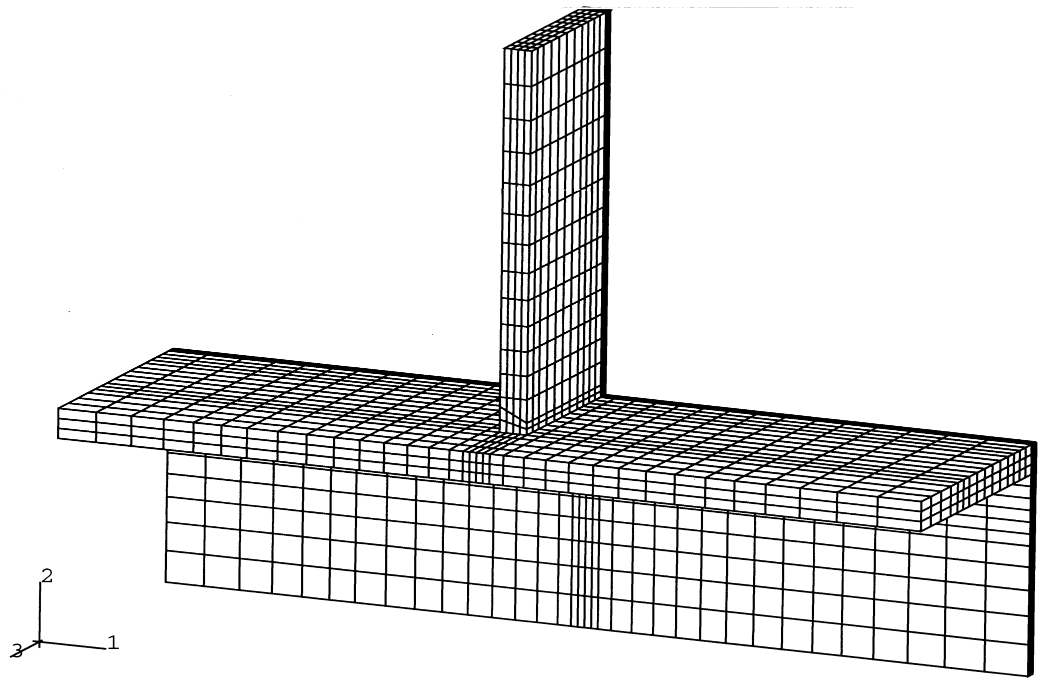

(a) Original Mesh

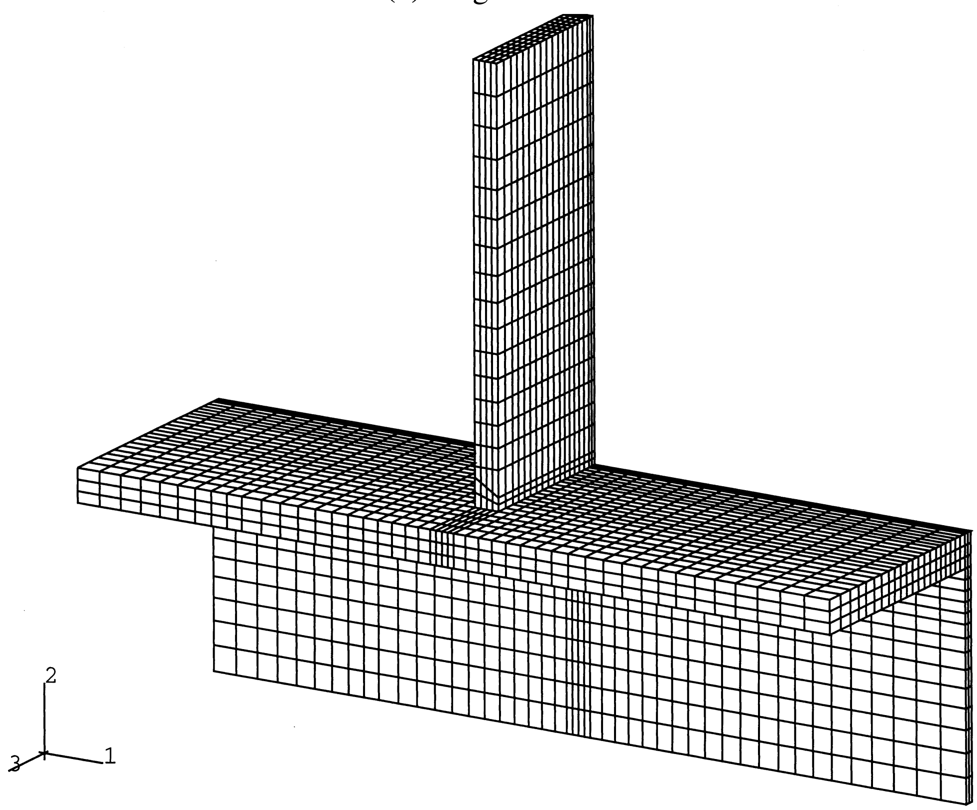

(b) Refined Mesh

Figure A.1: Comparison of Finite Element Meshing

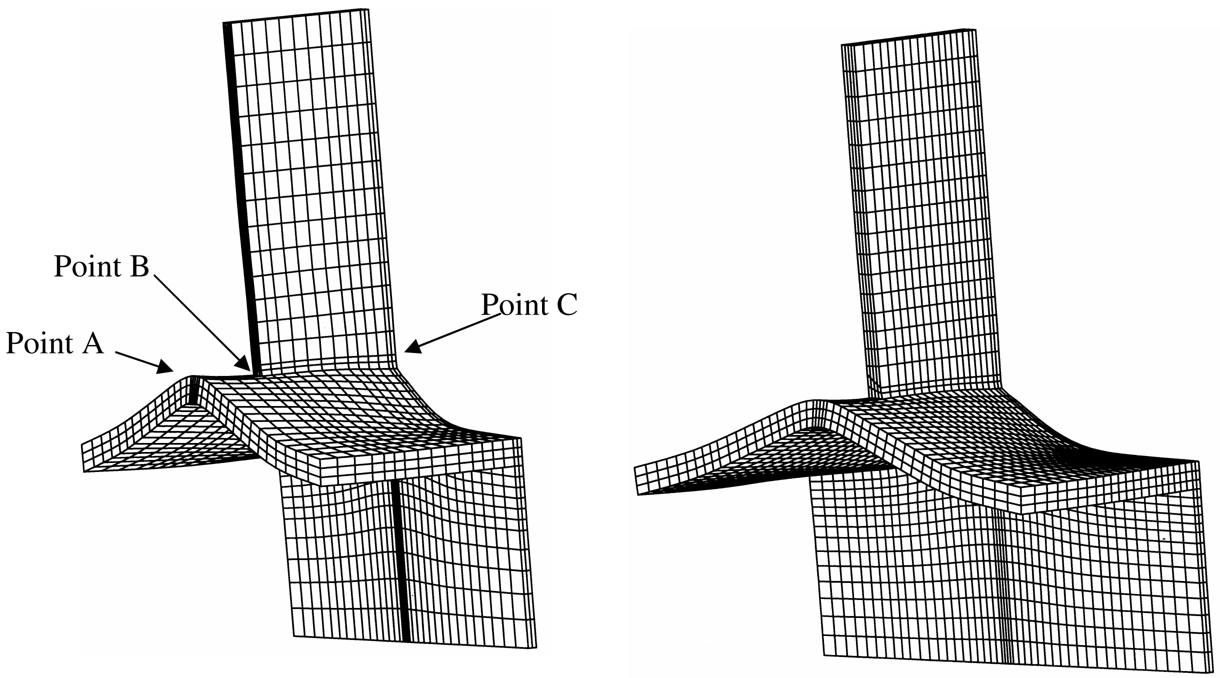

Original Mesh Model Refined Mesh Model

Figure A.2: Comparison of Deformed Shape

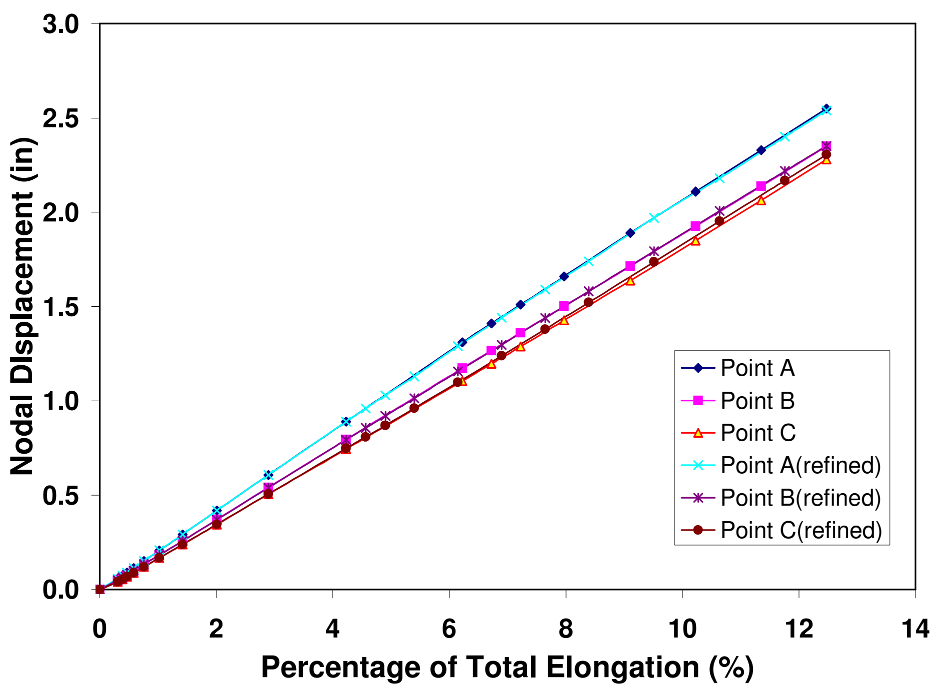

Figure A.3: Comparison of Displacement

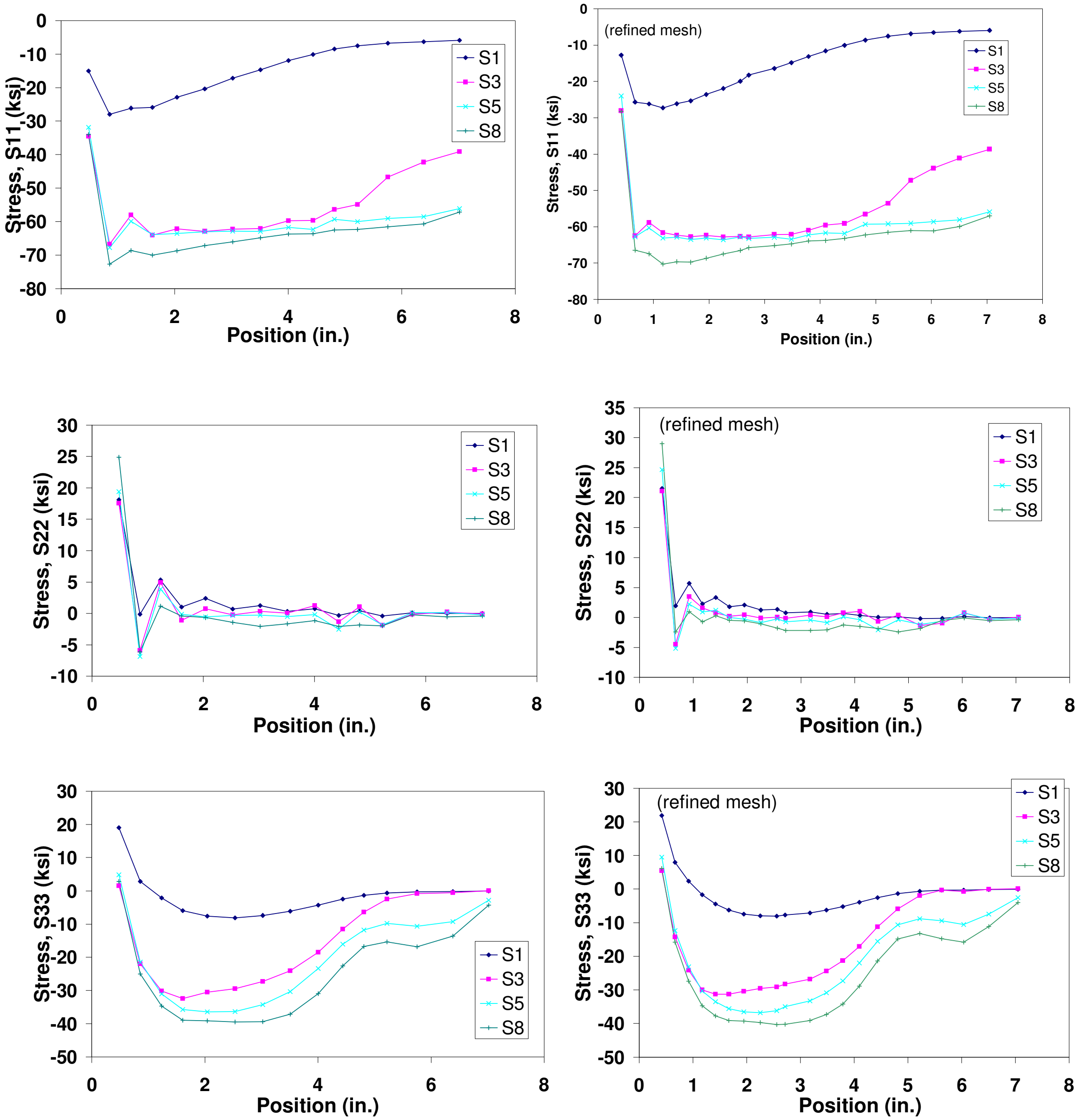

Figure A.4: Comparison of Stress in the Column Flange (FLA_Z-1)
(X-axis is the distance from the column web measured transverse to the column flange)

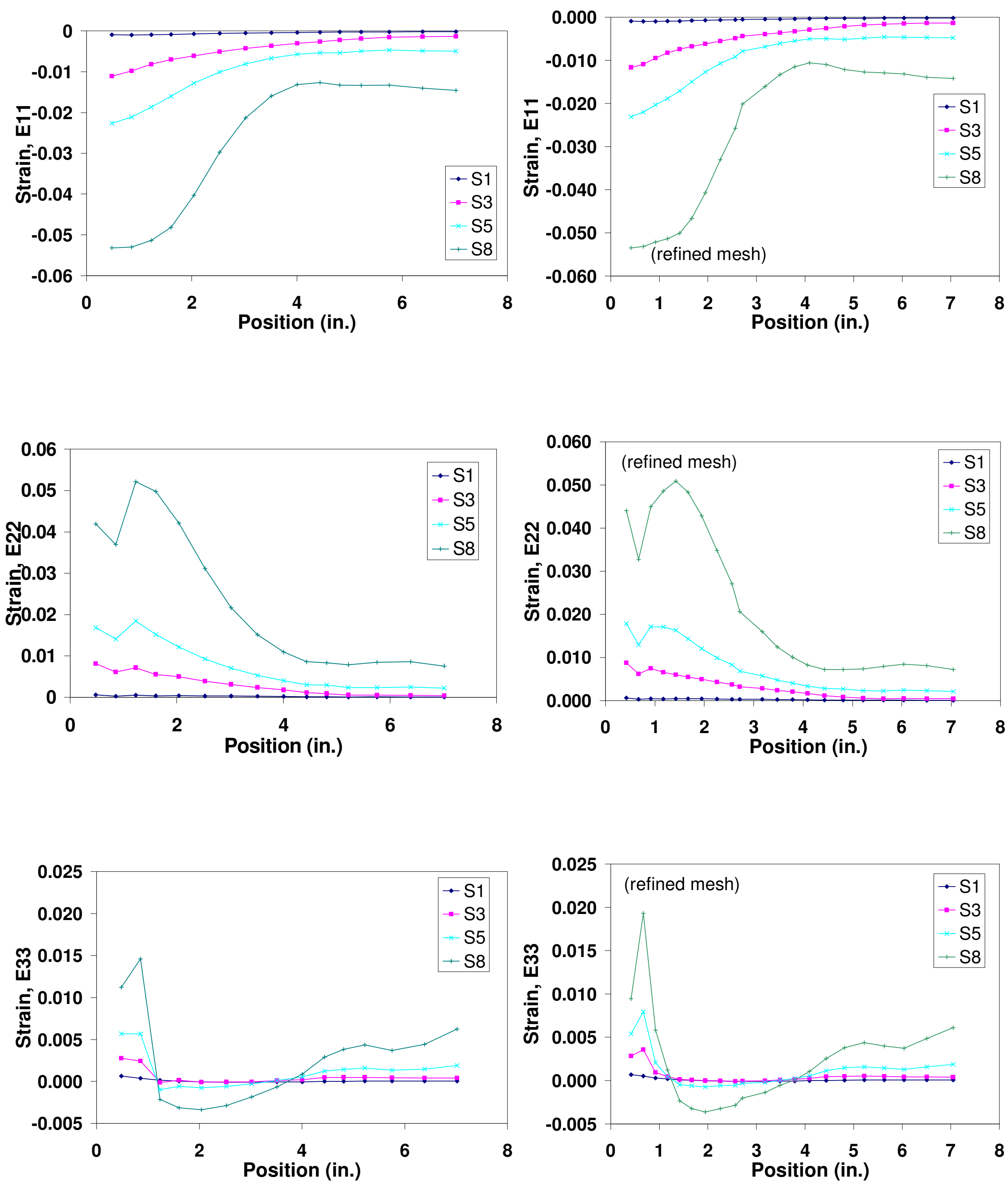

Figure A.5: Comparison of Strain in the Column Flange (FLA_Z-1)
(X-axis is the distance from the column web measured transverse to the column flange)

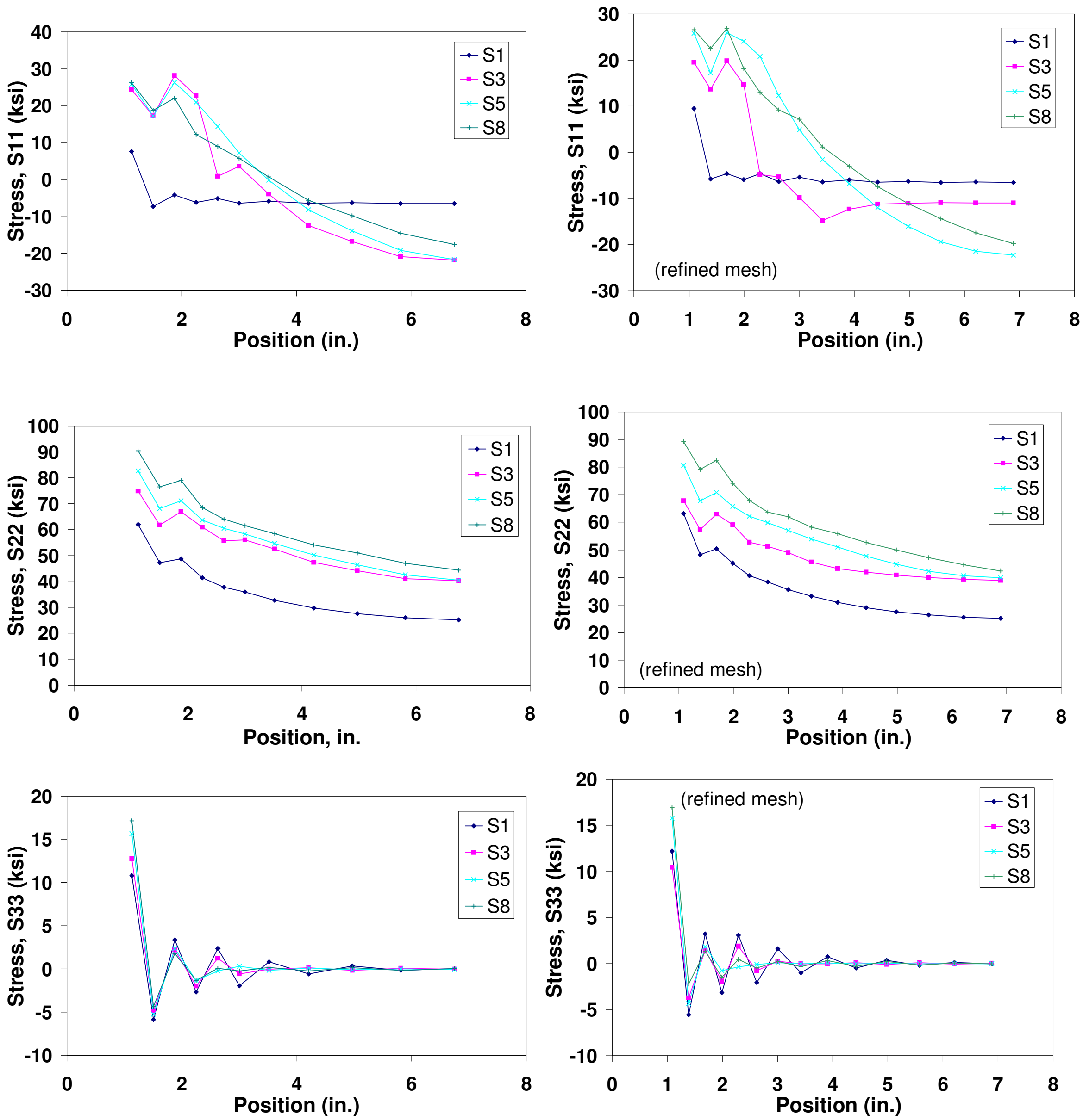

Figure A.6: Comparison of Stress in the Column Web (WEB_Y-1)

(X-axis is the vertical distance from the column flange)

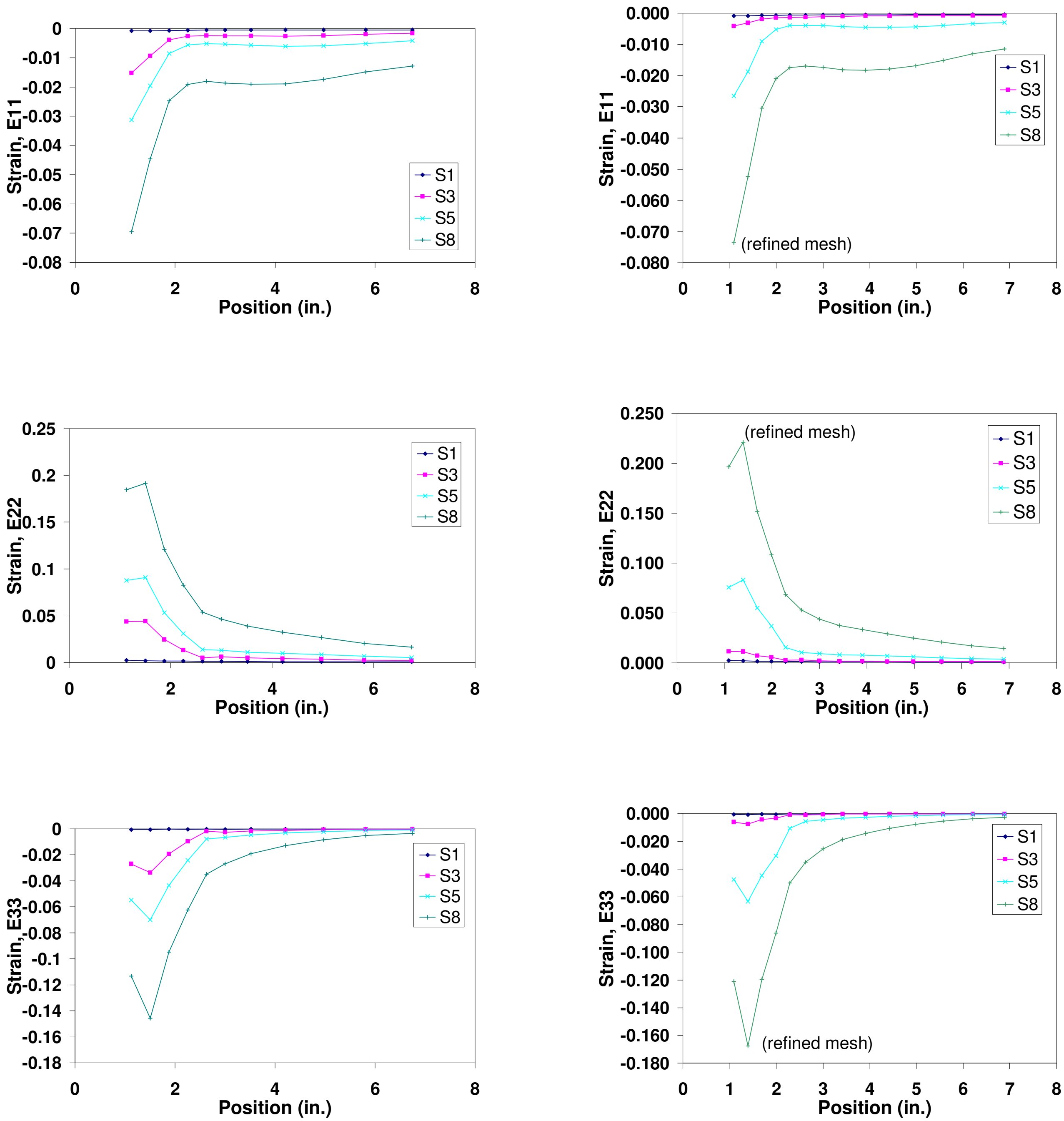

Figure A.7: Comparison of Strain in the Column Web (WEB_Y-1)

(X-axis is the vertical distance from the column flange)

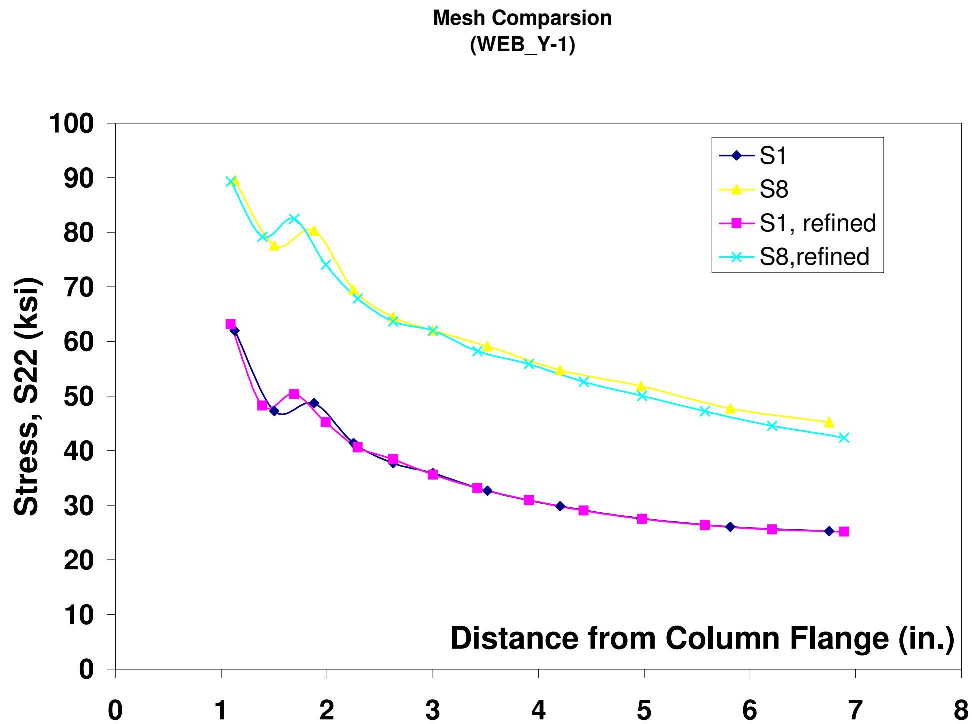

(a) Comparison of Stress in Column Web

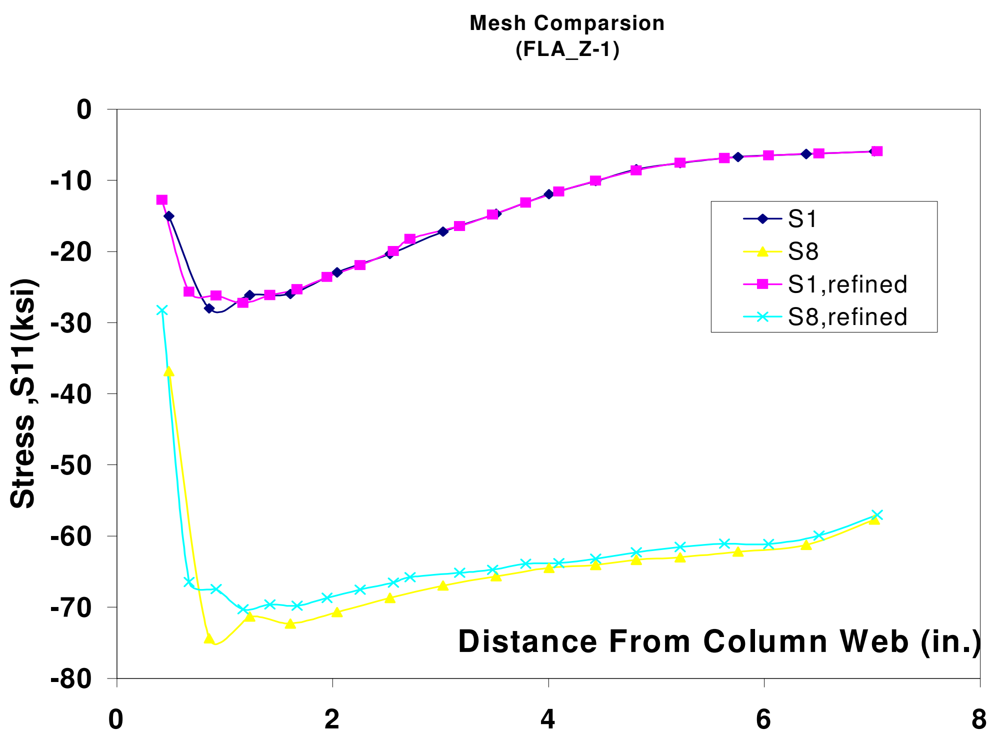

(b) Comparison of Stress in Column Flange

Figure A.8: Comparison of Stress

Appendix B

Mesh Refinement Study of the Cruciform Models

To examine the finite element meshing, mesh refinement studies were done on the cruciform specimen model. Based on the mesh studies for the pull plate models, only localized mesh refinement was done for the cruciform models. The location chosen was based on the stress and strain distribution pattern in the connection region. Mesh refinement was focused on the area near the girder flange-to-column flange welds and near the girder web access hole region, where higher stress and strain gradients were expected to occur. Shown in Figure B.1 are the two meshes used for comparison.

B.1 Mesh Refinement in the Girder flange

Shown in Figure B.2 is the comparison of the stress and strain distribution in the beam flange. The location is at the extreme layer of elements in the bottom flange (tensile flange) near the groove welds. The x-axis is the distance from the center of the beam web measured along the beam flange width. Only half of the beam flange width is plotted. The steps shown are detailed in Table 3.5. It can be seen from the plots that, in general, results from the two meshes compared favorably. Almost identical results were obtained for the first several load steps (up to 3% story drift). At higher inelastic deformation levels, the stress and strain at the center was higher in the refined mesh because the location of the Gauss point was closer to the welds. The stress and strain at the center of girder flange was somewhat sensitive to the finite element meshing. However, the difference from the two meshes at high strain levels was still within 2% for stress and 10% for strain.

Comparison of Von-Mises stress and plastic strain at the same location is shown in Figure B.2. Both meshes yielded essentially the same results. The difference is less than 1%. It is noted that at this high strain level, the beam flanges have yielded all across the flange width.

Similar results were compared for the top beam flange (in compression). Better converged results were obtained than that for bottom flange. Due to the asymmetry of the groove welds at the top and bottom flange, the top flange has less stress and strain concentration than the bottom one.

B.2 Mesh Refinement in the Girder Web

From the finite element analysis, it was observed that due to the constraints from the shear tab and the column flange, higher stress and strain gradient occurred near the top and bottom of girder web at the access hole region. Mesh refinement study was done at these locations. Shown in figure B.3 is the comparison of the shear stress distribution along the height of the beam web. The results were compared at three interstory drift levels: 0.375%, 3% and 5%. It is clear that at small deformation levels, the results are not sensitive to the finite element meshing. The difference from the two meshes increased with the increase of the inelastic deformation at the connection region. Furthermore, the results at the top showed a better convergence than that at the bottom of the girder web. It is noted that the access holes are not identical at the top and the bottom. Higher stress and strain gradients developed at the bottom access hole. However, the results from the two meshes still show good overall agreement. The difference at high inelastic deformation levels was still less than 12%.

The convergence study of the finite element meshing indicates that high stress and stain gradients occur at the center of girder bottom flange near the CJP welds and at girder web near the bottom access hole. The elastic behavior is not sensitive to the meshing. The analysis results are sensitive to the finite element meshing, the element type, and possibly the geometric configuration of the connection region at the locations of high strain concentrations. Caution shall be taken when comparing the results of these regions from different analyses. However, the finite element results can still provide an accurate prediction of the stress and strain distribution pattern in the connection region.

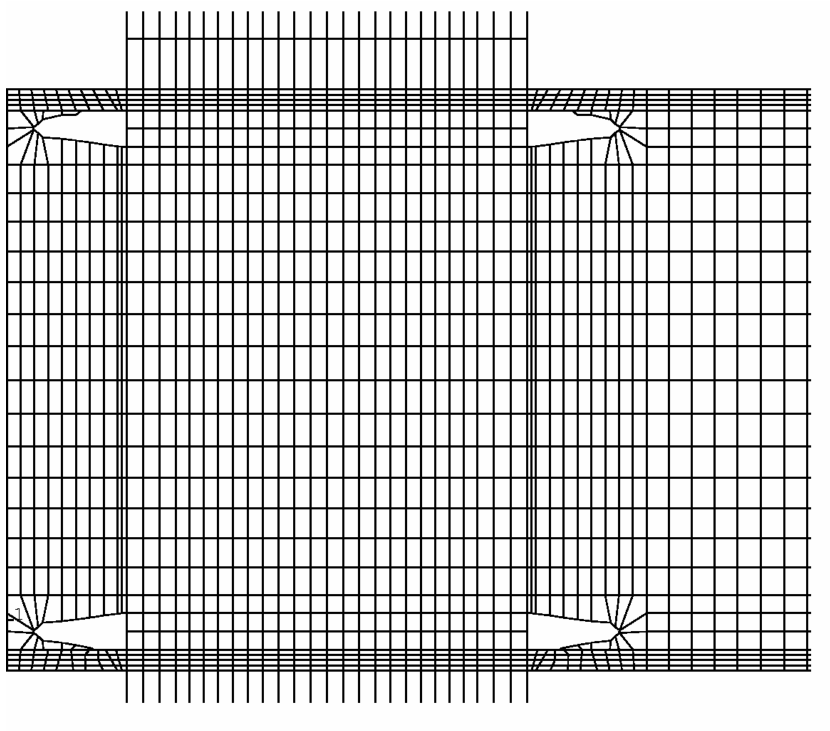

(a) Original Mesh

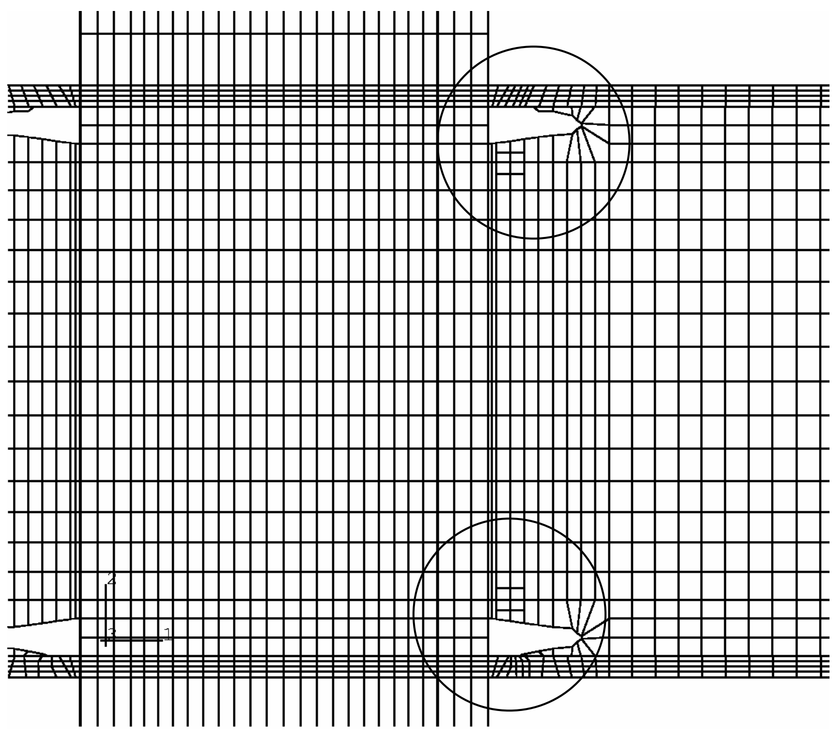

(b) Refined Mesh

Figure B.1: Mesh Refinement of the Cruciform Specimen Model

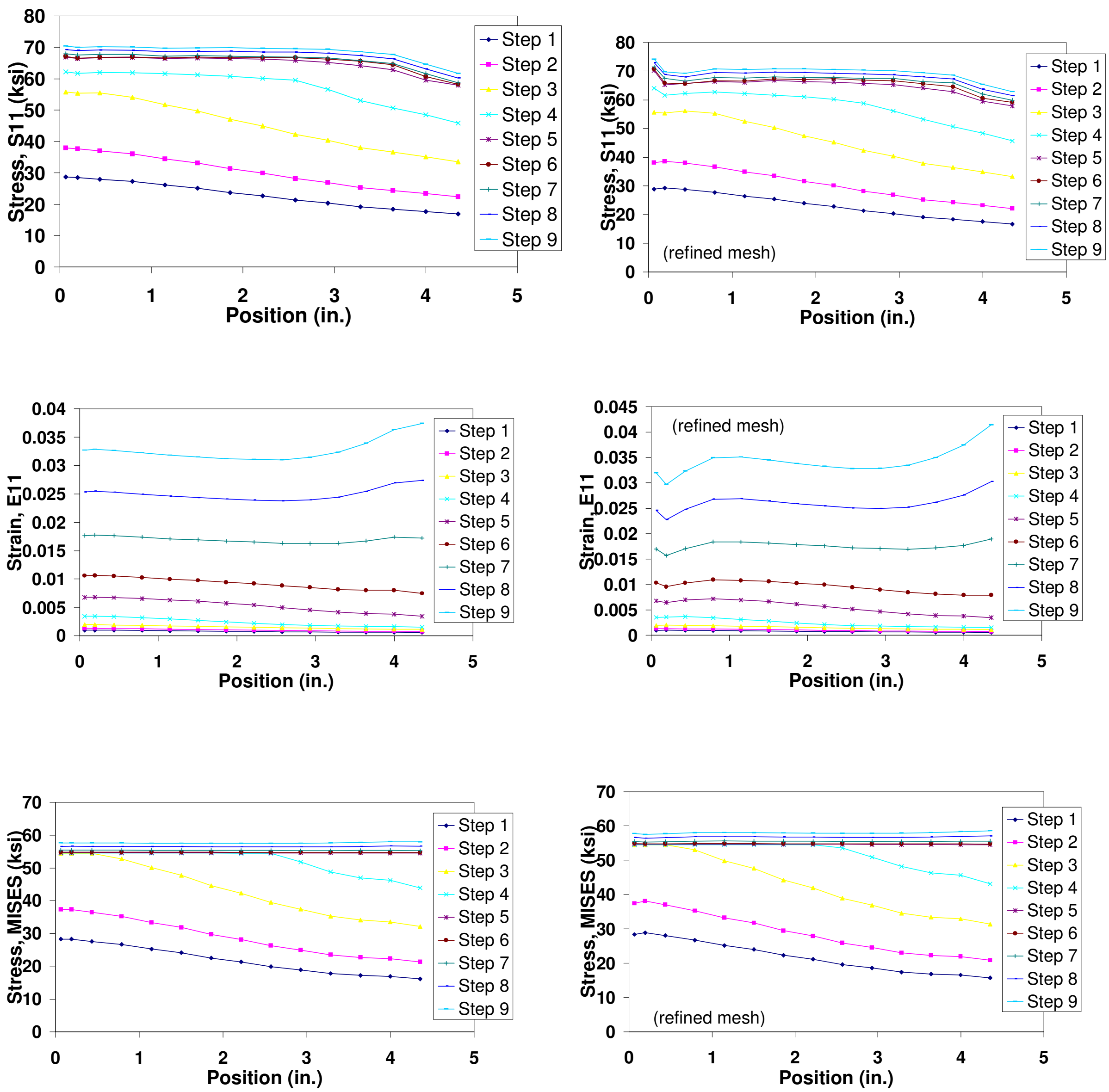

Figure B.2: Comparison of Stress and Strain along the Width in the Girder Flange
(The x-axis is the distance from the center of girder flange)
(Step 1-Step 9 are the load steps in Table 3.5)

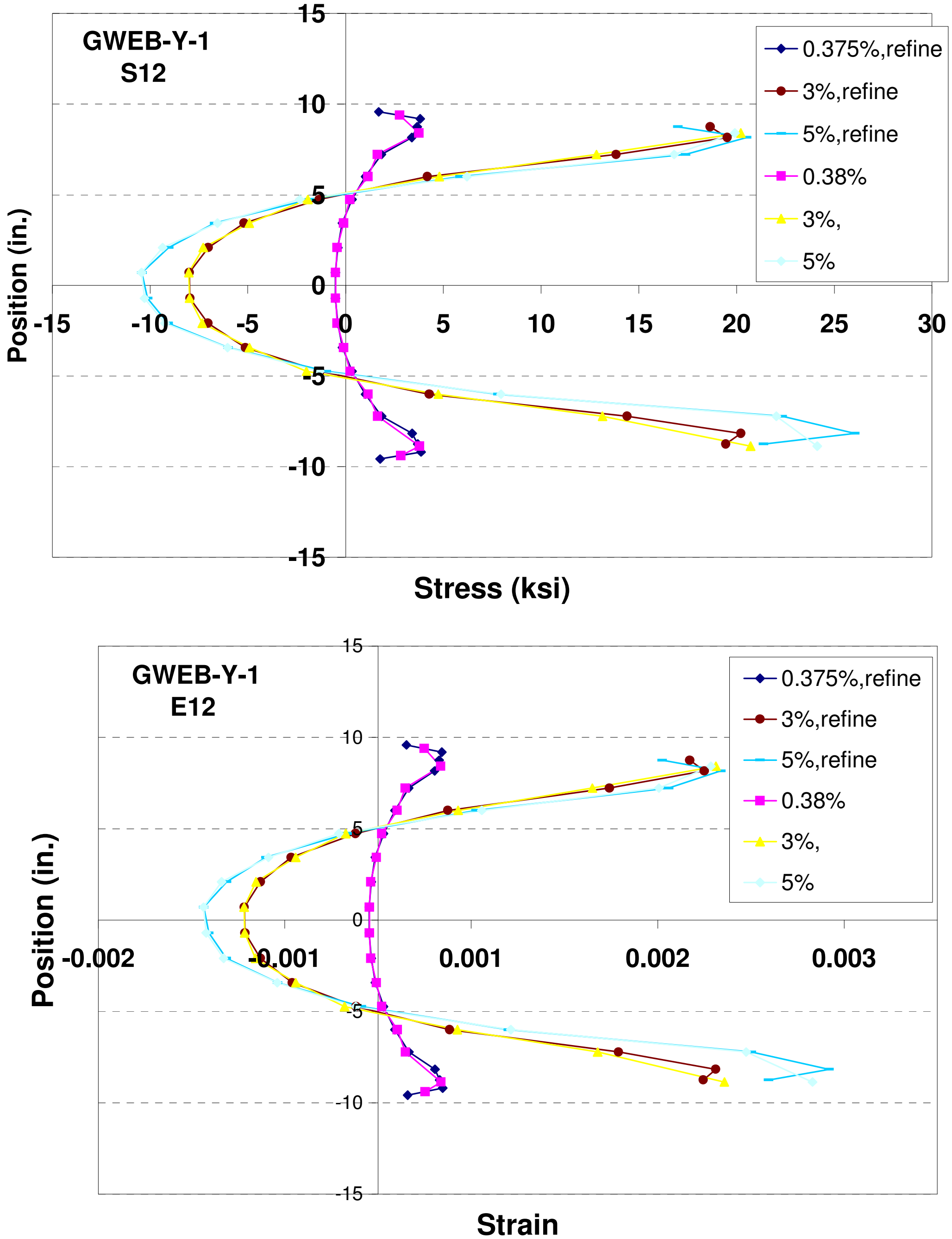

Figure B.3: Comparison of Shear Stress and Strain in the Girder Web (Y-axis is the distance from the center of the girder web centerline)

Appendix C

Justification of Column Stub Length for Pull Plate Tests

In the pull plate tests, only part of the column was used to study the connection behavior. Pull plate tests provide a convenient and economical way to study the LFB and LWY behavior. To ensure that the column stub length used in the tests are representative of the real connection behavior, a series of analyses using different column stub lengths were carried out and the results were compared.

An unstiffened pull plate specimen model (column size W14x120) was chosen to study the column stub length effect on the connection behavior. The reason for choosing a smaller unstiffened column is that the unstiffened section usually shows more significant local flange bending and local web yielding than large sections. The column stub length study on this section is applicable for large sections, which will only require a shorter length. Three different column stub lengths were studied: 2 feet, 3 feet, and 4 feet. Following are some results from the analysis used to determine the column stub length of pull plate tests.

The vertical column flange tip displacement (the same as pull direction) along the column stub length was used as one criterion to determine the column stub length effects. The objective was to find how far away from the center of the column the deflection curve went to flat. This indicates that the column stub length is long enough to represent the real connection behavior.

The results of the nodal displacements in increasing levels of load (represented by load steps S1 to S13) are plotted in Figure C.1. For all three cases, displacement for the 2-foot column model was always a little larger than that for the 3-foot and 4-foot column models. The vertical displacement dropped quickly as the distance from the column centerline increased. At about 10 inches away from the center, the displacement was only about 0.1 inches at 8% of total elongation. Several regions were studied in detail to compare the differences:

1. The vertical displacement from –3 inches to 3 inches from the column centerline (Table C.1):
   - The values for 3 feet and 4 feet were identical to 3 decimal digits for this region.
2. The region from 8 inches to 12 inches from the column centerline (Figure C.2):
   - Up to about 1.5% total elongation, values for 3-foot and 4-foot columns were identical to 3 decimal digits.
   - For larger elongations, the values for the 3-foot column were larger than that for the 4-foot column, but the difference begins at the third decimal digit.
3. The region beyond 12 inches from the column centerline (Figure C.2):
   - Up to about 1.0 % total elongation, values for 3-foot and 4-foot columns were identical to the second decimal digit.
   - For larger elongation, the values for the 3-foot section were larger than that for the 4-foot section, but the column web had been well yielded these larger load levels. The specimen will probably fail by pull plate yielding before reaching that load level.

The results from the displacements show that the 2-foot column length was not long enough for this smaller section. For the 3-foot and 4-foot column lengths, the results were nearly identical in the connection region. The difference beyond that region between the two cases was quite small.

The results from the stress and strain distributions were also checked. Most stress and strain distributions were concentrated near the intersection of the pull plate to the column flange. At a distance one foot from the column centerline, the stress and strain were quite small. The stress distribution along the column flange and the web at the specimen center are shown in Figure C.3. The stress distribution in the column flange was nearly identical for all three cases. The stress distribution in the column web was nearly identical for 3-foot and 4-foot sections, but was different from that of the 2-foot column, with the largest difference of 11%.

The analyses for three different column stub lengths suggest that the column stub length will not affect much of the connection behavior in the tests. For smaller unstiffened sections (W14x120), longer column lengths represented the real connection behavior better. It was decided to use the 3-foot column stub for all the pull plate tests.

Table C.1: Comparison of Displacement for Different Column Stub Length

	Flange Tip Displacement (in.) at 0.2% total elongation			Flange Tip Displacement (in.) at 1.5% total elongation		
Distance from column centerline (in.)	**2 feet**	**3 feet**	**4 feet**	**2 feet**	**3 feet**	**4 feet**
-3.238	0.0297	0.0289	0.0288	0.2372	0.2268	0.2258
-2.561	0.0318	0.0313	0.0311	0.2593	0.2505	0.2497
-1.922	0.0336	0.0331	0.0330	0.2789	0.2719	0.2713
-1.319	0.0349	0.0345	0.0344	0.2957	0.2904	0.2899
-0.75	0.0357	0.0353	0.0352	0.3081	0.3044	0.3041
-0.375	0.0359	0.0356	0.0356	0.3133	0.3106	0.3103
-0.1875	0.0360	0.0357	0.0356	0.3142	0.3119	0.3116
0	0.0360	0.0357	0.0356	0.3145	0.3123	0.3121
0.1875	0.0360	0.0357	0.0356	0.3141	0.3121	0.3119
0.375	0.0359	0.0357	0.0356	0.3130	0.3109	0.3107
0.75	0.0356	0.0356	0.0352	0.3075	0.3049	0.3046
1.319	0.0348	0.0356	0.0344	0.2945	0.2908	0.2906
1.922	0.0335	0.0319	0.0330	0.2773	0.2722	0.272
2.561	0.0317	0.0312	0.0311	0.2571	0.2507	0.2503
3.238	0.0295	0.0289	0.0288	0.2346	0.2268	0.2264

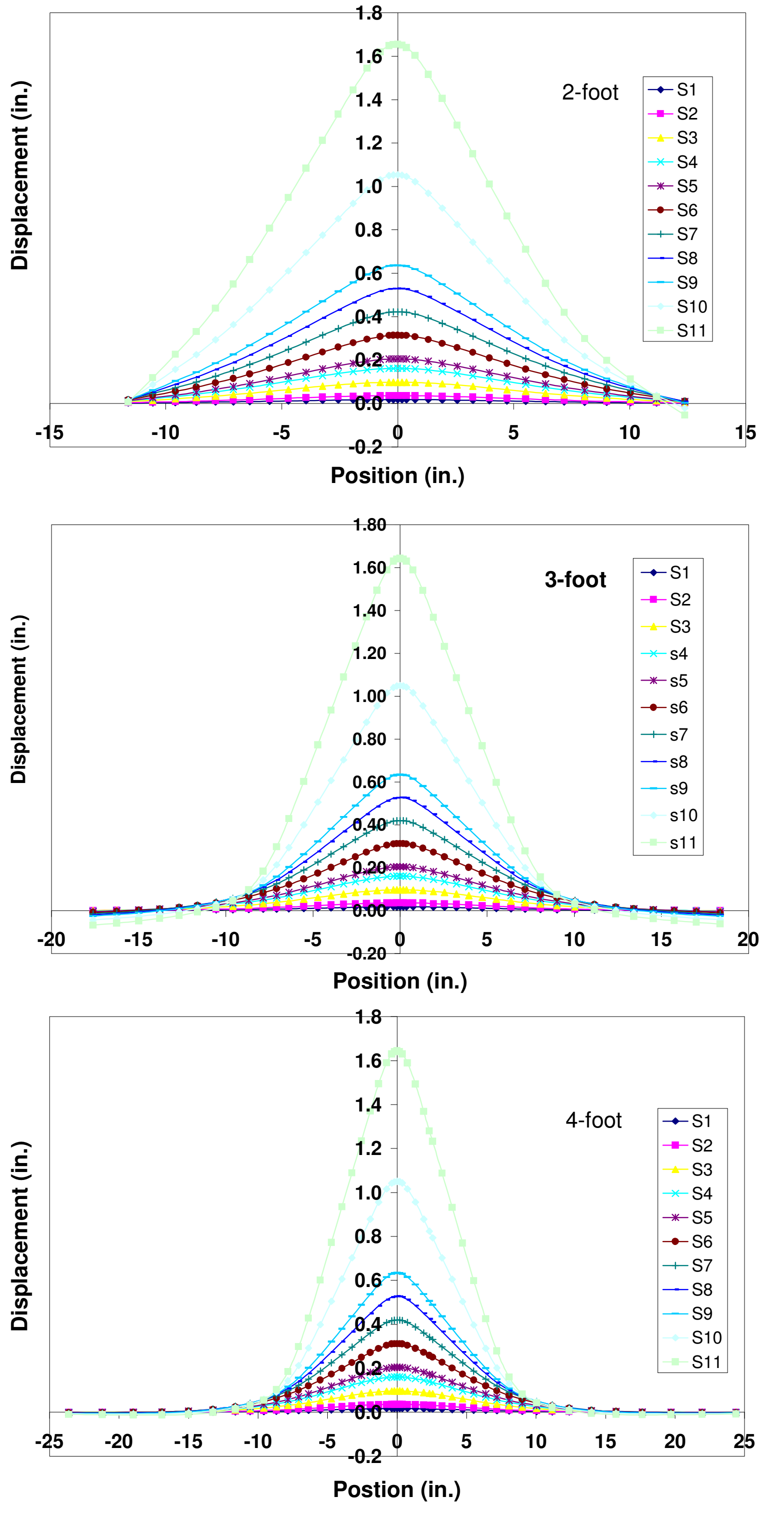

Figure C.1: Comparison of Flange Displacement for Different Column Lengths

(x-axis is the distance from the pull plate)
(S1-S11 correspond to load steps in Table 3.2)

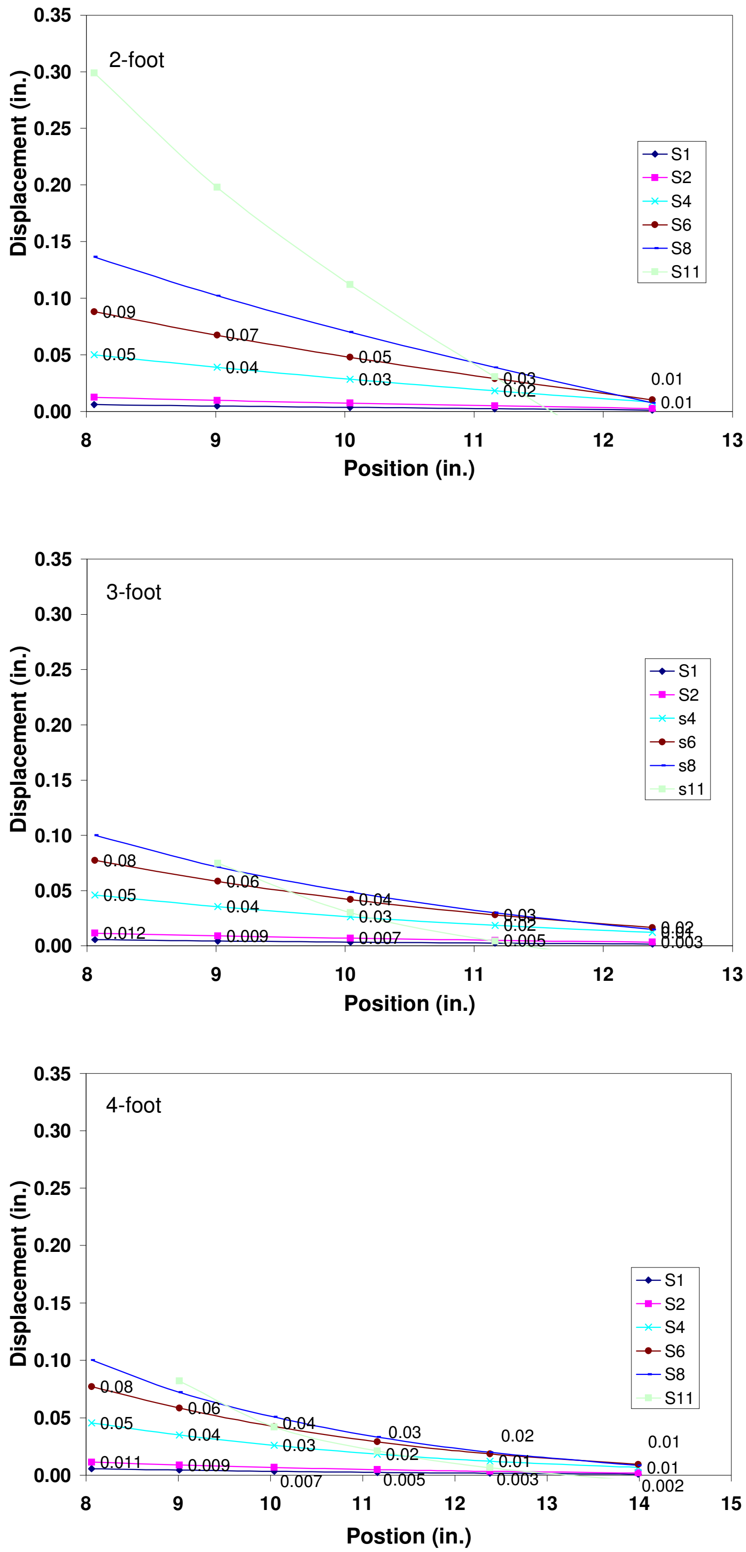

Figure C.2: Comparison of Displacement for Different Column Lengths

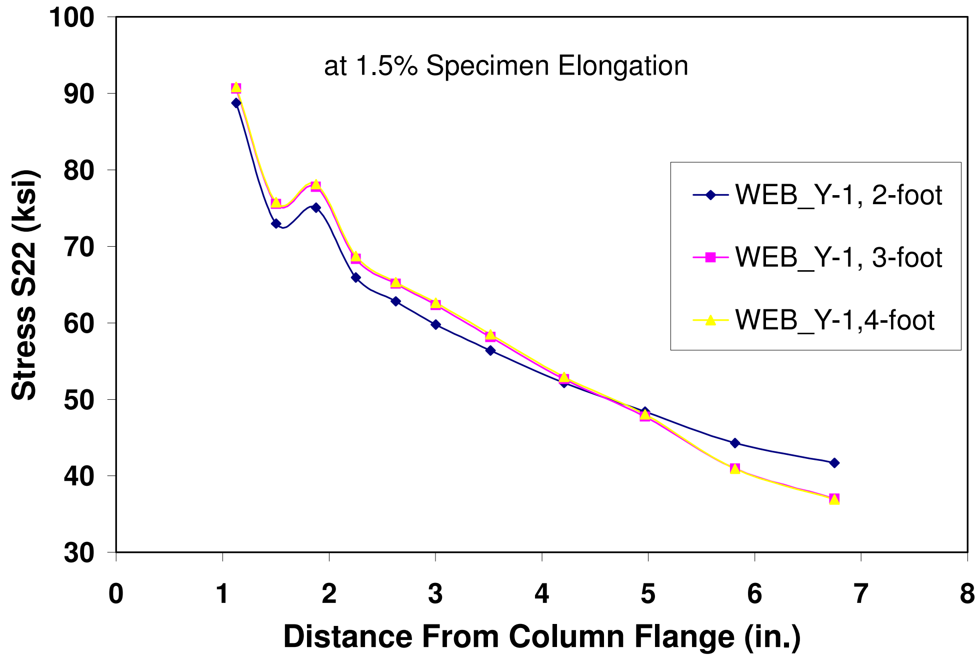

(a) Stress in Column Web

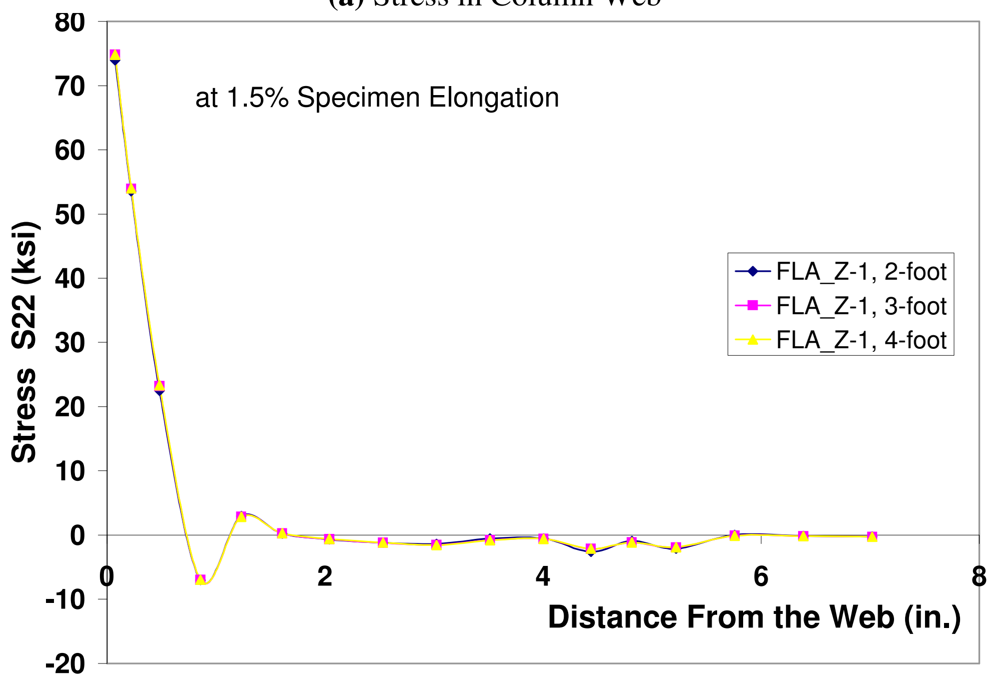

(b) Stress at Column Flange
(x-axis is the distance measured transverse to column flange)

Figure C.3: Comparison of Stress and Strain for Different Column Lengths

Appendix D

Summary of Equations Used in Specimen Calculations

The equations used in calculating the strength ratios in parametric study matrix are summarized in this appendix.

- **Strong-Column Weak-Beam Check**:

$$\frac{\sum Z_c \left(F_y - P_u / A_g\right)}{\sum 1.1 R_y F_y Z_g} > 1.0$$

- **Strength Ratios: girder tip loads to reach nominal strengths**

$$P_g = \frac{\sum F_y Z_g}{L_g}$$

$$P_z = \frac{0.6 F_y d_c t_p \left(1 + \frac{3 b_{cf} t_{cf}^2}{d_g d_c t_p}\right)}{\left(\frac{L_g}{d_g} - \frac{L_g + d_c/2}{L_c}\right)}$$

$$P_c = \frac{2 F_y Z_c}{\left(\frac{L_g + d_c/2}{L_c}\right)\left(L_c - d_g\right)}$$

- **Post-yield (Krawinkler) Term**:

$$K_{term} = \frac{3 b_{cf} t_{cf}^2}{d_g d_c t_p}$$

- **Panel Zone Demand**:

AISC (1997) Seismic: $R_u = 1.0 \sum \frac{1.1 R_y M_p}{d_g} - V_c$ (V_c = column shear)

FEMA (2000a) Seismic: $R_u = \frac{\sum M_{yield-beam}}{d_g} (\frac{L}{L - d_c})(\frac{h - d_g}{h})$

AISC (1993) Non-seismic: $R_u = 1.0 \frac{\sum M_p}{d_g} - V_c$

- **Local Flange Bending Demand**:

FEMA (2000a) Seismic: $R_u = 1.8 F_y b_f t_f$

AISC (1993) Non-seismic: $R_u = F_y b_f t_f$

From PZ: $R_u = \frac{1.1 R_y M_p}{d_g}$ [consistent with AISC PZ R_u]

- **Panel Zone and Local Flange Bending Nominal Resistance**:

Panel Zone:

AISC (1997) Seismic: $R_n = 0.6 F_y d_c t_p \left(1 + \frac{3 b_{cf} t_{cf}^2}{d_g d_c t_p} \right)$

FEMA (2000a) Seismic: $R_n = 0.55 F_y d_c t_p$

LFB:

AISC (1993) Non-seismic: $R_n = 6.25 F_y t_{cf}^2$

Appendix E

Panel Zone Deformation Calculation

Figure E.1 shows the shear deformation in the panel zone. From the figure, the following equations may be derived:

$$\gamma = \frac{\delta}{h} \quad , \quad \sin\beta = \frac{\Delta}{\delta} = \frac{b}{\sqrt{b^2 + h^2}} \Rightarrow \delta = \frac{\Delta\sqrt{b^2 + h^2}}{b}$$

$$\gamma = \Delta * \frac{\sqrt{b^2 + h^2}}{bh}$$

The distortion in the panel zone γ is taken as the average of the two diagonal values as:

$$\gamma^{ave} = \frac{|\Delta_1| + |\Delta_2|}{2} * \frac{\sqrt{b^2 + h^2}}{bh}$$

where:

Δ_1, Δ_2 =diagonal displacement in the panel zone

b, h=panel zone width and height respectively

The distortion at yield γ_y is defined as:

$$\gamma_y = \frac{F_y}{\sqrt{3} * G}$$

where,

Fy =yield stress

G = shear modulus

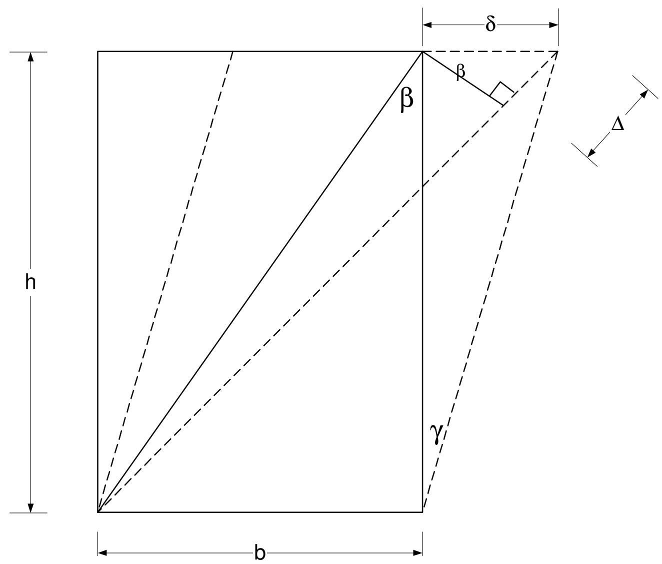

Figure E.1: Deformation in Panel Zone

References

American Institute of Steel Construction (AISC) (1993). "Load and Resistance Factor Design Specification for Structural Steel Buildings," Second ed., AISC, Chicago, Illinois.

AISC (1997). "Seismic Provisions for Structural Steel Buildings," AISC, Chicago, Illinois.

AISC (1999). "Stiffening of Wide-Flange Columns at Moment Connections: Wind and Seismic Applications," Steel Design Guide 13, AISC, Chicago, Illinois.

Bertero, V. V., Krawinkler, H., and Popov, E. P. (1973). "Further Studies on Seismic Behavior of Steel Beam-Column Subassemblages," Report No. EERC-73/27, Earthquake Engineering Research Center, University of California, Berkeley, California.

Carter, C. J. (1999). "Column Economy Considering Stiffening Requirements," *Structural Engineering in the 21st Century*, Proceedings of the ASCE Structures Congress, Avent, R. R. and Alawady, M. (eds.), New Orleans, Louisiana, April 18-21, 1999, ASCE, Reston, Virginia, pp. 552-555.

Cotton, S. C., Prochnow, S. D., Ye, Y., Hajjar, J. F., and Dexter, R. J. (2000). "Seismic Detailing of Continuity Plates and Web Doubler Plates in Steel Moment-Resisting Connections," Proceedings of the Fourth Workshop on Fracture Issues in Steel Buildings Subjected to Earthquakes, U.S.-Japan Partnership for Advanced Steel Structures, San Francisco, California, February 28-29, 2000.

Cotton, S. C., Dexter, R. J., Hajjar, J. F., Ye, Y., and Prochnow, S. D. (2001). "Column Stiffener Detailing and Panel Zone Behavior of Steel Moment Frame Connections," Report No. ST-01-1, Department of Civil Engineering, University of Minnesota, Minneapolis, Minnesota.

Deierlein, G. G., and Chi W. M. (1999). "Integrative Analytical Investigation on the Fracture Behavior of Welded Moment Resisting Connections," SAC Task 5.3.3, Final Project Report, SAC Joint Venture, Sacramento, California.

Dexter, R. J., Hajjar, J. F., Cotton, S. C., Prochnow, S. D, and Ye, Y. (1999). "Reassessment of Design Criteria and New Alternatives for Column Transverse Stiffeners (Continuity Plates) And Web Doubler Plates: Interim Report," *Structural Engineering Report* No. ST-99-3, Department of Civil Engineering, University of Minnesota, Minneapolis, Minnesota.

Dexter, R. J., and Melendrez, M. I. (1999). "Through-Thickness Properties of Column Flanges in Welded Moment Connections," *Journal of Structural Engineering*, ASCE, Vol. 126, No. 1, pp. 24-31.

El-Tawil, S., Mikesell, T., Vidarsson, E., and Kunnath, S. (1998). "Strength and Ductility of FR Welded-Bolted Connections," Report No. SAC/BD-98/01, SAC Joint Venture, Sacramento, California.

El-Tawil, S., Vidarsson, E., Mikesell, T., and Kunnath, S. (1999). "Inelastic Behavior and Design of Steel Panel Zones," *Journal of Structural Engineering,* ASCE, Vol. 125, No. 2, pp. 183-193.

Federal Emergency Management Agency (FEMA) (1995a). "Steel Moment Frame Structures: Background Reports," Report No. FEMA 288 (SAC-95-09), SAC Joint Venture, Sacramento, California.

FEMA (1995b). "Steel Moment Frame Structures: Interim Guidelines," Report No. FEMA 267 (SAC-95-02), SAC Joint Venture, Sacramento, California.

FEMA (1997). "Interim Guidelines Advisory No. 1," Report No. FEMA 267A (SAC-96-03), SAC Joint Venture, Sacramento, California.

FEMA (2000a). "Recommended Seismic Design Criteria For New Moment Resisting Steel Frame Structures" Report No. FEMA 350D, SAC Joint Venture, Sacramento, California.

FEMA (2000b). "State-of-the-Art Report on Connection Performance," Report No. FEMA 335D, SAC Joint Venture, Sacramento, California.

FEMA (2000c). "State-of-the-Art Report on Joining and Inspection," Report No. FEMA 355B, SAC Joint Venture, Sacramento, California.

Frank, K. H. (1999). "State-of-Art Report on Structural Steel Shapes," Internal Report, 80% draft, Department of Civil Engineering, University of Texas, Austin, Texas.

Graham, J. D., Sherbourne, A. N., Khabbaz, R. N., and Jensen, C. D. (1960). "Welded Interior Beam-to-Column Connections," Welding Research Council, Bulletin No. 63, pp. 1-28.

Hajjar, J. F., Leon, R. T., Gustafson, M. A., and Shield, C. K. (1998). "Seismic Response of Composite Moment-Resisting Connections. II: Behavior," *Journal of Structural Engineering*, ASCE, Vol. 124, No. 8, pp. 877-885.

Hibbit, Karlsson & Sorenson (HKS) (1994). *ABAQUS User's Manual*, Version 5.4, HKS Inc. Pawtucket, Rhode Island.

Krawinkler, H., Bertero, V. V., and Popov, E. P. (1971). "Inelastic Behavior of Steel Beam-to-Column Subassemblages," Report No. EERC-71/7, Earthquake Engineering Research Center, University of California, Berkeley, California.

Krawinkler, H. (1978). “Shear in Beam-Column Joints in Seismic Design of Steel Frames,” *Engineering Journal*, AISC, Vol. 15, No. 3, pp. 82-91.

Leon, R. T., Hajjar, J. F., and Gustafson, M. A. (1998). “Seismic Response of Composite Moment-Resisting Connections. I: Performance,” *Journal of Structural Engineering*, ASCE, Vol. 124, No. 8, pp. 868-876.

Lee, K.-H., Goel, S. C., and Stojadinovic, B. (1997). “Boundary Effects in Welded Steel Moment Connections,” Report No. UMCEE 97-20, Department of Civil and Environmental Engineering, University of Michigan, Ann Arbor, Michigan.

Prochnow, S. D., Dexter, R. J., Hajjar, J. F., Ye, Y., and Cotton, S. C. (2000). “Local Flange Bending and Local Web Yielding Limit States in Steel Moment-Resisting Connections,” Report No. ST-00-4, Department of Civil Engineering, University of Minnesota, Minneapolis, Minnesota.

Ricles, J.M., Mao, C., Lu, L., and Fisher, J. W. (2000). “Ductility Analysis of Welded Unreiforced Beam-to-Column Moment Connections,” Proceedings of the Fourth Workshop on Fracture Issues in Steel Buildings Subjected to Earthquakes, U.S.-Japan Partnership for Advanced Steel Structures, San Francisco, California, February 28-29, 2000.

Roeder, C. W. (1997). “An Evaluation of Cracking Observed in Steel Moment Frames,” Proceedings of the ASCE Structures Congress, Kempner, L. and Brown, C. (eds.), Portland, Oregon, April 13-16, 1997, ASCE, New York, pp. 767-771.

Roeder, C. W. (2000). “Doubler and Continuity Plates for Seismic Resistant Connections,” Proceedings of the Fourth Workshop on Fracture Issues in Steel Buildings Subjected to Earthquakes, U.S.-Japan Partnership for Advanced Steel Structures, San Francisco, California, February 28-29, 2000.

Yee, R. K., Paterson, S. R., and Egan, G. R. (1998). “Engineering Evaluations of Column Continuity Plate Detail Design and Welding Issues in Welded Steel Moment Frame Connections,” Welding for Seismic Zones in New Zealand, Aptech Engineering Services, Inc., Sunnyvale, California.